ISSN 1172-9511

The effect of floor flexibility on the seismic behaviour of post-tensioned timber buildings

By:

Wouter van Beerschoten

&

Michael P. Newcombe

Supervised by A. H. Buchanan and S. Pampanin

Research Report 2010-01

Department of Civil & Natural Resources Engineering
University of Canterbury
Christchurch, New Zealand

March 2010

Abstract

This report describes in-plane experimental testing and numerical modelling of timber-concrete floor diaphragms. The experimental tests investigated the in-plane stiffness of the diaphragm and the stiffness and strength of different connections between the diaphragm and the lateral load resisting system. The test model was 1/3 scale and three meters square in plan. Seven tests with a different kind of connection between the floor and the rigid lateral supports (which simulated a timber lateral load resisting system) have been performed. The results of the experimental testing are used to calibrate numerical models which are used to investigate the effects of the floor flexibility on the seismic behaviour of post-tensioned timber buildings.

For the experimental tests, screw and nail fasteners were used to connected to floor unit to the lateral supports. These fasteners were embedded into the concrete slab or timber edge joints at different orientations. The stiffness of the diaphragm connections was vastly different for each detail. Screws installed at a 45° angle (inclined) to the lateral supports were four times stiffer than the screws installed orthogonal to the lateral supports. The initial stiffness of the inclined fasteners was similar for timber-to-timber and concrete-to-timber connections. For the timber-to-timber connections the orientation did not seem to influence the strength of the connection. The tested diaphragm had an uncracked stiffness of 4000 kN/mm and a cracked stiffness of 300 kN/mm. For the tested floor unit it was concluded that the influence of the diaphragm flexibility was negligible compared to the connector flexibility.

The floor flexibility can be idealized as three different parts, the deformation of the connectors, the shear deformation of the diaphragm and the flexural deformation of the diaphragm. The numerical analyses showed that in most perceivable situations the connection deformation will govern the in-plane seismic response of the floor. Hence, it is justified to model it as a single-degree-of-freedom (SDOF) element.

The influence of the floor flexibility on the seismic response of post-tensioned timber buildings is small. In most cases neglecting the floor flexibility is a conservative approach for the structural design of the building. However, structures with stiff walls and long floor spans there can be a significant amplification of the seismic response. For that case, a simple SDOF representation is proposed.

Code-based recommendations for predicting the peak floor accelerations are found to be inadequate. A methodology is proposed to more accurately predict the expected peak floor accelerations for design

Table of Contents

Acknowledgements

The authors would like to thank their supervisors Andy Buchanan, Stefano Pampanin, David Carradine, Frank Bijlaard, Jan-Willem van de Kuilen and Pierre Hoogenboom.

The assistance from Gavin Keats and Russell McConchie during the experimental testing in the laboratory is greatly appreciated.

Finally, Anna Brignola and Stefano Pampanin are thankfully acknowledged for their contributions to the design of the experimental test apparatus.

Glossary of Terms

DBD	Displacement Based Design
EC	Eurocode
FAM	Floor Acceleration Magnification (=PFA/PGA)
IBC	International Building Code
LLRS	Lateral Load Resisting System
LVL	Laminated Veneer Lumber
MDOF	Multi Degree of Freedom
PFA	Peak Floor Acceleration
PGA	Peak Ground Acceleration
SDOF	Single Degree of Freedom
TCC	Timber Concrete Composite
THA	Time History Analysis

List of tables

List of figures

1 Introduction

New structural systems for multi-storey timber buildings are under development at the University of Canterbury in collaboration with the Structural Timber Innovation Company Ltd (STIC). These systems are suitable for a wide range of building types, including commercial structures. They have the potential to compete with existing forms of construction (concrete and steel) in Australia and New Zealand in terms of cost, flexibility of structural form and structural performance [Buchanan *et al.*, 2008]. The system incorporates large timber structural frames or walls, constructed of Laminated Veneer Lumber (LVL) and connected by steel post-tensioning.

To achieve the long floor spans required in commercial timber buildings, Timber Concrete Composite (TCC) floor systems have been developed [Lukaszewska *et al.*, 2007; Yeoh *et al.*, 2008]. To date there has been little research into the performance of TCC floors acting as a diaphragm or the performance of the diaphragm connection to the lateral load resisting system (LLRS). The connection details could prove crucial to the effectiveness of the structural system under seismic loads. Furthermore, flexibility of the connections and the thin concrete diaphragm could result in amplification of building displacements and floor accelerations [Rivera, 2008]. The objective of this report is to determine if diaphragm flexibility should be considered in the design of the multi-storey timber buildings and establish which type of structural systems, if any, could be susceptible to increased floor accelerations and interstorey drift demands. Conversely, it may be more cost effective to consider the flexibility of the diaphragms in design as it can result in lower demands for the LLRS [Nakaki, 2000].

1.1 Background

During the 1994 Northridge earthquake several structures collapsed due to larger than expected floor diaphragm forces [Hall, 1995] and high drift demands on gravity systems [Iverson *et al.*, 1994a]. The higher mode response of structures with flexible floor diaphragms results in an amplification of the peak floor accelerations above the peak ground acceleration [Rodriguez *et al.*, 2002], often in excess of the design values predicted by international design codes [FEMA 450, 2003; International Code Council., 2003; UBC, 1997], which can result in costly damage to a building [Reinoso *et al.*, 2005]. The flexibility of the diaphragm can also amplify the interstorey drift demands on gravity systems [Fleischman *et al.*, 2001a]. The amplification of floor accelerations and interstorey drifts depend on both the stiffness of the LLRS and the diaphragm stiffness.

International codes [CEN, 2004b; International Code Council., 2003; Standards New Zealand, 2004] define a diaphragm as being ‘flexible’ or ‘rigid’, however, these definitions vary substantially. New Zealand Standards (NZS) and the International Building Code (IBC) classify a diaphragm as flexible when its deformation is larger or equal to the interstorey

displacement of the building. However, Eurocode specifies that a diaphragm is flexible when the floor deformation exceeds 10% of the building displacement at any level. If a diaphragm is flexible it shall be modelled, NZS specifies; “diaphragms shall be modelled in a three-dimensional model response spectrum or three-dimensional numerical integration time history analysis”. The codes then specify that a concrete diaphragm shall be modelled with a cracked stiffness of 0.4 to 0.5 of the gross section stiffness and designed to resist higher mode amplification and overstrength actions. For TCC floors, it is possible that the deformation of the diaphragm connections may significantly contribute to the deformation of the slab. Hence, it is unclear how a flexible TCC floor shall be modelled and if the cracked section stiffness suggested by the codes is appropriate.

As described by Brignola *et al* [2008a] for timber floors, the in-plane stiffness of the TCC diaphragm is a combination of the flexural and shear deformation of the floor unit and the deformation of the connectors between the floor unit and the LLRS. For similar systems in precast concrete, no distinction is typically made between the deformation of the connectors and the deformation of the diaphragm [Fleischman *et al.*, 2001a; Lee *et al.*, 2007; Nakaki, 2000]. Instead, an over-all effective flexural stiffness is used that takes into account cracking of the concrete and the deformation of the discrete connections between floor units (as low as 5% of the gross section stiffness). While for some types of concrete diaphragms this may be reasonable, for TCC floors it is possible that most of the floor deformations comes from the diaphragm connectors. If this is the case, the structural two-dimensional response of the floor (for a regular structure) could be simplified to a single degree of freedom (SDOF) system. This would have implications for the expected peak floor accelerations and displacements of the floors during an earthquake.

1.2 Objectives

The main objective of this study is to investigate the influence of the floor flexibility on the seismic response of post-tensioned timber buildings.

The in-plane flexibility of TCC floors is evaluated by experimental testing. A 1/3 scale timber-concrete composite (TCC) floor unit model was constructed in the structural laboratory. The goals of the experimental testing are to acquire data about the strength and stiffness of different connectors between the floor diaphragm and the LLRS, and the concrete floor diaphragm.

Numerical models are created to simulate the seismic response of TCC floor diaphragms, based of the results of the experimental testing. Parameters that influence the floor response are identified and simplified modelling approaches are proposed. Once accurate floor models are developed, they are combined with models that represent the LLRS. The combined seismic response of the floor and LLRS is analysed to establish the effects of floor flexibility for a range of building geometries.

1.3 Organisation

Chapter two gives a literature review about the development of post-tensioned timber buildings, an overview of other research performed on diaphragm flexibility and the strength of different types of fasteners. Finally, a summary of diaphragm design information from different building codes.

The third chapter describes the test setup for the experimental testing. It reviews the materials which are used, the fasteners and their characteristics, the loading procedure and the recycling of the floor after the test. The forth chapter gives an overview of the seven tests performed and the results of these tests. The test results are evaluated in chapter five.

Chapter six is the start of the numerical analysis. This chapter describes the models which are made to investigate the different deformation components of the floor. In chapter seven the lateral load resisting system is added to the models to model a single-storey building. In chapter eight a detailed analysis of a six storey building is described.

2 Literature study

Firstly, this literature review describes the development of post-tensioned timber buildings and illustrates why it may be necessary to consider floor flexibility. Secondly, a summary of previous research on diaphragm flexibility and its influence on the seismic response is given. Subsequently, an overview of methodologies used to design of connections is provided. Finally, current code-based recommendations for diaphragm design are listed.

2.1 Post-tensioned timber buildings

New forms of multi-storey timber buildings are being developed in the STIC research consortium at the University of Canterbury. The structural systems are either frames or walls connected by steel post-tensioning tendons [Palermo *et al.*, 2006]. The post-tensioning creates simple moment resisting connection, facilitating easy of assembly and providing excellent structural performance. This system gives the opportunity to create large open spaces and provide a good resistance to earthquakes. This gives them the potential to compete with concrete or steel structures within New Zealand [Smith, 2008].

Another key aspect is the floor system. The timber-concrete composite (TCC) floor system is most viable for multi-storey buildings due to its low weight, good acoustic performance and limited deflections at larger spans [Buchanan *et al.*, 2008]. A lot of research has focussed on the timber-to-concrete connections in order to achieve a high degree of composite action [Deam, 2007; Linden, 1999; Lukaszewska *et al.*, 2007; Seibold, 2004].

So far the effect of the in-plane diaphragm stiffness on the seismic response of multi-storey timber buildings has had little attention. However, there is the potential that in-plane floor deformations may be significant for post-tensioned timber buildings due to the long spans and thin concrete toppings that are used in design. These deformations may significantly alter the seismic response of post-tensioned timber buildings; this is focal point of this report.

2.2 In-plane diaphragm stiffness and seismic response

During the 1994 Northridge earthquake several structures collapsed due to larger than expected floor diaphragm forces [Hall, 1995] and high drift demands on gravity systems [Iverson *et al.*, 1994b]. The higher mode response of structures with flexible floor diaphragms results in an amplification of the peak floor accelerations above the peak ground acceleration [Rivera, 2008; Rodriguez *et al.*, 2002], often in excess of the design values predicted by international design codes [FEMA 450, 2003; IBC, 2003; UBC, 1997], which can result in costly damage to a building [Reinoso *et al.*, 2005]. The flexibility of the diaphragm can also amplify the interstorey drift demands on gravity systems [Fleischman *et al.*, 2001b]. The

amplification of floor accelerations and interstorey drifts depend on both the stiffness of the LLRS and the diaphragm stiffness.

Fleischman and Farrow [2001a] showed that long-span precast concrete diaphragms can be highly flexible when compared to the LLRS. This can lead to increased diaphragm forces and non-ductile diaphragm failure or structural instability due to high drift demands in the gravity system. They conclude that current design procedures based on rigid diaphragms are not adequate to predict the seismic demands on structures with flexible diaphragms. It is likely that long span TCC floors will be similarly flexible.

Studies of the stiffness of concrete diaphragms [Lee *et al.*, 2007; Nakaki, 2000] have mainly focussed on the stiffness of precast concrete elements with discrete connectors. An overall effective flexural stiffness is used that takes into account cracking of the concrete and deformation of the discrete connections between floor units. While for some types of concrete diaphragms this may be reasonable, for TCC floor units it is possible that the most significant deformation component comes from the discrete connectors between the LLRS and the diaphragm. If this is the case, the structural response of the floor could be simplified to a single degree of freedom (SDOF) system. This would have implications for the expected peak floor accelerations and displacements during an earthquake.

As described by Brignola *et al* [2008b] for timber floors, the in-plane stiffness of the TCC diaphragm can be represented as a combination of the flexural and shear deformation of the floor unit and the deformation of the connectors between the floor unit and the LLRS. The adopted modelling approach (see Figure 2.1) excludes the possibility of higher modes of response from the combination of the two different elements.

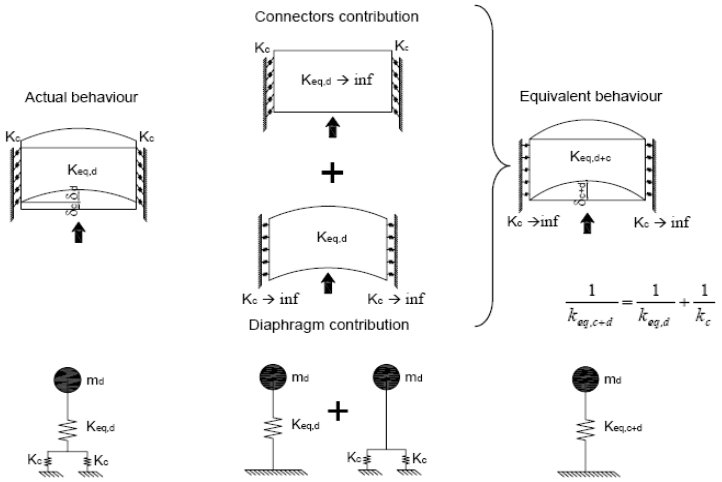

Figure 2.1 – Schematic contributions of connectors and diaphragm stiffness to the overall floor system stiffness [Brignola et al., 2008a]

2.3 Fasteners Design

To provide an adequate connection between the concrete floor diaphragm and the LLRS wood-type fasteners are considered. Johansen's yield theory is widely used to calculate the load carrying capacity of timber-to-timber and timber-to-steel connections [CEN, 2004b]. Dias [2005] showed that the formulas from EC5 are also applicable to concrete-to-timber connections. The theory of Johansen's yield theory has been expanded to inclined screws in timber-to-timber connections [Bejtka, 2002] and for inclined screws in concrete-to-timber connections [Kavaliauskas, 2007]. However, all of these studies only focus on uni-directional loading, not on cyclic loading, as will be the case under earthquake loading. Further research on the cyclic degradation of screwed fastener is required.

2.4 Building Standards and Guidelines

This section gives an overview of the sections from the New Zealand standard [1993; 2004; 2006], the Eurocode [CEN, 2004b; CEN, 2004c; CEN, 2004d] and the International Building Code [International Code Council., 2003] relevant for this report. In general, it is noted that there is a lack of design guidelines for diaphragms connections for timber buildings.

2.4.1 Diaphragm stiffness

For the ease of the design process, diaphragms are classified as rigid or flexible. This is done in the following way by the three standards.

NZ1170.5 Rigid diaphragm: A diaphragm that is sufficiently rigid that the maximum lateral deflection is less than twice the average inter-storey deflection at that level.

EC8 The diaphragm is taken as being rigid, if, when it is modelled with its actual in-plane flexibility, its horizontal displacements nowhere exceed those resulting from the rigid diaphragm assumption by more than 10% of the corresponding absolute horizontal displacements in the seismic design situation.

IBC A diaphragm is rigid for the purpose of distribution of story shear and torsional moment when the lateral deformation of the diaphragm is less than or equal to two times the average story drift.

These definitions are explained with the help of Figure 2.2. The average inter-storey drift (or for a single storey building, the total horizontal displacement) is u_{llrs}. The horizontal deflection of the diaphragm is u_{floor}. The New Zealand standard and the IBC require for a rigid diaphragm that:

$u_{floor} + u_{llrs} \leq 2 \times u_{llrs}$ or $u_{floor} \leq u_{llrs}$.

EC8 requires that:

$u_{floor} \leq 10\% \times u_{llrs}$.

It can be seen that there is a factor ten difference between the two standards.

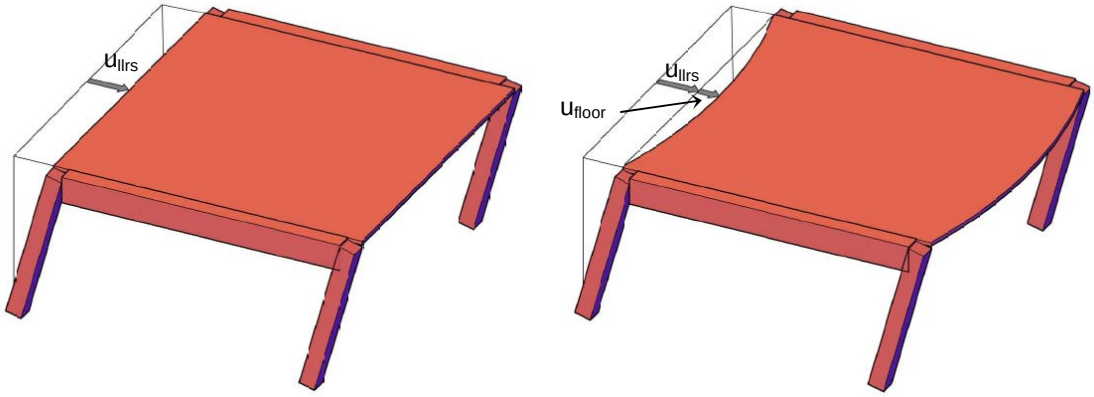

Figure 2.2 – Explanation of flexible and rigid diaphragm

2.4.2 Diaphragm design

Eurocode 8 [CEN, 2004d] gives several design rules for (concrete) diaphragms. A short overview is presented below.

4.2.1.5.(2) Floor systems and the roof should be provided with in-plane stiffness and resistance and with effective connection to the vertical structural system.

4.3.1.(7) Unless a more accurate analysis of the cracked element is performed, the elastic flexural and shear stiffness properties of concrete and masonry elements may be taken to be equal to one-half of the corresponding stiffness of the uncracked elements.

4.4.2.5.(1) Diaphragms and bracings in horizontal planes shall be able to transmit, with sufficient overstrength, the effects of the design seismic action to the lateral load-resisting system […].

4.4.2.5.(2) The recommended value [for γ_d (overstrength)] for brittle failure modes, such as shear in concrete diaphragms is 1.3.

5.10.(1) A solid reinforced concrete slab may be considered to serve as a diaphragm, if it has a thickness of not less than 70 mm […].

5.10.(4) Action-effects in reinforced concrete diaphragms may be estimated by modelling the diaphragm as a deep beam […].

Section 4.2.1.5.(2) mentions an 'effective connection', but what characteristics result in an effective connection is not mentioned. In this report there are several different connections analysed and compared.

Section 4.3.1.(7) gives a reduction factor of 0.5 for the stiffness of a cracked concrete diaphragm. Eurocode 5 [CEN, 2004c] states the following:

5.2.(5) [...] As a simple approach the stiffness of the cracked part of the concrete cross-section may be taken as 40% of the stiffness in un-cracked condition.

The determination of the stiffness of the diaphragm is part of the experimental testing and the results will be used to check the validity of these factors, which is presented in Section 5.5 and Section 6.4.

The New Zealand standard for earthquake loading [Standards New Zealand, 2004] provides the following information about floor diaphragms:

6.1.4.1 For structures over 15 m in height where the structure is classified as irregular […], diaphragms shall be modelled in a three-dimensional model response spectrum or three-dimensional numerical integration time history analysis. Where diaphragms are not rigid compared to the vertical elements of the vertical action resisting system, the model should include representation of the diaphragm's flexibility.

6.1.4.2 Actions within the diaphragm shall account for higher mode effects and the influence of overstrength actions […].

Section 6.1.4.1 raises the question how to model the diaphragm's flexibility. This is evaluated in Chapter 6.

In the New Zealand standard for Timber Structures [Standards New Zealand, 1993] only covers the design for diaphragms consisting of wood passed panels. As mentioned before, in the design of multi-storey timber buildings the most likely floor system will be a TCC floor. The diaphragm design of this floor system is not covered by the timber standard. The New Zealand concrete standard [Standards New Zealand, 2006] does cover the diaphragm design, but the connection between the diaphragm and the LLRS is less than adequate.

13.3.7.5 Connections by means of reinforcement from precast or cast-in-place concrete diaphragms to components of the primary force-resisting systems shall be adequate to accommodate the expected deformations at the interface while maintaining load paths.

No connection by means of reinforcement is possible between the TCC floor and a timber frame or wall. Several possible connections are described in Chapter 4.

Six notches were machined into each joist and two 5.3x80mm coach screws were positioned in the centre of the notch, providing a high degree of composite action between the LVL joists and the concrete slab. At each end, the joists were connected to the primary gravity beams, which also had notched slab connections. The floor unit rested on timber corbels which, in the prototype structure, would be attached to the face of the columns.

3 Experimental testing

This chapter describes the objectives of the test, the layout of the TCC floor, the test setup and the materials used. An overview is given of the testing of the fasteners which were used. Also described are the loading procedure and the recycling of the floor after the test.

3.1 Objectives

The main objective of the experimental testing is to acquire data about the strength and stiffness of different connectors between the floor diaphragm and the LLRS. Also the in-plane stiffness of the diaphragm will be investigated.

To evaluate the floor flexibility a 1/3 scale test setup of a TCC floor system was designed and build in the laboratory. This floor was subjected to 7 tests each with a different connection between the floor diaphragm and the LLRS. The results are described in Chapter 4.

3.2 Floor and test setup

A 3 x 3 m TCC floor system has been constructed in the structural testing laboratory of the Department of Civil and Natural Resources Engineering at University of Canterbury. This setup can be seen in Figure 3.1. The floor consisted of 7 LVL joists (45 x 150 mm) and a 25 mm concrete layer. Notched connections, designed according to Yeoh *et al* [2008], made sure there was a good composite action between the joists and the concrete layer. At each end, the joists were connected to the primary gravity beams, which also had notched slab connections. The floor unit rested on timber corbels which, in the prototype structure, would be attached to the face of the columns.

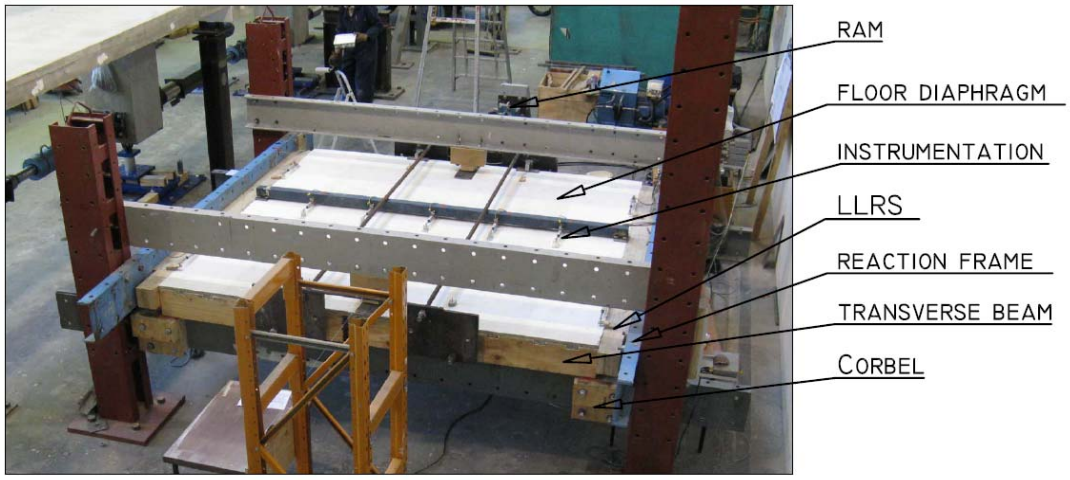

Figure 3.1 – Test setup in the laboratory

On each side of the floor a LVL beam represented the LLRS. This beam was connected to the steel reaction frame by four threaded bars, which were epoxyed into the timber and bolted to the steel frame. Some movement in this connection was possible due to oversize holes in the steel frame. This affected the rigidity of the whole setup, which influenced the last test.

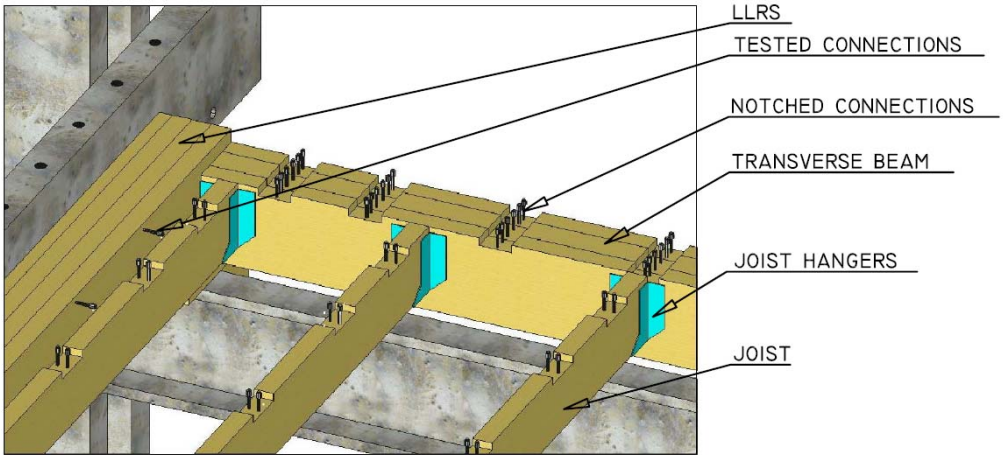

Figure 3.2 –Details of test setup, c.o. Lorent (unpublished work)

In Figure 3.2 various details of the test setup can be seen. The gap between the outer joist and the LLRS was filled with an LVL packer, which was glued to the joist (see also Figure 4.9). This has been done in order to test additional timber-to-timber connections without a gap. Calculations showed that the timber-to-timber connections with the gap would have been too weak to be realistic.

Figure 3.3 shows the instrumentation utilized to monitor displacements on the floor. Five linear pots, 50mm travel and 5000 steps, were attached to a rectangular hollow section (RHS) section, which spanned across the floor and was attached to the floor with silicon only near the edges of the diaphragm. These pots were used to measure the deflection of the diaphragm. Two pots were attached along each edge of the floor and to the LLRS. They were used to measure the displacement of the connections. Two more pots were connected to the steel reaction frame in order to measure the displacement between the LLRS and the reaction frame. This data was used to get an indication for the displacement of the reaction frame.

At one end a 250 kN ram was connected to the floor. Four threaded bars made it possible to apply the cyclic loading to the floor. At one end a load cell measured the force acting on the floor, at the other end a rotary pot was connected to control the displacement (the tests were displacement based). A positive displacement was extension of the rotary pot, which meant a pulling force in the ram, so movement of the floor towards the west.

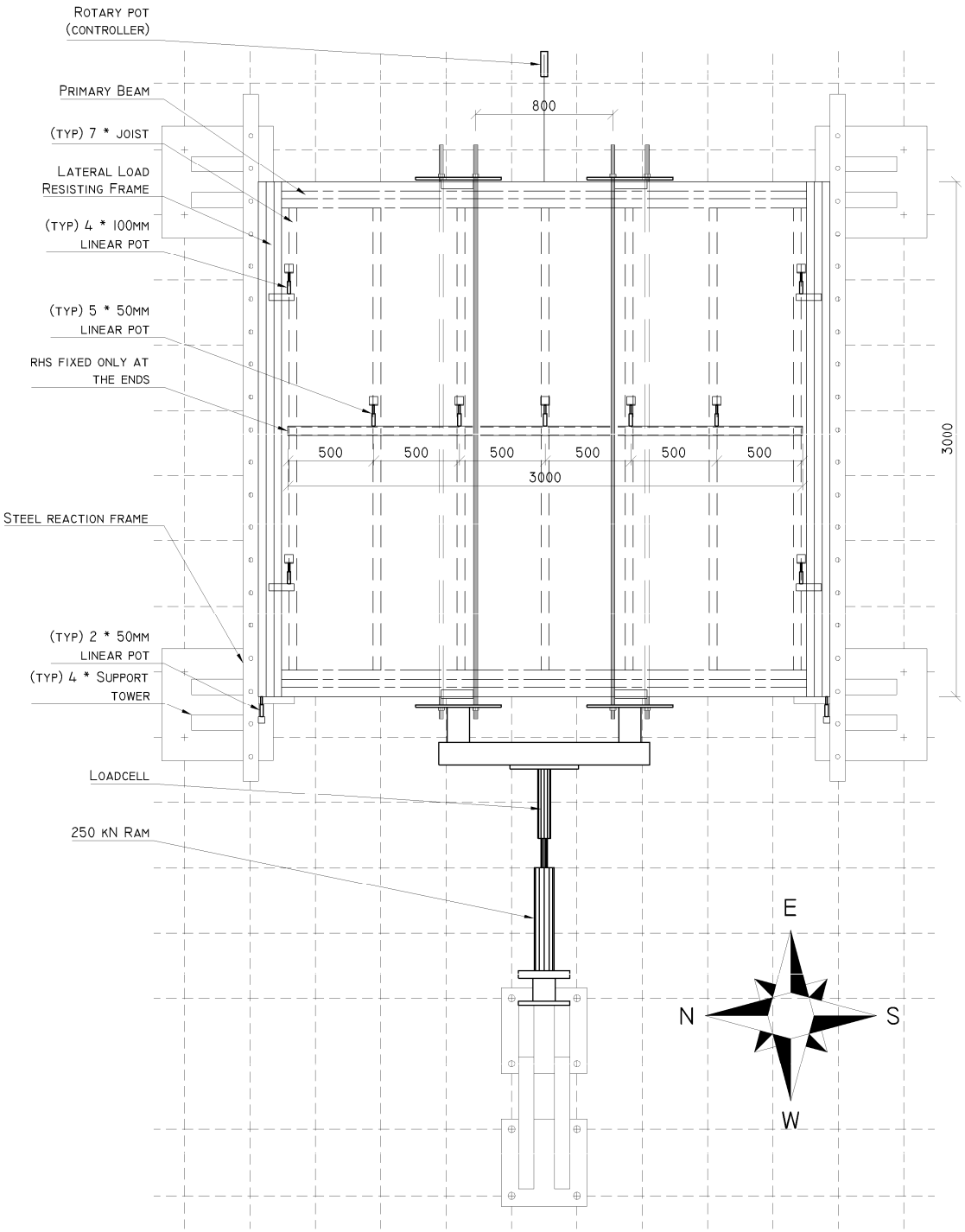

Figure 3.3 –Measurement instrumentation on the floor

3.3 Materials

3.3.1 Laminated Veneer Lumber

The timber used for the testing was LVL10 from NelsonPine. The characteristics can be seen in Table 3.1

Table 3.1 – Strength characteristic for Timber, Glulam and LVL [Buchanan, 2007]

Brand	Bending strength	Compression strength	Tension strength	Shear in beams	Compression perpendicular	Modulus of elasticity	Modulus of rigidity
	f_b (MPa)	f_c (MPa)	f_t (MPa)	f_s (MPa)	f_p (MPa)	E (GPa)	G (MPa)
CHH hySPAN*	48	45	33	5.3	12	13.2	660
NelsonPine LVL10*	48	45	30	6.0	12	10.7	535
Glulam GL8	19	24	10	3.7		8.0	530
Timber MSG 8	14	18	6	3.0	8.9	8.0	

*Both companies manufacture other grades

3.3.2 Concrete

The constructed floor had a 25 mm thick concrete layer. The concrete consists of the components shown in Table 3.2. After 28 days the test cylinders reached a compressive strength of 24 MPa. The day that the first test took place, the strength was around 36 MPa. A fine steel wire mesh was used as reinforcement.

Table 3.2 – Concrete mix [Le Heux, 2008]

	per $1m^3$	per 80 L	
Cement	280	22.4	kg
Water	150	12	kg
6mm aggregate	1050	84	kg
Sand	900	72	kg
RMCO1	1800	144	mL
Control 40	5000	400	mL

3.3.3 Grout

After the first test some of the concrete had to be taken out in order to make a different connection between the concrete layer and the timber frame, as can be seen in Figure 3.4. Grout has been used to fill this gap after the connection was made. This was done to not have to wait for a month for the concrete to cure.

Figure 3.4 – Gap in the concrete which was filled with grout

The grout used was *"Sika Grout GP"*, a high strength, shrinkage compensated, pourable cementitious grout [Sika Ltd, 2008]. Four test cylinders (Ø50 mm, 100 mm high) were made and tested at the day of the test, which was 12 days after the casting. Two cylinders were tested for compressive strength and two for tensile strength, by performing a splitting test. The results can be seen in Table 3.3. Figure 3.5 shows the tested cylinders.

Figure 3.5 – Tested grout cylinders – on the left the failure in the compression test, right the failure in the splitting test

Table 3.3 – Test results grout cylinders

Test	Force [kN]	Strength [MPa]
Compression 1	93	47
Compression 2	110	56
Split 1	30	3.8
Split 2	45	5.7

3.4 Fasteners

Six different types of fasteners have been used for the testing, five different types of screws and one type of nails. No specifications were available so the ASTM F 1575-03 [2003] was used to obtain the bending strength of the fasteners. These tests were performed after the floor testing, due to time constraints in the lab. Therefore the results of these tests are used as an evaluation of the test results, but not as a prediction of the performance.

The test setup can be seen in Figure 3.6 and Figure 3.7. The maximum possible deflection of the fasteners in the test setup was 12 mm, except for the last test. Five fasteners of each type were tested. Table 3.4 gives an overview of all the tested fasteners. Figure 3.8 gives the different loading positions.

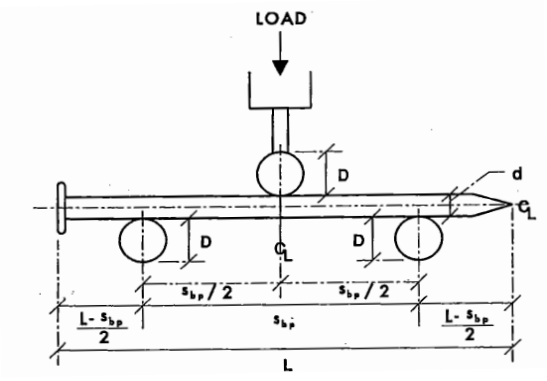

Figure 3.6 – Schematic test setup [ASTM, 2003]

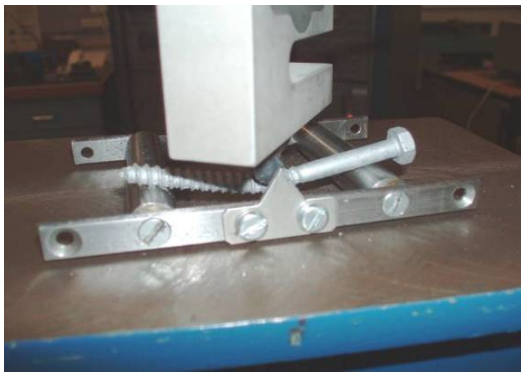

Figure 3.7 – Photo of fastener testing

Table 3.4 – Test results fastener testing

Type	Test nr	Diameter [mm]	Loading position	Failure
75 mm	1	5.50	thread	stop at 10 mm
	2	5.42	thread	stop at 10 mm
	3	5.40	thread	stop at 10 mm
	4	5.46	thread	stop at 10 mm
	5	5.38	thread	stop at 10 mm
100 mm	1	4.95	shank	stop at 12 mm
	2	4.93	interface	failure at 7 mm
	3	5.02	interface	failure at 8.5 mm
	4	4.92	shank	stop at 12 mm
	5	4.97	thread	failure at 4.5 mm
125 mm	1	5.16	shank	stop at 12 mm
	2	5.17	shank	stop at 12 mm
	3	5.20	interface	failure at 4.5 mm
	4	5.15	interface	failure at 9 mm
	5	5.22	interface	failure at 10 mm
150 mm	1	5.02	shank	failure at 4 mm
	2	4.95	shank	failure at 8 mm
	3	4.93	interface	failure at 7.5 mm
	4	4.99	interface	failure at 4 mm
	5	5.00	thread	failure at 8 mm
200 mm	1	5.15	shank	failure at 2 mm
	2	5.09	shank	failure at 4 mm
	3	5.17	shank	failure at 3 mm
	4	5.08	interface	failure at 2.5 mm
	5	5.14	interface	failure at 3.5 mm
nails (125 mm)	1	5.35	shank	stop at 12 mm
	2	5.33	shank	stop at 12 mm
	3	5.28	shank	stop at 12 mm
	4	5.34	shank	stop at 12 mm
	5	5.31	shank	stop at 18 mm

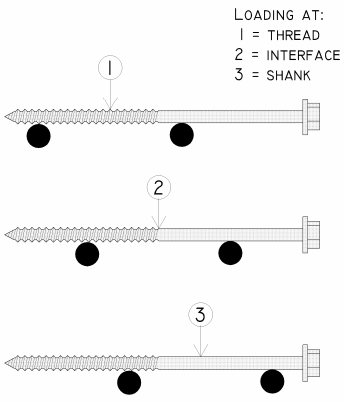

Figure 3.8 – Three different loading positions for fastener testing

Figure 3.9 gives six load displacement graphs, one for each type of connectors.

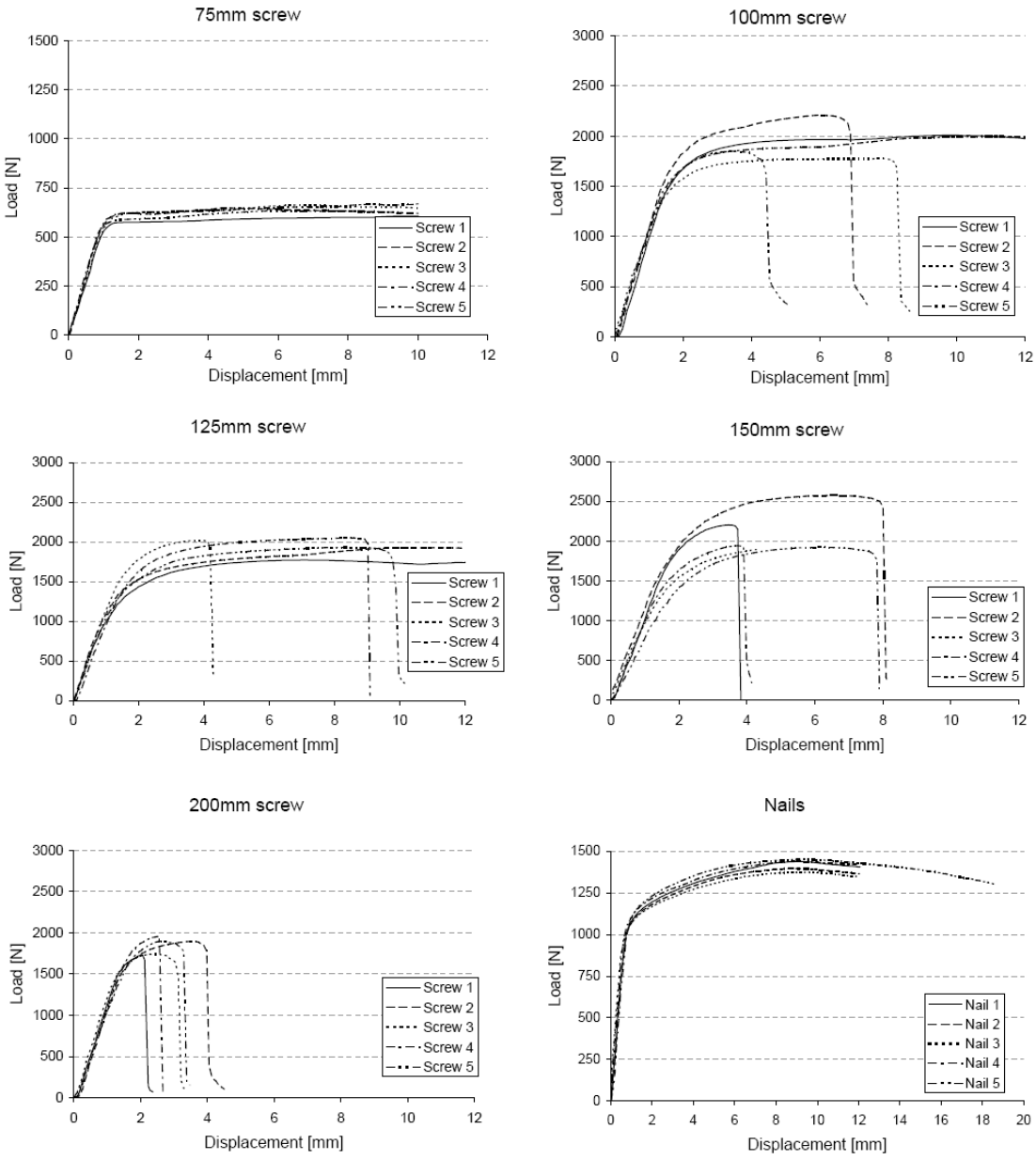

Figure 3.9 – Load displacement graphs of fastener testing

Eq. 3.1 and Eq. 3.2 [ASTM, 2003; Kavaliauskas, 2007] were used to calculate the average yield moment and the corresponding yield stress from the yield load. The results can be seen in Table 3.5. The characteristic values are not shown, since the purpose of the test was to find the real strength, and not the design strength. A normal distribution of the strength of the fasteners can be assumed [CEN, 2006]. These distributions are shown in Figure 3.10.

$$M_y = \frac{1}{4} * F * l \qquad \text{(where } l = 60\ mm\text{, } s_{bp} \text{ in Figure 3.9)} \qquad \textit{Eq. 3.1}$$

$$M_y = 0.8 * f_y * \frac{d^3}{6} \qquad \textit{Eq. 3.2}$$

Table 3.5 – Test results from fastener bending

Type	Average diameter [mm]	Average yield load [N]	Standard deviation [N]	Average yield moment [N-mm]	Average yield stress [N/mm2]	Failure mode
75mm screw	5.43	564	11	8460	396	Max. bending
100mm screw	4.96	1504	149	22560	1387	Breaking at interface & max. bending
125mm screw	5.18	1248	217	18720	1010	Breaking at interface & max. bending
150mm screw	4.98	1492	278	22380	1359	Brittle failure
200mm screw	4.98	1670	105	25050	1521	Brittle failure
125mm nail	5.32	1010	54	15150	755	Max. bending

Some general remarks can be made from these tests.

- The nails and 75 mm screws were ductile; they did not break during the bending tests.
- There was a difference in ductility if the fastener was loaded on the shank or on the thread. In general when fasteners were loaded on the thread they failed earlier, but not necessary at a lower load.
- The higher the steel quality (yield stress), the more brittle the fastener.

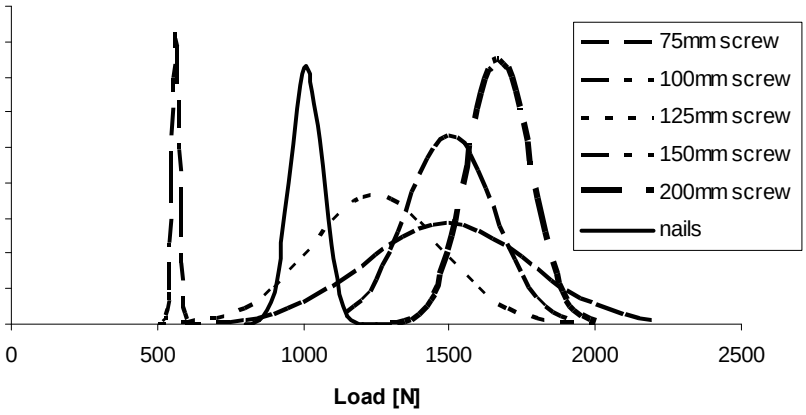

Figure 3.10 – Normal distributions of the fasteners (vertical axis is scaled differently for each graph)

3.5 Loading

The loading protocol used for testing was based on ISO CD 21581 [2007]. Even though the testing is performed on a floor slab and not a shear wall, this code provides a more extensive test protocol (especially at lower amplitudes) then EN 12512 [CEN, 2001].

For each test an ultimate displacement was assumed which determined the displacement increments. The maximum displacement for each test (except Test 2) was 20mm in order to get a good comparison between the different tests. Each displacement level during testing was cycled three times, although during some tests the higher displacement cycles were only performed twice, in order to save time. An example of a loading protocol is given in Figure 3.11.

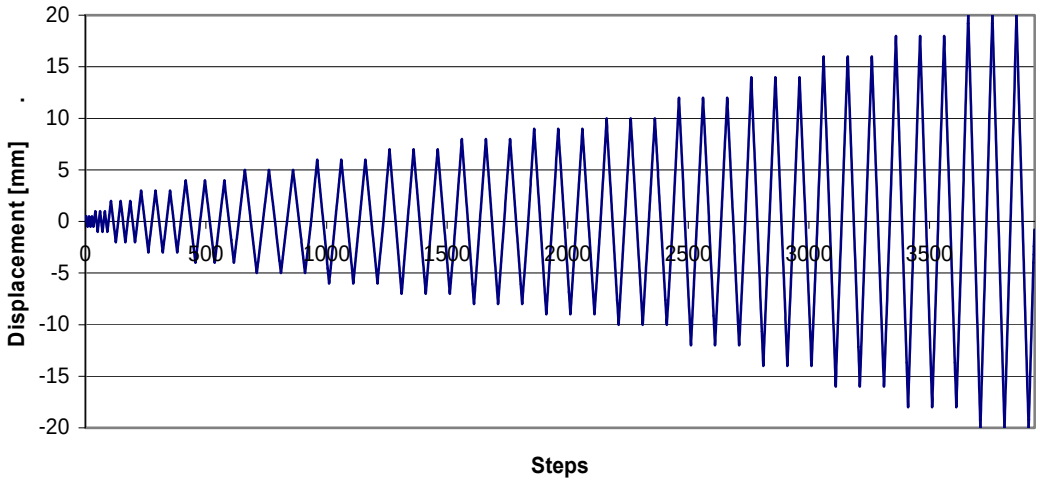

Figure 3.11 – Example loading protocol according to ISO CD 21581

4 Results experimental testing

A total of seven tests were performed, as shown in Table 4.1. Each test used a different kind of connection between the floor and the frame.

Table 4.1 – Overview of connections per test

Test nr.	Connection between	Fasteners	Size [mm]	Amount	Angle [°]
1	Timber-to-concrete	Screws	Ø5.3 – 75	10	90
2	Timber-to-concrete	Screws	Ø5.3 – 100	12	45
3	Timber-to-timber	Screws	Ø5.3 – 125	10	90
4	Timber-to-timber	Nails	Ø5.3 – 125	20	90
5	Timber-to-timber	Screws	Ø5.3 – 150	12	45
6	Timber-to-timber	Screws	Ø5.3 – 200	10	90
7	Diaphragm test	*			

** The last test was performed with 8 coach screws, Ø15 mm, and 6 steel angles to restrain the connection.*

4.1 Test 1 – Timber-to-concrete, screws, 90°

Description

The first test was performed with a connection between the timber and the concrete. Ten coach screws, Ø5.3 – 75 mm, installed at a 90° angle with the timber frame were used.

Prediction

Previous full-scale research [Smith, 2008] showed that the bearing capacity of the concrete was the governing failure mode. The capacity of one connector was estimated at 6.8 kN with formulas given by EC 5 [CEN, 2004b]. The total capacity of all ten screws would be 68 kN.

Test results

The hysteresis loops in Figure 4.2 show how the floor behaved under the cyclic loading. The yield force reached was 32 kN. From the larger displacement loops a residual force of 7 kN was a result of friction between the floor and the supports. The remaining 25 kN was resistance provided by the connectors.

After taking away some timber and concrete around one of the connectors, see Figure 4.1, the failure mode could be seen. It was not the expected failure of the concrete, but instead, double hinge yielding in the screw took place.
The capacity of this failure mechanism can be estimated using the formulas given in Eurocode 5 for steel-to-timber

Figure 4.1 – Double yielding in the fastener [Le Heux, 2008]

connections. The thick steel plate analogy is used to simulate the screw being held in the concrete. This failure mode occurs at 2.8 kN per screw, see Appendix A, if the rope effect is not taken into account. This is higher than the results found in the test, 10 * 2.8 > 25 kN.

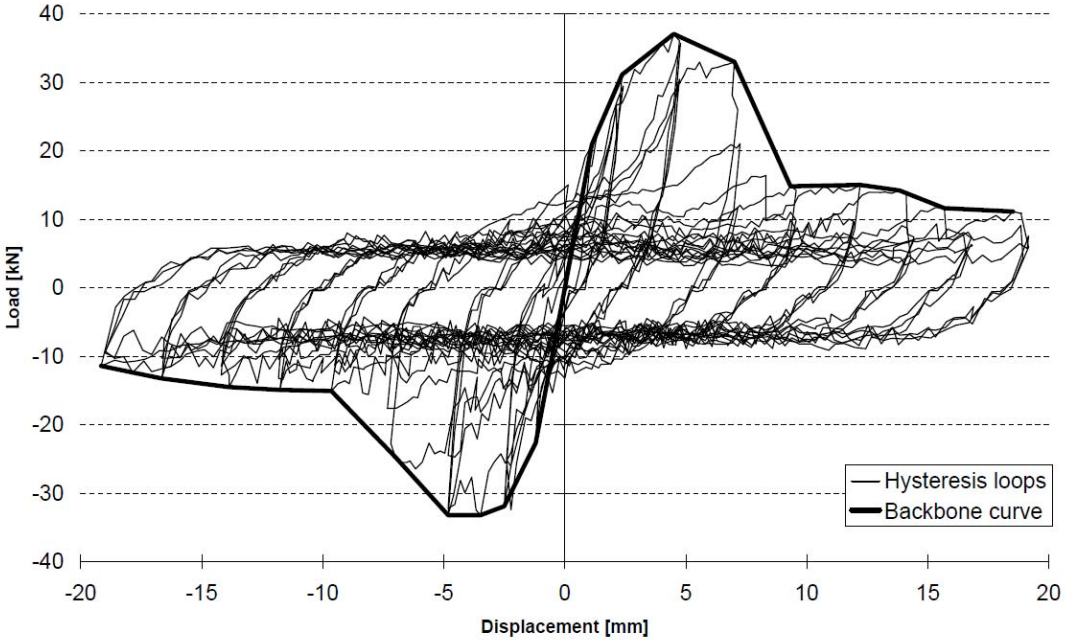

Figure 4.2 – Hysteresis loops Test 1

4.2 Test 2 – Timber-to-concrete, screws, 45°

Description

The second test was done to see how inclined screws would perform in the timber-to-concrete connection. A total of 12 coach screws, length of 100 mm, Ø5.3, were placed at a 45º angle with the timber framing, see Figure 4.3. This length of screws gave the same perpendicular depth in the timber as the screws used for Test 1.

Figure 4.3 – Timber-to-concrete connection with screws under a 45° angle

To speed up the testing sequence, a high strength grout (see Chapter 3.3.3) was used to fill the gap around the connectors that was necessary to remove the fasteners from the previous test.

Prediction

A paper by Kavaliauskas [2007] gives three formulas for possible failure modes in screws installed at an angle in the timber. These formulas are derived from Johansen's yield theory. The governing failure mode (III) is double yielding in the screw, as shown in Figure 4.4, at a load of 12.4 kN.

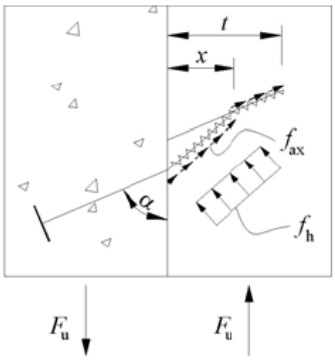

Figure 4.4 – Failure mode III [Kavaliauskas, 2007]

The problem however is that no information could be found about inclined screws when subjected to cyclic loading. All the available information was based on inclined screws in tension; while during cyclic loading compression also occurs. Therefore the assumption was made by us that only the screws under tension would contribute to the force transfer in the connections. This seemed reasonable since the stiffness of screws under tension is probably larger then under compression. But more research is needed in this area. The total capacity of the connectors is predicted to be 6 * 12.4 = 75 kN.

Test results

The failure mode was not in the screw and the timber but in the grout, as can be seen in Figure 4.5.

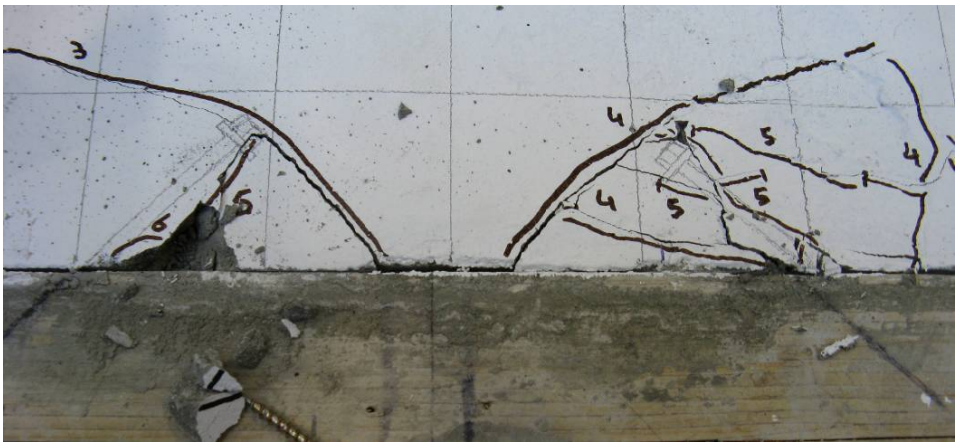

Figure 4.5 – Failure in the grout

During this test, not only rigid body movement but also rotation of the floor diaphragm took place. This can be concluded from Figure 4.6. The dashed line is the movement of the ram, in the middle of the floor. A large variation in movement between the connections on the north and south side can be seen. This difference was caused by the movement of the reaction frame, which resulted in a rotation of the floor.

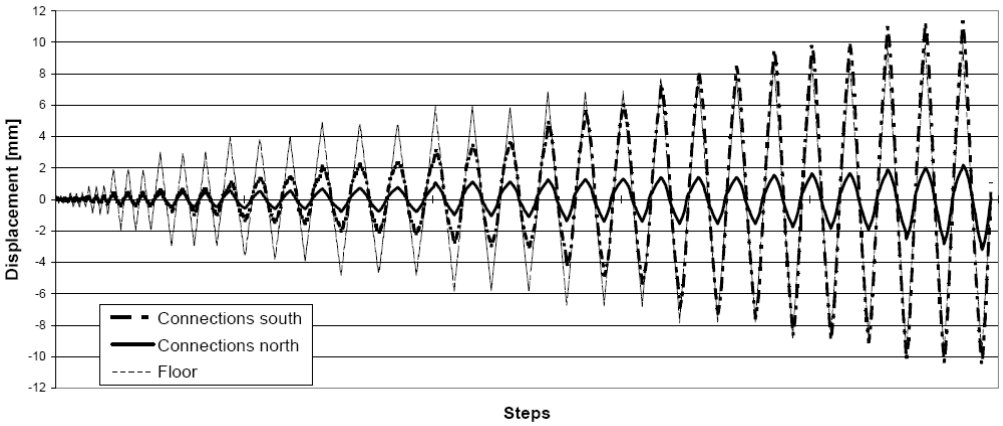

Figure 4.6 – Connection displacement for Test 2

Figure 4.7 shows the development of the hysteresis loops. Each graph shows three series of three displacement cycles. The first and second graphs show an elastic response from the connectors. The third and forth graph show a more ductile behaviour.

Besides the rotation, there was also some movement between the timber frame and the steel reaction frame and in the steel reaction frame itself. Therefore not the total displacement of the floor, but the average displacement over the connections was used for the hysteresis data. This is why the 10mm displacement cycles (the last cycles in Figure 4.6) did not result in a 10mm displacement, but only 7mm, as can be seen in the last graph of Figure 4.7.

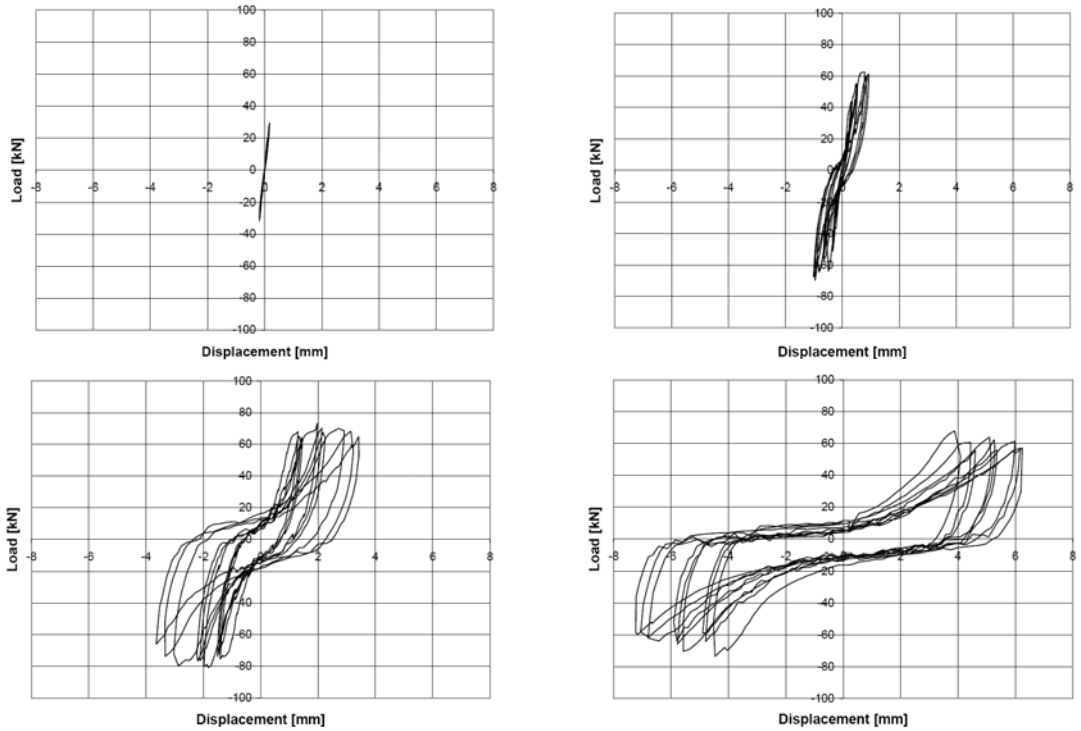

Figure 4.7 – Hysteresis loops Test 2, 4 graphs with each three series of three displacement cycles

Figure 4.8 shows all the hysteresis loops in one graph and the backbone curve. This curve is the envelope that shows the maximum force which is reached for each displacement. During the test the maximum force reached was 79 kN. From the previous test it was concluded that approximately 7 kN was friction. This resulted in a shear force of 72 kN for all connectors, or 12 kN per connector (in tension).

Calculations done after the fastener testing (see Appendix A) show that the screws would fail at 9 kN. But the failure in the grout indicated that this value was not reached. This shows that the screws in compression also were contributing to the load resisting behaviour of the system. The screws in compression should contribute at least for 50% of the capacity. So that each screw in tension resisted a force of 8 kN and the ones in compression 4 kN.

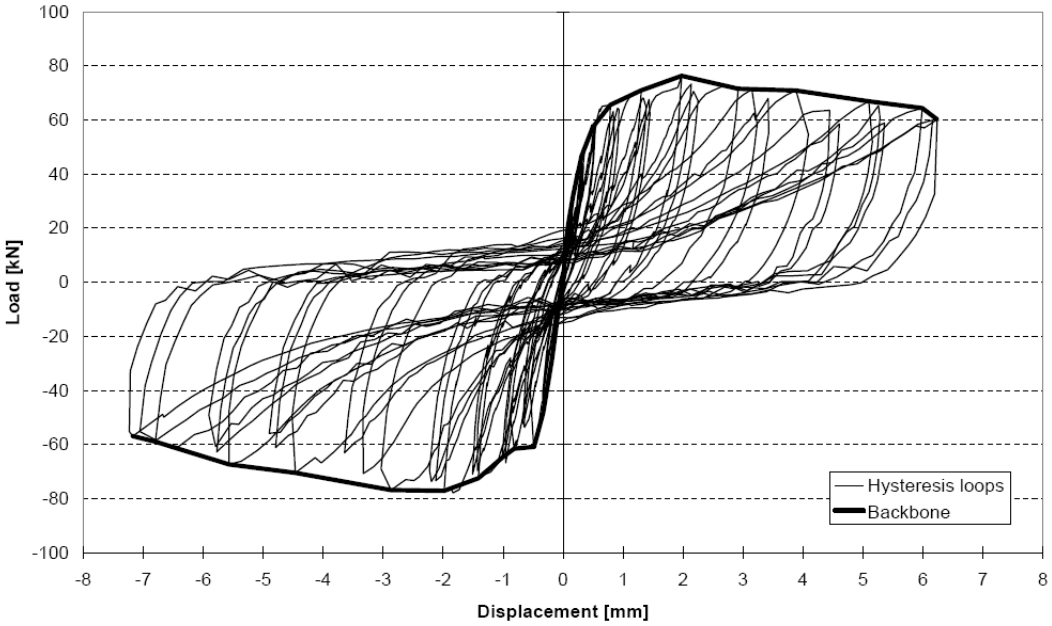

Figure 4.8 – Hysteresis loops Test 2

4.3 Test 3 – Timber-to-timber, screws, 90°

Description

After an earthquake it is difficult to repair a connection between the concrete layer and the timber floor. The concrete around the old connectors needs to be taken out; the connection needs to be replaced and new concrete or grout would need to be poured. This is not something which is desirable based on cost and building occupancy requirements. An alternative is a connection between the outer joist and the timber frame. These connections are easy to fabricate and easy to repair.

For this test ten 125 mm long Ø5.3 mm screws were used, placed as shown on Figure 4.9. Half of this length was threaded, so the threaded portion was at the interface between the frame and the joist. The screws were self-drilling.

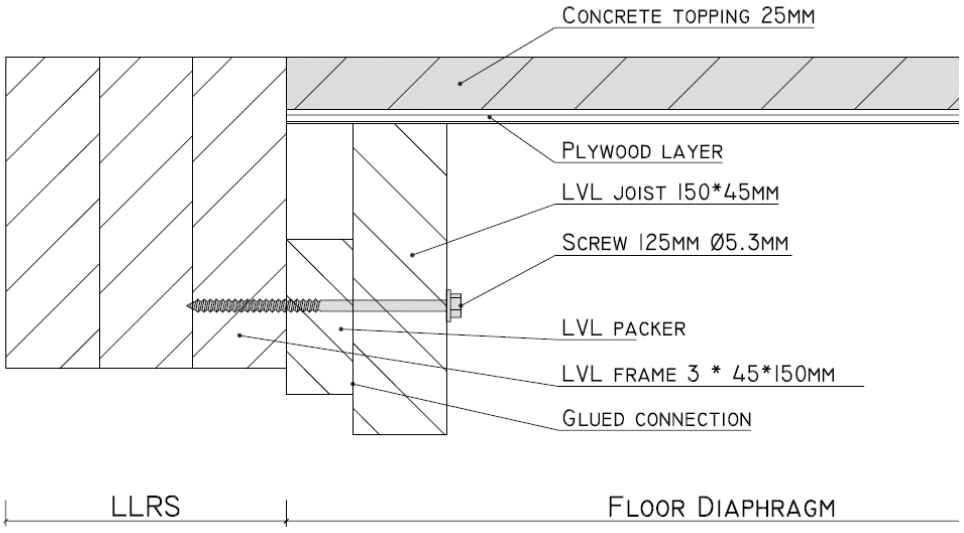

Figure 4.9 – Connection Test 3

Prediction

This connection was a fairly straight forward timber-to-timber connection, of which the capacity can be calculated utilizing formulas from Eurocode 5 [CEN, 2004b]. There are 6 different failure modes possible, see Figure 4.10.

The calculated capacities are as follows:

a. 12.2 kN
b. 7.6 kN
c. 19.7 kN
d. 6.9 kN
e. 6.8 kN
f. 3.9 kN

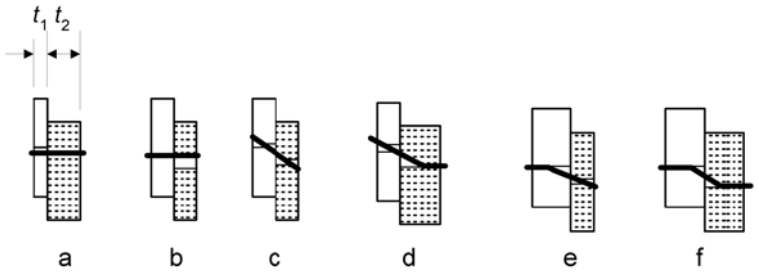

Figure 4.10 – Six failure modes according to EC5 [CEN, 2004b]

The rope effect was taken fully into account in these predictions. The expected failure mode was f; double yielding in the screw and bearing failure in the timber. So the total capacity of the 10 connectors was predicted at 39 kN.

Test results

Figure 4.11 –Failure of the fastener

Figure 4.11 shows the remainder of the fastener. It was broken at two places, about 26 mm apart. So the prediction of the failure mode was correct. The maximum force reached during the test was 45 kN at a displacement of 6 mm, as can be seen on Figure 4.12. Again, approximately 7 kN was assumed for the friction, so the connectors resisted 38 kN. After the fastener testing the six failure modes were calculated again (see Appendix A). Without the rope effect the screws would fail at 2.9 kN, with the full rope effect the capacity would be 5.3 kN. From this it can be concluded that only a part of the rope effect can be taken into account for screws under cyclic loading.

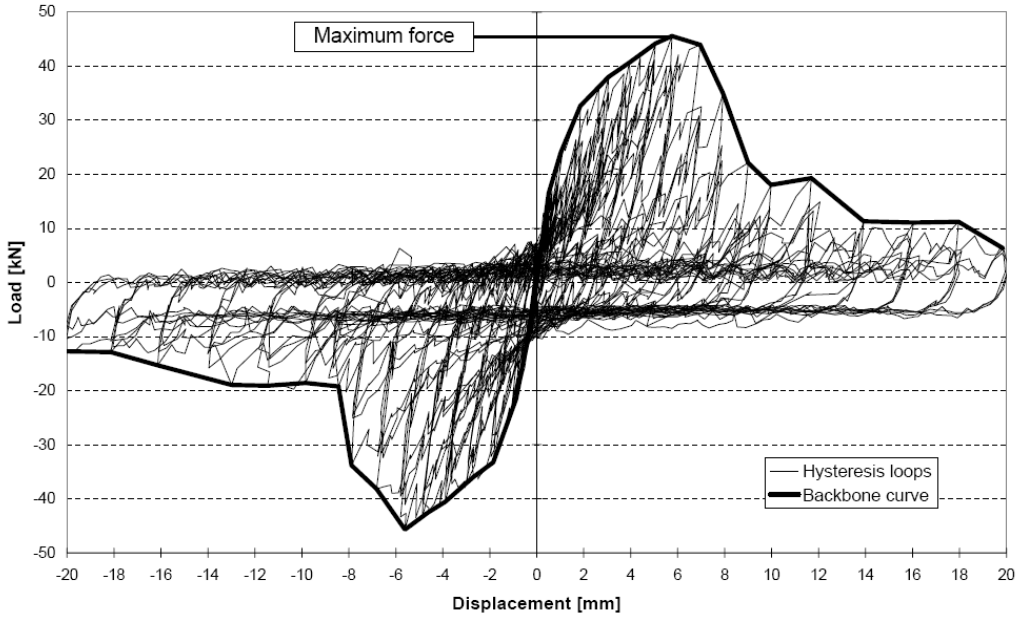

Figure 4.12 – Hysteresis loops Test 3

4.4 Test 4 – Timber-to-timber, nails, 90°

Description

Nails were tested as an alternative to screws. Only nails installed at a 90° angle were tested, since the withdrawal capacity of nails is lower then that of screws. Therefore, Eurocode 5 limits the rope effect to 15% of the Johansen part for round nails, compared to 100% for screws.

For this test 20 nails have been used. The nails had a 5.3 mm diameter and a length of 125 mm. The first 20 mm were predrilled to get a start for hammering in the nails.

Prediction

The same formulas as for Test 3 were used to calculate the capacity of the nails, except that the rope effect was limited to 15% of the connector capacity. The failure mode was still mode f; double yielding and bearing failure. The capacity of one nail was 2.25 kN, so in total a maximum force of 45 kN was expected.

Test results

The results of this test are shown in Figure 4.13. The maximum force resisted was 78 kN and was reached at a displacement of 14 mm. This hysteretic response shows that nails created a very ductile connection.

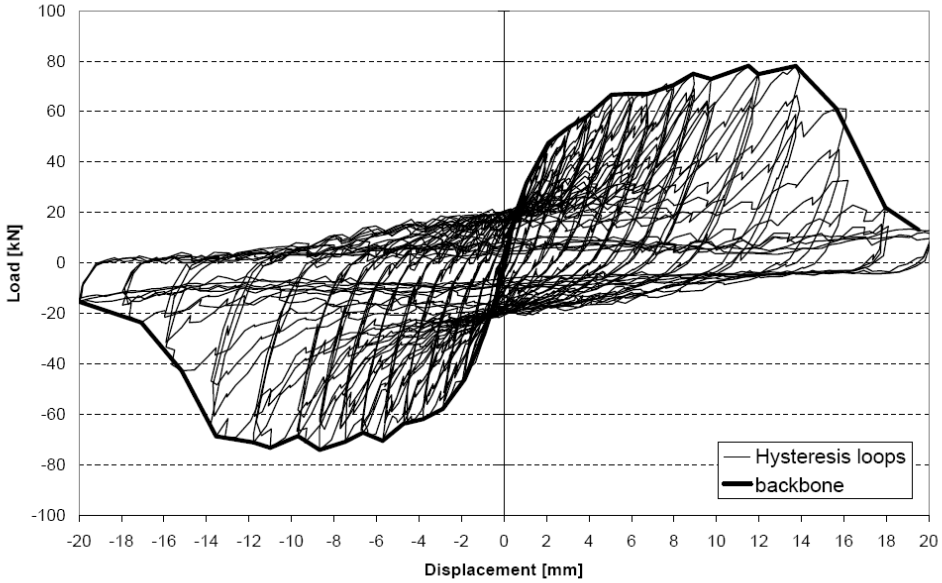

Figure 4.13 – Hysteresis loops Test 4

The maximum force was much higher then expected, which is probably caused by limiting the rope effect in the prediction. Table 4.2 shows the various capacities of the connection with different contributions of the rope effect. See Appendix A for the calculations. The connectors resisted a force of approximately 71 kN (78 kN minus 7 kN of friction). Similar to test 3, it can be seen that only a part of the rope effect can be taken into account. The 15% limit set by EC5 seems to be very conservative.

Table 4.2 – Influence of the rope effect on the capacity

% rope effect	Capacity per connector [kN]	Capacity all connectors [kN]
0	2.5	50
15	2.9	58
100	4.0	80

4.5 Test 5 – Timber-to-timber, screws, 45°

Description

A test of timber-to-timber connections with screws under a 45° angle is performed in order to get a good comparison between screws under a 45° and a 90° angle. Twelve screws with a length of 150 mm were used for this test.

Prediction

In a paper by Bejtka [2002] an adaptation of the Johansen's yield theory for inclined screws is given. Three different failure modes are possible. The adapted form of double yielding is the governing failure mode and results in an estimated strength of 8.1 kN per screw in tension.

The behaviour of inclined screws under cyclic loading is still not well known, as already mentioned in Chapter 4.2.2. Therefore the assumption was made again that the screws in compression did not contribute to the strength of the connection. The maximum force was predicted at 49 kN (6 times 8.1 kN).

Test results

Figure 4.14 shows the result of Test 5. The maximum force achieved was 61 kN, at a displacement of only 2 mm. Again, some rotation of the floor diaphragm was noticed during the test, but less than during Test 2.

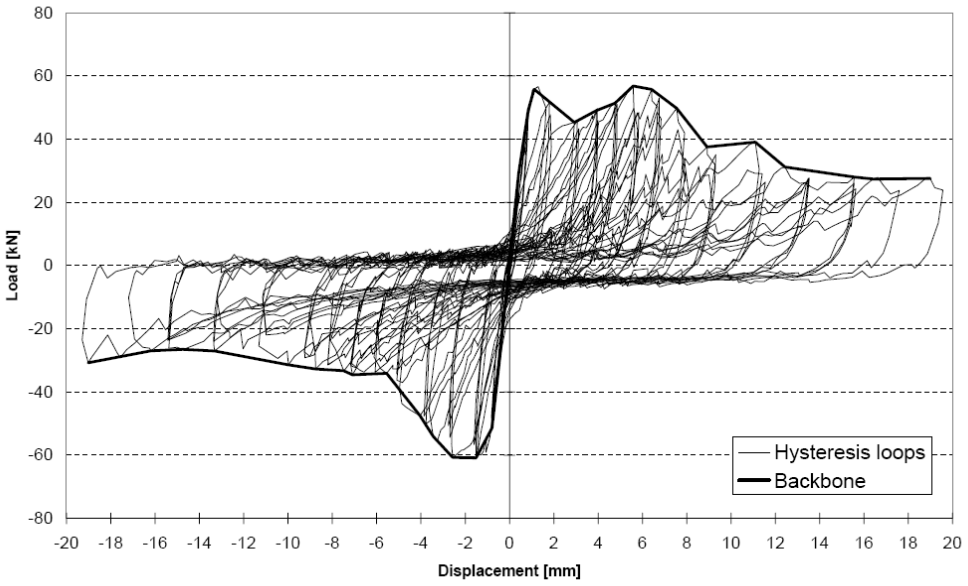

Figure 4.14 – Hysteresis loops Test 5

After the test the screws were removed and, surprisingly, three of them (all in tension under positive displacement) had not broken. The screws had yielded, but the ultimate strength had not been reached. The failure was in the timber, as can be seen in Figure 4.15. This explains why the loops of the hysteresis graph are not symmetrical (between 4 and 12 mm) and why the last loops maintained a high resistance.

Figure 4.15 – Failure in the timber frame and the screw still fixed to the joist

The calculations in Appendix A show that failure mode 2b (single yielding in the fastener and failure in the timber) and failure mode 3 (double yielding of the fastener) occur both at approximately 7 kN. This explains why two different failure mechanisms are seen. According to the assumption that only the screws in tension take up the force, the capacity would be 42 kN (6 times 7 kN). Figure 4.14 shows that a strength of 61 kN is reached, of which 7 kN is friction, so the connectors take up 55 kN. The difference of 13 kN is the contribution of the screws in compression. That would mean that they take up approximately 25% of the total force.

After the screws were taken out, the 20 mm cycles were repeated. This was done to see how much friction there was in the system. The black line in Figure 4.16 shows the average result of this test. The increase of friction towards the end may be explained by the remainders of connectors from the previous tests. It was not possible to take the old connectors completely out since they were broken. This probably resulted in some resistance at larger displacements.

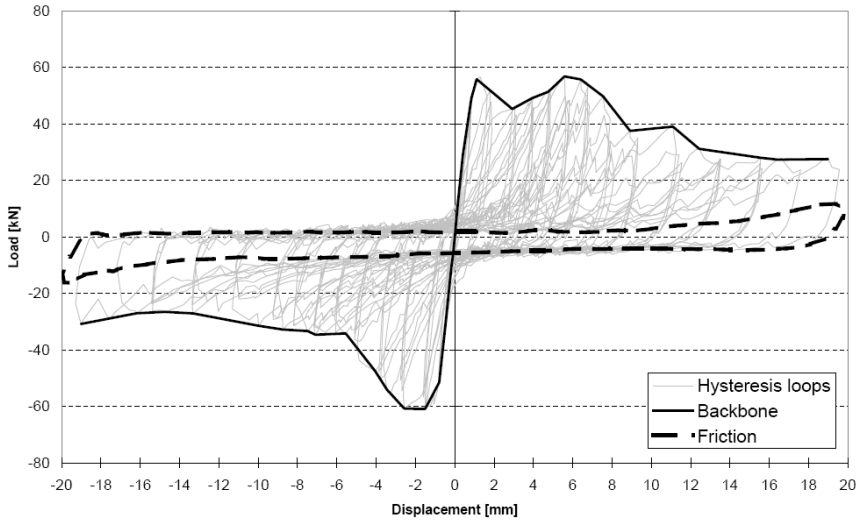

Figure 4.16 – Hysteresis loops and friction loop Test 5

4.6 Test 6 – Timber-to-timber, long screws, 90°

Description

During Test 3 (timber-to-timber, screws, 90°) the screws broke in the threaded part. Test 6 was conducted to see if it made any difference if the yielding (and finally breaking) of the screws took place in the shank. This could give a more ductile connection, like with the nails. This time screws with a length of 200 mm, Ø5.3 mm and a threaded length of only 75 mm were used. These screws were self-drilling.

Prediction

The prediction was the same as for Test 3, so 39 kN.

Test results

Figure 4.17 shows the hysteresis loops of this test. The maximum force resisted was 35 kN at 4 mm displacement. The friction found after the previous test is also plotted in Figure 4.18. This explains why it seems that the strength is increasing towards the end (backbone is going up). But the difference between the maximum applied load (backbone) and the friction is actually decreasing. Figure 4.17 does not show the expected ductile behaviour. This is due to the high steel grade of the fasteners, which made them brittle, as is seen during the fastener testing.

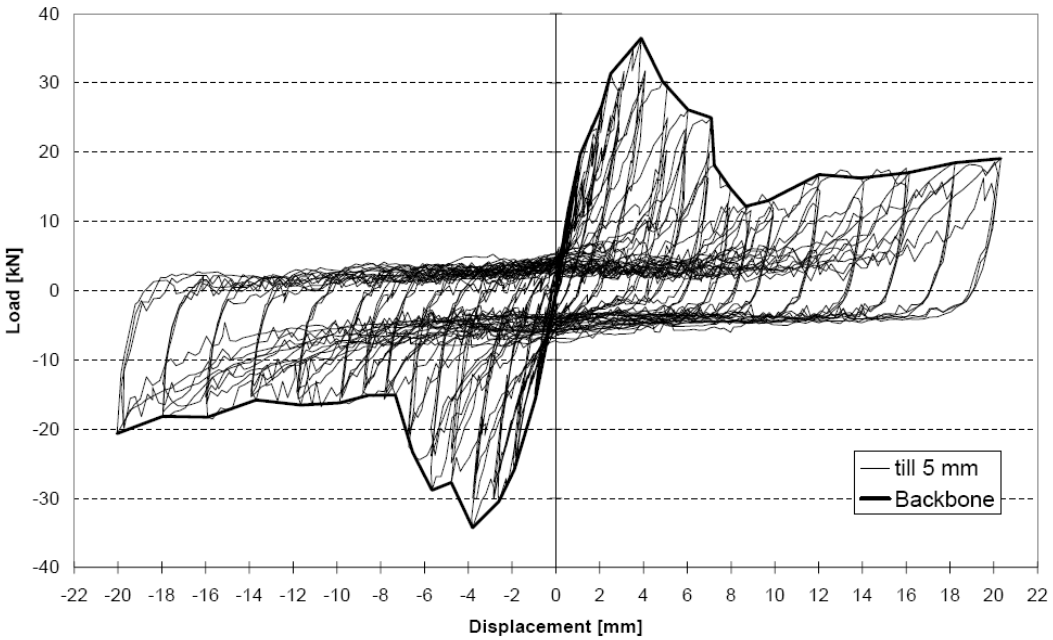

Figure 4.17 – Hysteresis loops Test 6

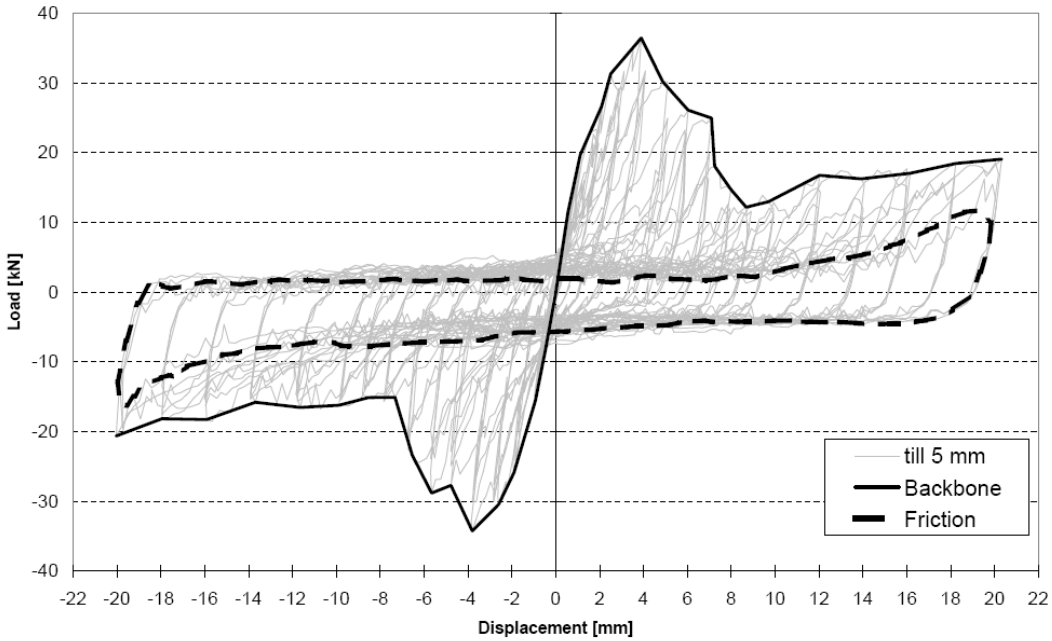

Figure 4.18 – Hysteresis loops and friction loop Test 6

4.7 Test 7 – Diaphragm stiffness

Description

The final cyclic diaphragm test was performed in order to get information about the stiffness of the diaphragm. Previous testing, focused on retrofitting of existing buildings [Brignola *et al.*, 2008a], had been done on different kinds of timber floors. A TCC floor was one of the alternatives as a retrofit technique, but no testing had been done for the type of floor under investigation here.

For this test the connections between the floor diaphragm and the LLRS had to be much stronger than during previous tests, to allow for a higher capacity of the hydraulic actuator to be reached. This was needed in order to get as much displacement as possible in the diaphragm and to determine the strength of the concrete diaphragm, instead of the strength of the connectors. Therefore eight Ø15 mm coach screws, placed between the outermost joist and the LLRS frame, and 6 steel angles, see Figure 4.19, were used to fix the floor to the frame.

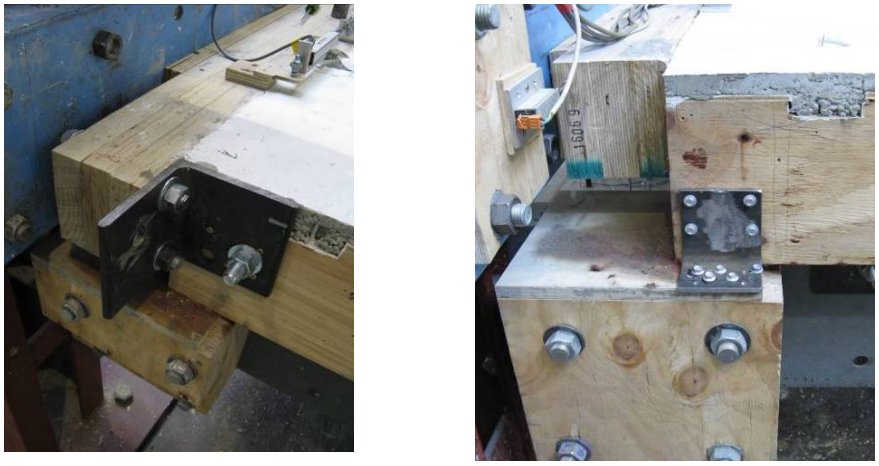

Figure 4.19 – Steel angles to fix the floor diaphragm

The deformation of the diaphragm was measured at 5 places, 500 mm center to center, spread out over the width of the floor, as shown in Figure 3.3. The displacement of the connectors was measured with 4 linear pots, two at each side. The displacement of the whole system was measured with the rotary pot at the middle of the floor.

Test results

There are three deformation components to be considered when looking at floor system diaphragm test data, the movement in the reaction frame, the movement in the connections and the movement of the diaphragm. Figure 4.20 shows the hysteresis data for the whole

system. Figure 4.21 shows the hysteresis data of only the connections, and Figure 4.22 shows the hysteresis data of the diaphragm.

Figure 4.23 shows the backbone curves of the displacement of all three components during the test. It can be seen that the displacement of the diaphragm was very small compared to the total displacement.

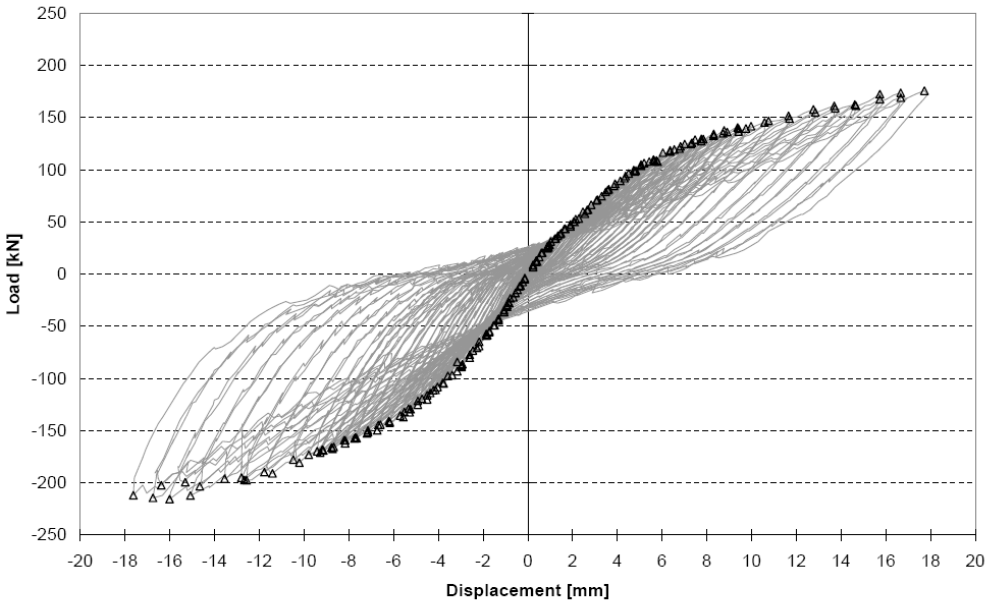

Figure 4.20 – Hysteresis loops of the whole system

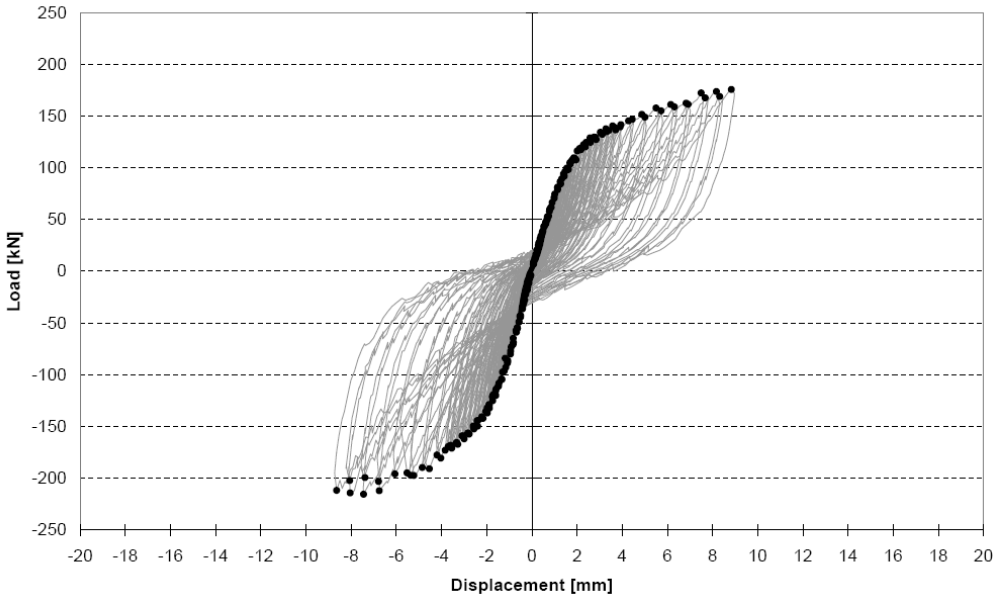

Figure 4.21– Hysteresis loops of the connection

Zooming in on the stiffness of the diaphragm as in Figure 4.22, it can be seen that the diaphragm did not have the same stiffness in both loading directions. This may have been caused by an accident during construction, which resulted in a large crack (and probably some micro-cracks) on the side of the positive movement.

During the 7 mm cycle a crack started to form in the middle of the floor, see Figure 4.26. From Figure 4.20 it can be seen that this was under a load of approximately 120 kN on the positive side and 150 kN on the negative side. Figure 4.22 shows a distinct change in the stiffness of the diaphragm at exactly these force levels. So, due to the cracking, the stiffness of the floor slab decreased significantly.

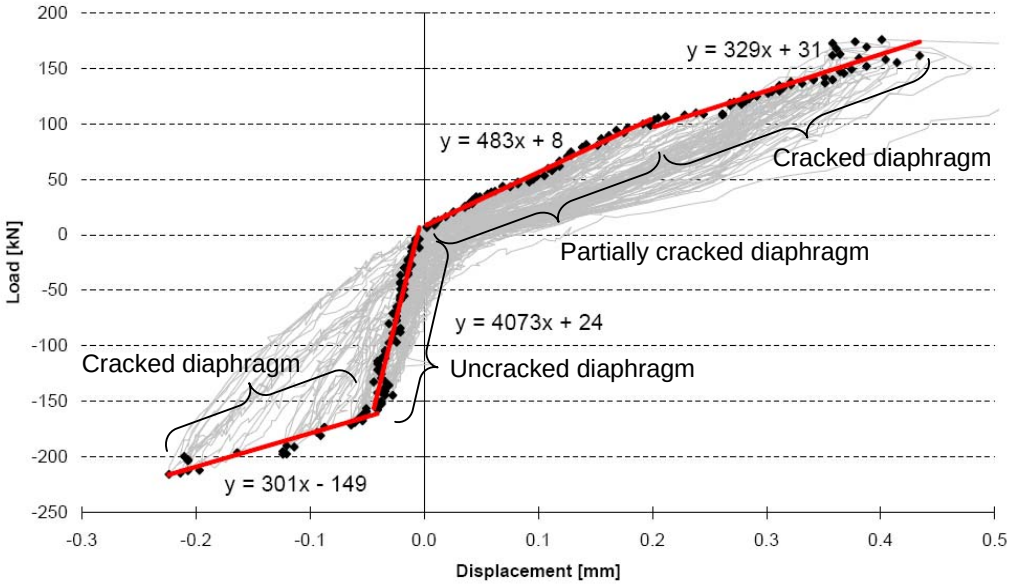

Figure 4.22 – Hysteresis loops and stiffness of the diaphragm

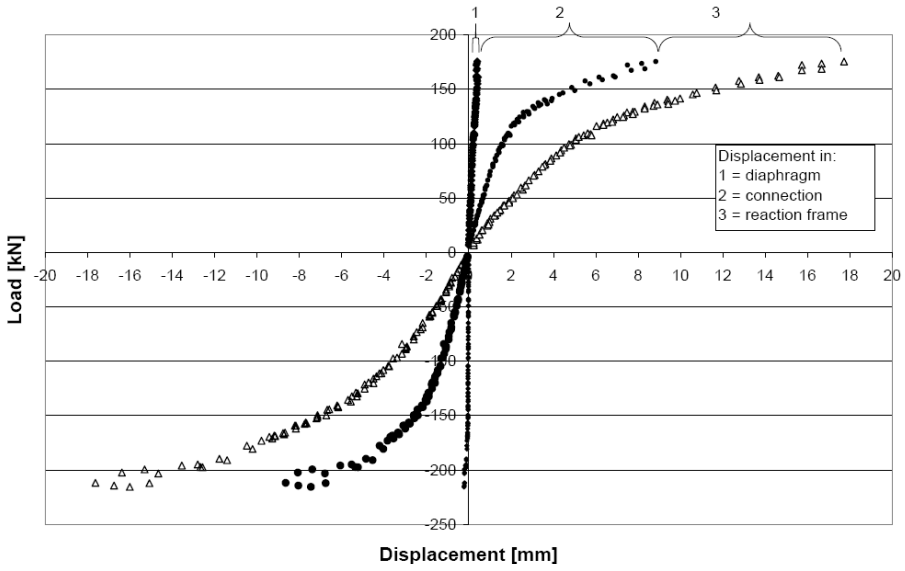

Figure 4.23 – Stiffness comparison of the diaphragm, the connection and the reaction frame

The displacement at 5 locations on the diaphragm, at the peak displacement of some cycles, is shown in Figure 4.24. From these lines it can be seen that the diaphragm showed some bending and shear deformation, although the magnitude was fairly small.

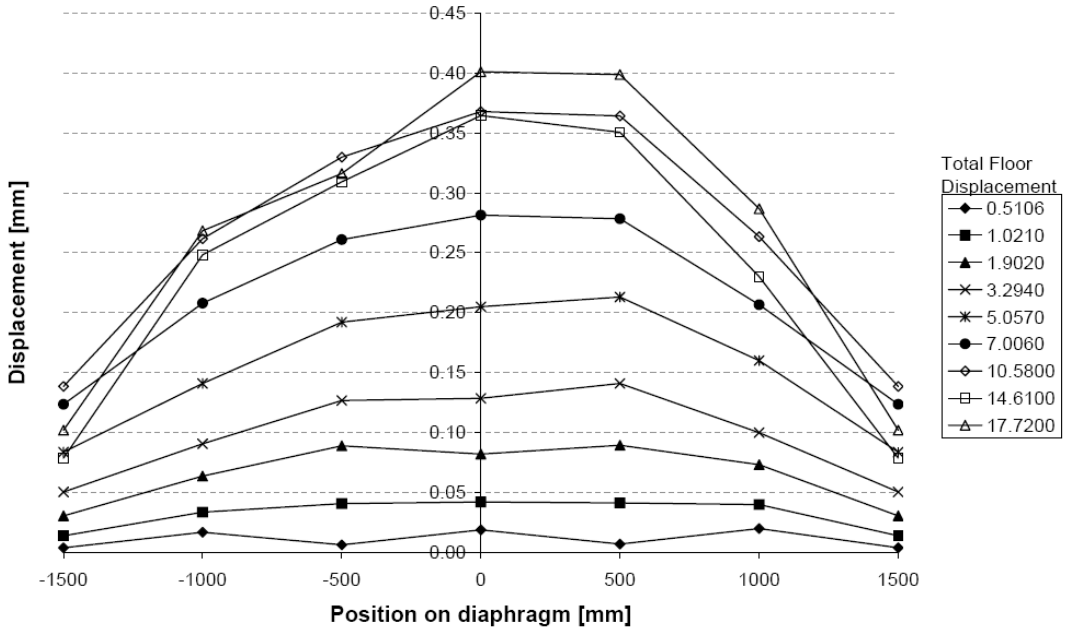

Figure 4.24 – Displacement of the diaphragm

During the test the concrete started to crack in the corners where it was fixed by the steel angles. A crack width of over 2 mm was recorded during the test, see Figure 4.25.

The complete cracking pattern can be seen in Figure 4.26. In the corners a lot of cracks were formed due to the steel supports which resulted in tensile forces in the concrete. Also significant cracking could be seen around the top and bottom of the floor, which was from Test 2, due to the timber to concrete connections. A big flexural crack can be seen from left to right, which occurred during the final test at a displacement of 7mm.

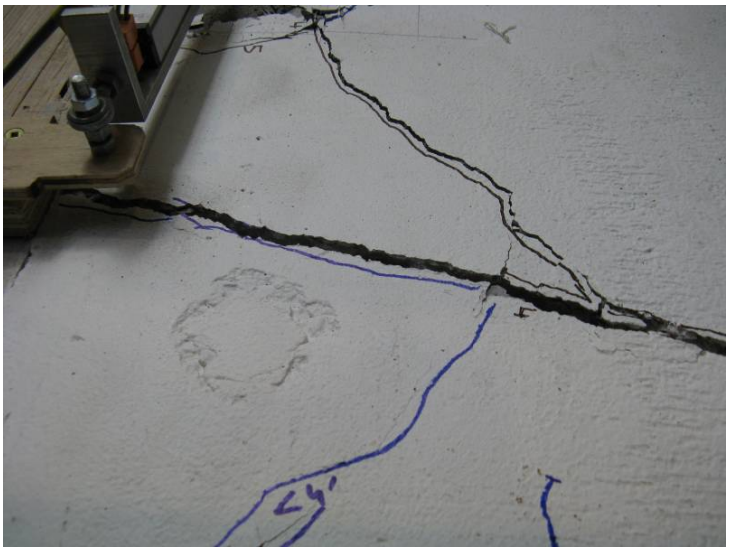

Figure 4.25 – Cracking of the concrete

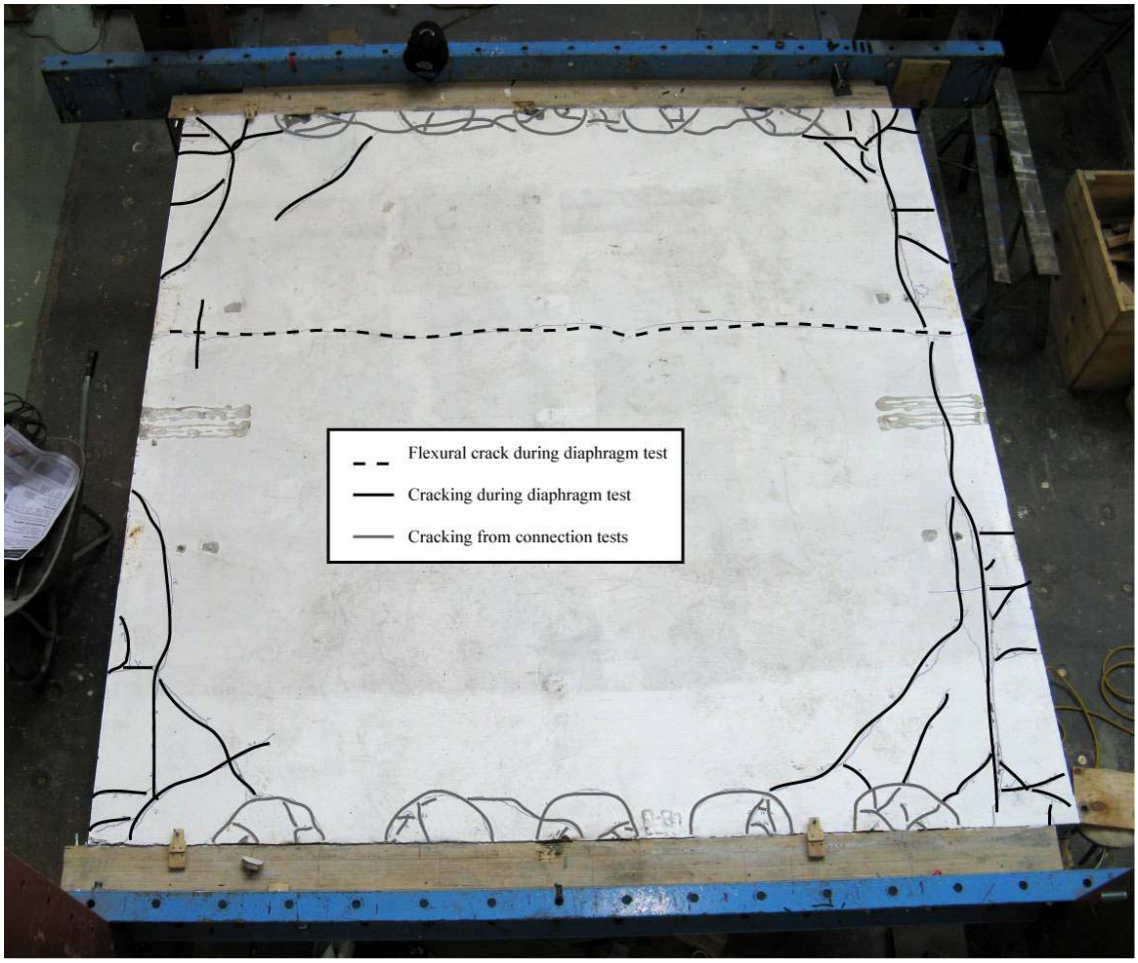

Figure 4.26 – Complete cracking pattern in the concrete

5 Discussion and conclusions of experimental results

This chapter discusses the results of the experimental testing and conclusions are drawn from the comparison between the tests. The strength and stiffness of the different connections are compared. Also the difference between screws and nails is discussed, as well as the effect of having the threaded part or the shank of a connector at the interface of the connection.

5.1 Connection strength

Figure 5.1 shows the backbone curves from the timber-to-concrete (1 & 2) and timber-to-timber (3 & 5) tests with the screws. For easy comparison, the curves have been modified to show the result of only 10 fasteners per test (instead of 20 for the nails and 12 for the 45° connections).

The maximum strength is also shown in Table 5.1. It can be seen that there is a significant difference between the two timber-to-concrete connections. The timber-to-concrete connectors placed at a 45° angle were nearly twice as strong as the connectors at a 90° angle. This is because the timber to concrete connection couldn't develop its full strength, which would include the rope effect, due to low cycle fatigue of the fastener. The timber-to-timber connections show very comparable results regarding the strength of the connection.

The maximum force was reached at a displacement of around 2 mm if the connectors were installed at a 45° angle, compared to 5 mm if the connectors were installed at a 90° angle.

Table 5.1 – Overview of maximum strength for timber-to-concrete and timber-to-timber connections

Test	Angle [degrees]	Maximum strength (positive) [kN]	Maximum strength (negative) [kN]
1 – Timber-to-concrete	90	37	-33
2 – Timber-to-concrete	45	64	-64
3 – Timber-to-timber	90	45	-45
5 – Timber-to-timber	45	46	-50

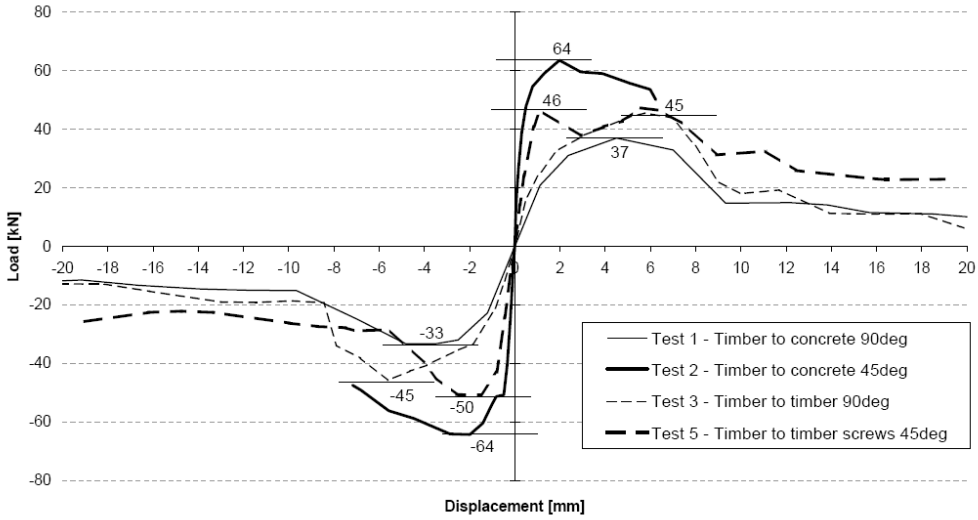

Figure 5.1 – Comparison between the maximum strength for the timber-to-concrete and timber-to-timber connections

5.2 Connection stiffness

Figure 5.2 shows the same backbone curves as Figure 5.1. It can clearly be seen that the initial stiffness of the connectors installed at a 45° angle, 80 kN/mm, was four times as stiff compared to the connectors place at a 90° angle, 20 kN/mm.

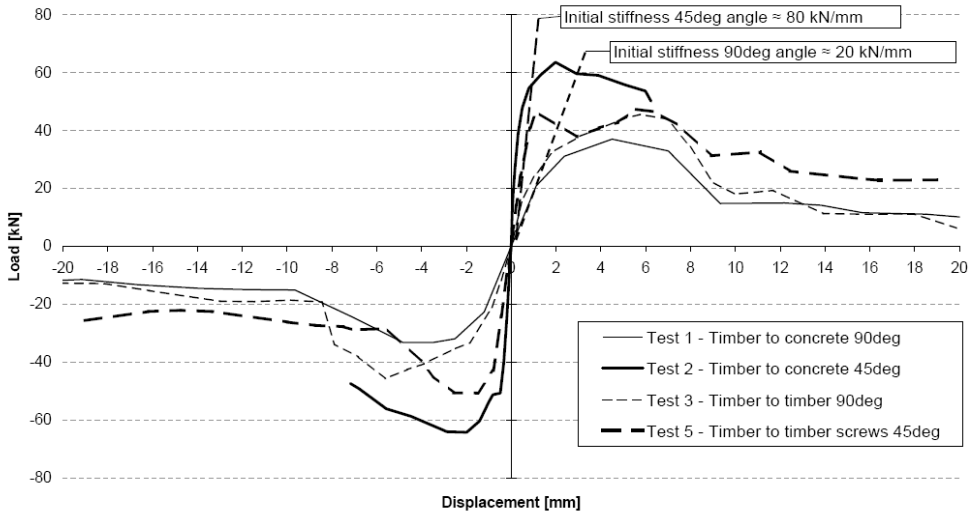

Figure 5.2 – Comparison between the stiffness for the timber-to-concrete and timber-to-timber connections

5.3 Comparison between screws and nails

Figure 5.3 shows the backbone curves for the tests with nails and screws installed at a 90° angle between the timber joist and the LLRS. The initial stiffness of both connectors is the same. The screws were a bit stronger than the nails, which was mainly caused by the difference in steel quality. The failure modes were the same, both showed double yielding. The displacement at which the connectors failed was quite different. The screws reached their maximum force at approximately 5 mm and the nails at approximately 14 mm of displacement. Clearly the nails exhibited much more ductile behaviour than the screws.

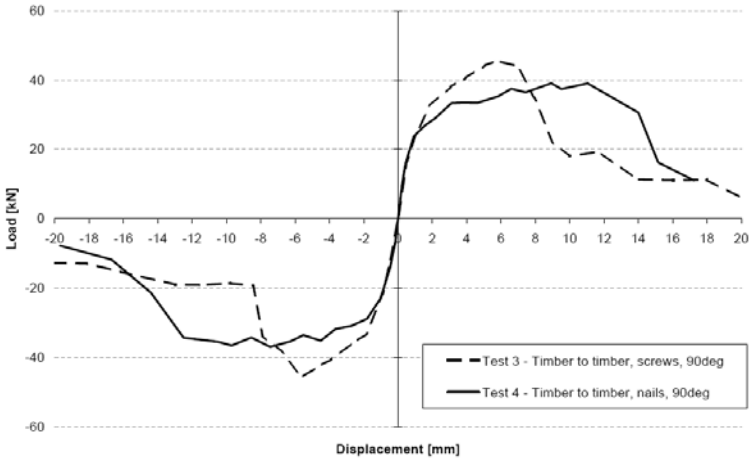

Figure 5.3 – Comparison between screws and nails as connectors

5.4 Comparison between thread and shank at connection interface

The threaded section of the screw can influence the ductility of the connections as is shown in the testing of the fasteners in Section 3.4. Test 6 has been performed with long screws so that the yielding would take place in the shank. But the long screws used were very brittle, as can be seen in Table 3.4. Therefore, unlike the nails, they broke at a lower displacement and did not exhibit the desired ductile behaviour as can be seen in see Figure 5.3.

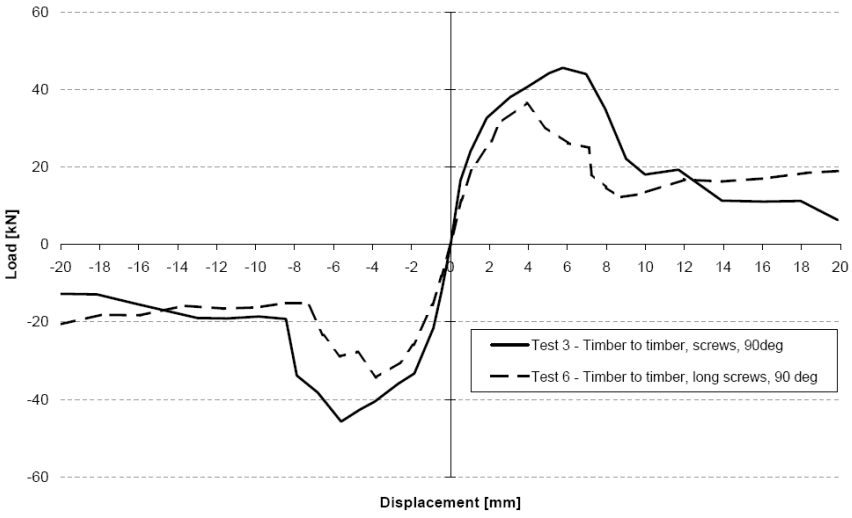

Figure 5.4 – Comparison between fasteners with the thread and shank at the interface of the connection

5.5 Diaphragm

The stiffness of the diaphragm is largely dependent on the cracking in the concrete. The uncracked diaphragm showed a stiffness of approximately 4000 kN/mm. The cracked diaphragm showed a stiffness of approximately 300 kN/mm. It has to be noted that the displacements of especially the uncracked diaphragm were within 0.04 mm. The experimental stiffness value might not be very accurate due to irregularities in the test specimen, unconsidered effects like friction and the accuracy of the instrumentation at that level of displacement.

The stiffness of a floor system consists of two parts, the stiffness of the floor slab and the stiffness of the connection between the floor slab and the LLRS. The range of stiffness of the connectors is from 20 to 80 kN/mm, as can be seen from Figure 5.2. Table 5.2 gives the influence of the diaphragm stiffness on the total stiffness of the floor. It is assumed that the stiffness of the connectors and the stiffness of the diaphragm can be modelled as serial springs, as is proposed by Brignola [2008a].

Table 5.2 – Influence of the diaphragm stiffness

	Most flexible option	**Most stiff option**
Diaphragm stiffness	500 kN/mm (cracked)	4000 kN/mm (uncracked)
Connector stiffness	20 kN/mm (90° angle)	80 kN/mm (45° angle)
Combined stiffness	$(\frac{1}{20}+\frac{1}{500})^{-1}=19.2kN/mm$	$(\frac{1}{80}+\frac{1}{4000})^{-1}=78.4kN/mm$
Influence of the diaphragm stiffness	$\frac{19.2-20}{20}\times 100\%=-3.8\%$	$\frac{78.4-80}{80}\times 100\%=-2.0\%$

The influence of the diaphragm stiffness is less than 4% in both options. So the in-plane floor stiffness of the floor used in this experiment can be modelled by only the connection stiffness. The diaphragm stiffness of the TCC floor used in this experiment can be neglected in the seismic design.

5.6 Summary

The experimental testing showed that the major structural difference between the different connections was the stiffness. The stiffness of the connections with screws installed at a 45° angle was approximately 80 kN/mm. This was four times stiffer than the screws installed at a 90° angle. No difference in initial stiffness between the nails and the screws was found, but the screws showed a much more ductile behaviour.

The timber-to-concrete connection with screws installed at a 45° angle was nearly twice as strong as the screws at a 90° angle. The reason for this is the different failure mechanism between the two tests. For the timber-to-timber connections the orientation did not seem to influence the strength of the connection, both times the connections could reach their ultimate strength. The displacement at maximum force was approximately 2 mm for the screws at a 45° angle, compared to 5 mm for the screws at a 90° angle and 14 mm for the nails.

The threaded part of the screws is influencing the ductility of the connectors. This is shown by the fastener testing. Making connections with the shank at the interface could result in a more ductile connection. But this could not be confirmed by the experimental testing.

The concrete-to-timber connections showed the highest ductility. This might be good for the design but the connection also showed extensive damage to the concrete. After an earthquake this would result in costly repairs. The timber-to-timber connection achieved a slightly lower ductility level but would be much easier to repair.

The rope effect which is used for the design of screwed connectors in EC5 can not be taken fully into account for screwed connections at a 90° angle under seismic (cyclic) loading. More research is needed in order to determine which part of the rope effect can be taken into account.

There is not enough information available for the design of inclined screws under seismic loading. Only information on inclined screws under tension is available. A conservative design approach would be to neglect the strength of the screws in compression.

The stiffness of the uncracked TCC floor diaphragm which was tested was approximately 4000 kN/mm. In a cracked state this reduces to approximately 300 kN/mm. For the floor used in this experimental test it can be concluded that the flexibility of the diaphragm can be neglected in comparison with the flexibility in the connectors.

6 Numerical analysis of a floor unit

This chapter describes the first part of the numerical analysis, which has been performed to determine the effect of the floor flexibility on the seismic behaviour of multi-story timber buildings. The numerical model is described and the important parameters for the design are identified. Five designs with different slenderness ratios of the floor have been made. The design parameters for each design are calculated, and are used for a numerical time-history analysis with Ruaumoko [Carr, 2008]. The results from these analyses are discussed in the end of this chapter.

6.1 Introduction

The goal of this part of the numerical analysis is to describe the components that influence the floor flexibility and to determine how the floor flexibility can be modelled. Therefore the LLRS is assumed rigid and only the stiffness of the diaphragm and the connectors is considered. In later stages (Chapter 7 and 8) of the analysis the influence of the floor flexibility on the global response of a structure will be looked at.

The floor flexibility consists of three different parts, the deformation of the connectors, the shear deformation in the diaphragm and the flexural deformation in the diaphragm, as shown in Figure 6.1. In the experimental part it was already determined that, for the geometry considered, the flexibility of the diaphragm could be neglected.

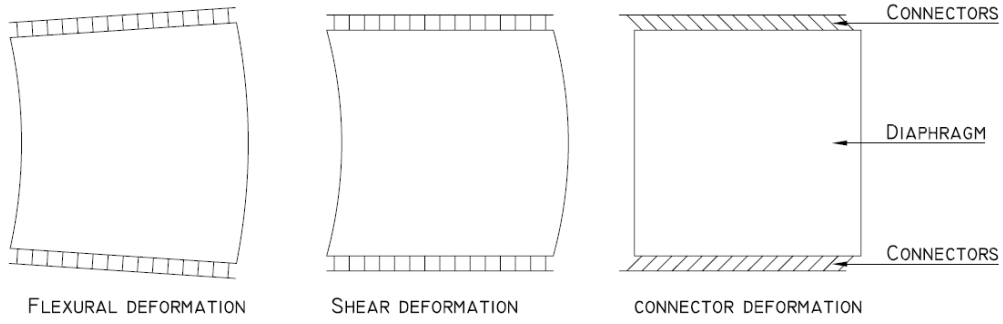

Figure 6.1 – Three floor deformation components

6.2 Numerical Model

Three different models have been made. The first model is a multi degree-of-freedom (MDOF) model, which represents a real floor system as closely as possible. The mass of the floor needs to be distributed to a number of points, since a distributed mass would result in infinite degrees of freedom in the model. Therefore the floor is represented as 8 beam elements, which is enough to get an accurate result [Spooner, 2008]. The connectors are

represented as springs with a linear stiffness. This is valid as long as the forces imposed on the connectors are not larger than the elastic limit.

The second model is a single degree-of-freedom model, named 'SDOF-1' hereafter, which only takes the stiffness of the connectors into account. This model is made to determine if the influence of the diaphragm can be neglected completely. The third model, named 'SDOF-2' hereafter, is made to include the diaphragm stiffness by representing it as a spring. The stiffness of this spring will consist of the shear and flexural stiffness of the diaphragm. This stiffness will be combined with the connector stiffness according to Eq. 6.1. This model does include the diaphragm stiffness, but not the possibility of the development of higher modes of response. Other researchers [Fleischman *et al.*, 2001a] shown that these higher modes of response can significantly influence the forces generated in the structure.

$$k_{eff} = \frac{1}{\frac{1}{k_{conn}} + \frac{1}{k_{diaphragm}}} \qquad \textit{Eq 6.1}$$

All the three models are shown in Figure 6.2. The nodes which represent the mass of the floor have thick lines. Movement is allowed in the x-direction but restricted in the y-direction. Rotation is only allowed for the nodes 2 to 10 in the MDOF model.

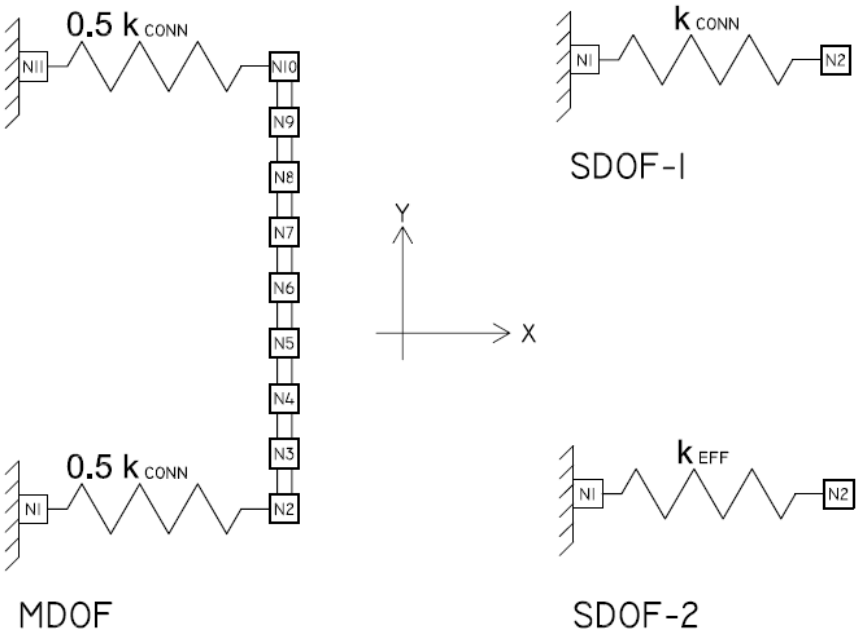

Figure 6.2 – Three numerical models

6.3 Design Parameters

Two important parameters in the design are the depth and the length (the span) of the floor. These parameters determine the total area and thus the mass of the floor. This mass generates inertial forces when subjected to accelerations during an earthquake. These forces have to be transferred from the diaphragm into the LLRS. So the design of the connectors depends on the mass, and thus the floor depth and floor span.

The ratio of the floor span (L) over the floor depth (D) is the aspect ratio (λ) of the floor. Five designs have been considered with different aspect ratios, as shown in Figure 6.3. The cross-section, the shear area and the second moment of inertia are calculated according to Eq. 6.2(a)-(c) and are shown in Table 6.1.

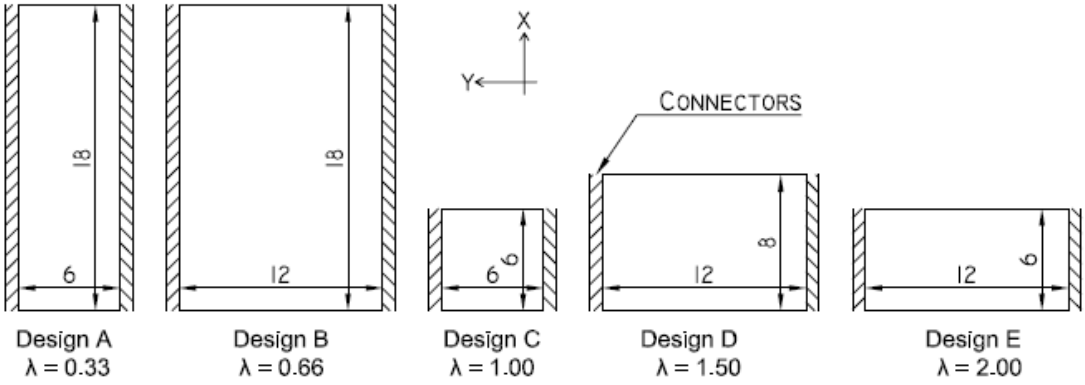

Figure 6.3 – Five designs with different aspect ratios

Table 6.1 – Overview section properties

Design	A [m^2]	A_s [m^2]	I [m^4]
A	1.26	1.05	34.02
B	1.26	1.05	34.02
C	0.42	0.35	1.26
D	0.56	0.47	2.99
E	0.42	0.35	1.26

$$A = t \times D \qquad \textit{Eq. 6.2(a)}$$

$$A_s = \frac{5}{6} \times t \times D \qquad \textit{Eq. 6.2(b)}$$

$$I = \frac{1}{12} \times t \times D^3 \qquad \textit{Eq. 6.2(c)}$$

Besides the two parameters mentioned above, there are also some parameters which stayed constant during the analysis. These are shown in Table 6.2. Also shown is a reference to a chapter where the parameter is discussed.

Table 6.2 – Fixed design parameters

Parameter	Symbol	Magnitude	Chapter
Thickness floor slab	t	70 mm	
Modulus of elasticity of concrete	E	28.000 kN/mm	6.4
Shear modulus of concrete	G	11.000 kN/mm	6.4
Factor for cracked EI	n	0.2	6.4
Floor mass	W	3.3 kN/m^2	6.5
Design Peak Ground Acceleration	PGA	0.70 g	6.6
Floor Acceleration Magnification	FAM	1 or 3	6.6
Connector yield strength	f_y	1000 N/mm^2	6.6
Connector diameter	d	10 mm	6.6 & 6.7

An overview of the design process which leads to the diaphragm stiffness can be seen in Figure 6.4. This figure also shows references to a chapter where the step of the design procedure is discussed. Figure 6.5 shows the design process for the calculation of the period of the connectors. This parameter will be used as the major variable in the presentation of the results.

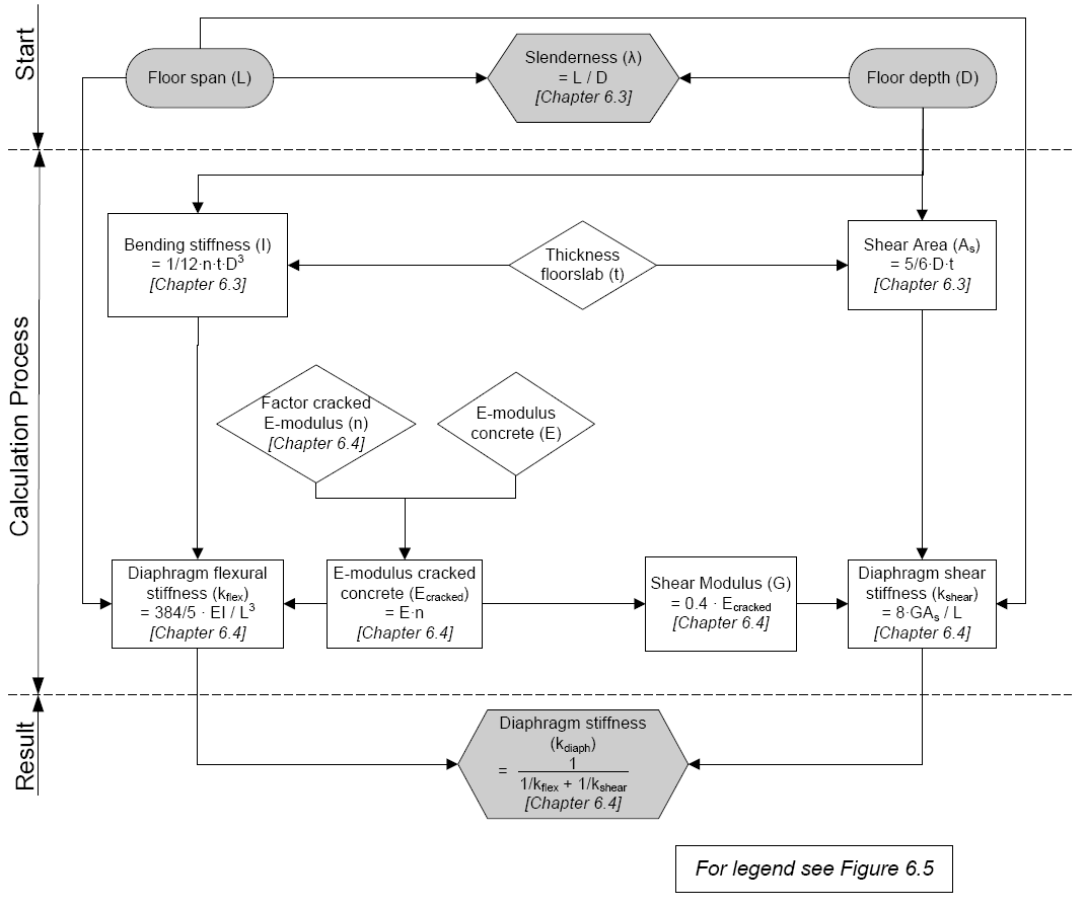

Figure 6.4 – Schematics of the calculations of the diaphragm stiffness

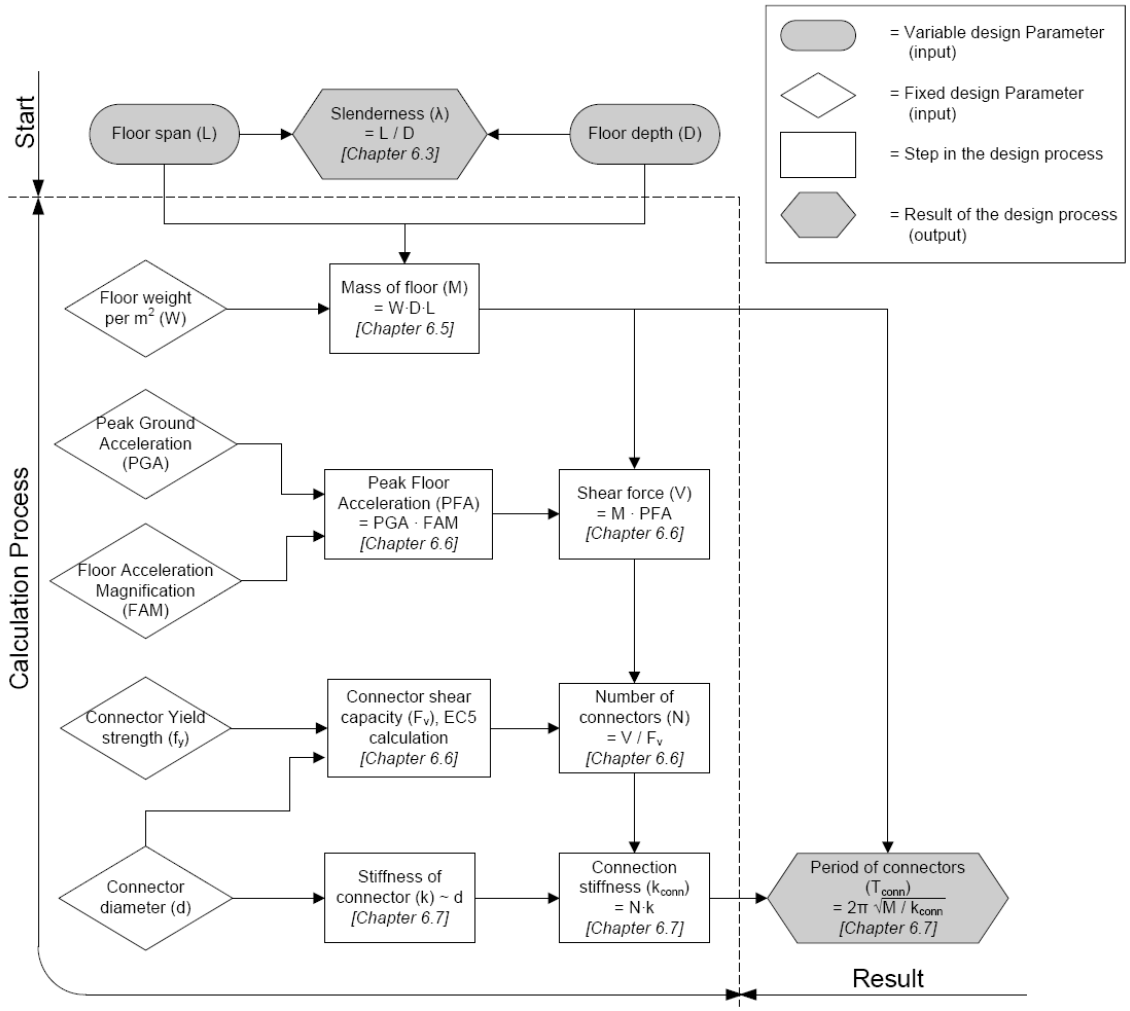

Figure 6.5 – Schematics of the calculations of the period of the connection

6.4 Stiffness of the diaphragm

The stiffness of the diaphragm needs to be known for the SDOF-2 model. The diaphragm stiffness consists of two parts, the flexural and the shear stiffness. The experimental results from the diaphragm test will be used to determine these two stiffness values.

The tested diaphragm will be idealized as a beam which is clamped at both ends, because the test rig prevented the ends from rotating. This idealization is shown in Figure 6.6.

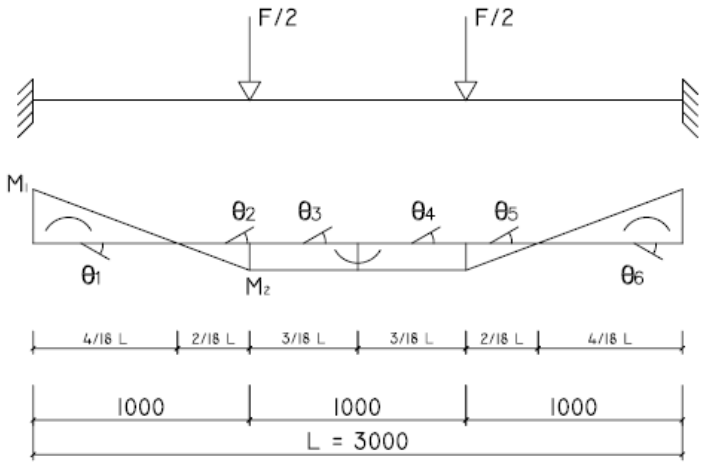

$$M_1 = \frac{2}{18} Fl$$

$$M_2 = \frac{1}{18} Fl$$

Figure 6.6 – Beam model of the diaphragm for determining the flexural stiffness

The flexural stiffness of the diaphragm will follow from the deflection in the middle of the span. The values of θ can be expressed as the area underneath the M/EI line, as shown in Eq 6.3(a)–(c).

$$\theta_1 = \theta_6 = \frac{M_1 \times \frac{1}{2} \times \frac{4}{18} l}{EI} = \frac{1}{81} \times \frac{Fl^2}{EI} \qquad \textit{Eq. 6.3(a)}$$

$$\theta_2 = \theta_5 = \frac{M_2 \times \frac{1}{2} \times \frac{2}{18} l}{EI} = \frac{1}{324} \times \frac{Fl^2}{EI} \qquad \textit{Eq. 6.3(b)}$$

$$\theta_3 = \theta_4 = \frac{M_2 \times \frac{3}{18} l}{EI} = \frac{1}{108} \times \frac{Fl^2}{EI} \qquad \textit{Eq. 6.3(c)}$$

The flexural deformation in the middle of the span can be described by Eq. 6.4.

$$\delta_m = \theta_1 \times \frac{23}{54} l - \theta_2 \times \frac{11}{54} l - \theta_3 \times \frac{1}{12} l \qquad \textit{Eq. 6.4}$$

Eq. 6.4 together with Eq. 6.3 forms Eq. 6.5

$$\delta_m = \frac{1}{81}\times\frac{23}{54}\frac{Fl^3}{EI} - \frac{1}{324}\times\frac{11}{54}\frac{Fl^3}{EI} - \frac{1}{108}\times\frac{1}{12}\frac{Fl^3}{EI} = \frac{5}{1296}\times\frac{Fl^3}{EI} \qquad \textit{Eq. 6.5}$$

Figure 6.7 compares the result of Eq. 6.5 with two other loading cases. The deflection under the two point loads is less than the deflection under one point load, but more than the deflection under a distributed load.

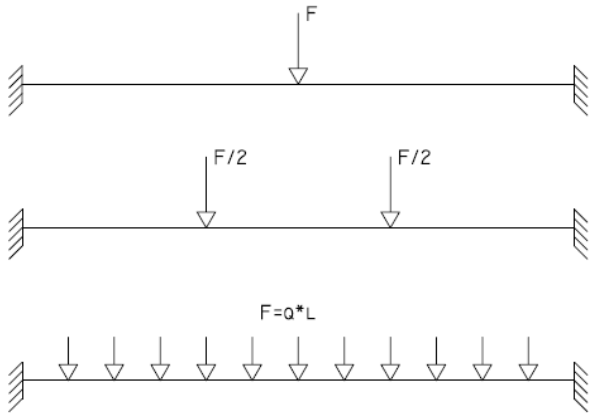

$$\delta_m = \frac{1}{192}\times\frac{Fl^3}{EI} = 0.0052\times\frac{Fl^3}{EI}$$

$$\delta_m = \frac{5}{1296}\times\frac{Fl^3}{EI} = 0.0038\times\frac{Fl^3}{EI}$$

$$\delta_m = \frac{1}{384}\times\frac{ql^4}{EI} = 0.0026\times\frac{Fl^3}{EI}$$

Figure 6.7 – Comparison of the deflection under three different loading configurations

From Eq. 6.5 the flexural stiffness of the clamped beam can be derived as shown in Eq. 6.6.

$$F = k\times\delta = k\times\frac{5}{1296}\times\frac{Fl^3}{EI} \quad\rightarrow\quad k_{flex} = \frac{1296}{5}\times\frac{EI}{l^3} \qquad \textit{Eq. 6.6}$$

A similar derivation can be done for the shear stiffness, as shown in Figure 6.8 and Eq. 6.7 and Eq. 6.8.

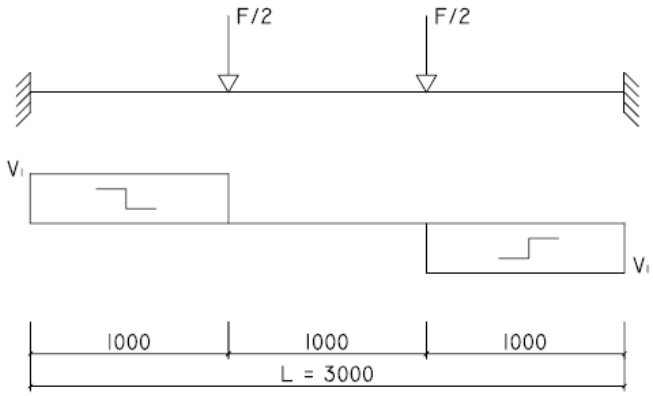

$$V_1 = \frac{F}{2}$$

Figure 6.8 – Beam model of the diaphragm for determining the shear stiffness

$$\delta_m = \frac{1}{3} l \times \frac{F/2}{GA_s} = \frac{1}{6} \frac{Fl}{GA_s} \qquad \textit{Eq. 6.7}$$

$$F = k \times \delta = k \times \frac{Fl}{6GA_s} \quad \rightarrow \quad k_{shear} = \frac{6GA_s}{l} \qquad \textit{Eq. 6.8}$$

Assuming that the flexural and shear deformation are independent, they can be combined according to Eq 6.9.

$$k_{diaphragm} = \frac{1}{\frac{1}{k_{flex}} + \frac{1}{k_{shear}}} \qquad \textit{Eq. 6.9}$$

The modulus of elasticity of the concrete is of big influence on both stiffness values. Therefore this value is calibrated using the results from the experimental testing.

The concrete used in the experimental test had an average compressive strength of 35 Mpa [Le Heux, 2008]. Design standards give different formulas for the modulus of elasticity as can be seen in Eq. 6.10(a)–(c).

$$E = 22\left(\frac{f_{cm}}{10}\right)^{0.3} \approx 32GPa = 32000MPa \quad \text{[CEN, 2004a]} \qquad \textit{Eq. 6.10(a)}$$

$$E = 4700\sqrt{f_c'} \approx 28000Mpa \quad \text{[ACI Committee 318, 2005]} \qquad \textit{Eq. 6.10(b)}$$

$$E = 3320\sqrt{f_c'} + 6900 \approx 26500MPa \quad \text{[Standards New Zealand, 2006]} \qquad \textit{Eq. 6.10(c)}$$

The value from the American Standard (ACI) has been chosen from these three results, since it is the median value.

The modulus of rigidity is given by Eq. 6.11.

$$G = 0.4E = 0.4 * 28000 \approx 11000MPa \quad \text{[Standards New Zealand, 2006]} \qquad \textit{Eq. 6.11}$$

The equations 6.6, 6.8 and 6.9 give the following stiffness values for the uncracked diaphragm:

$$\left.\begin{aligned} k_{flex} &= 15120\ kN/mm \\ k_{shear} &= 1680\ kN/mm \end{aligned}\right\} \quad k_{diaphragm} = 1512\ kN/mm$$

The stiffness of the tested diaphragm is shown in Figure 6.9. The initial, uncracked, stiffness is around 4000 kN/mm, while the cracked stiffness is approximately 300 kN/mm. The theoretical stiffness of 1500 kN/mm is in the range of the experimental value. It has to be

noted that the displacements of especially the uncracked diaphragm were very small. The experimental stiffness value might not be very accurate due to irregularities in the test specimen, unconsidered effects like friction and the accuracy of the instrumentation at that level of displacement.

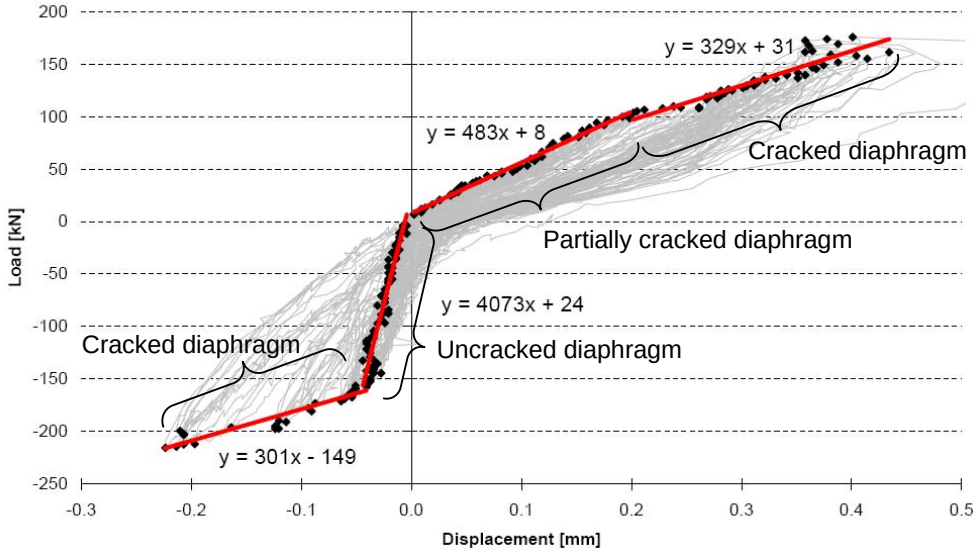

Figure 6.9 – Experimental stiffness of the diaphragm

The cracked diaphragm stiffness is used to determine the reduced E-modulus of the cracked concrete. A value of $E_{cracked} = 0.2E$ gives the following stiffness values:

$$\left.\begin{aligned} k_{flex} &= 3024\ kN/mm \\ k_{shear} &= 336\ kN/mm \end{aligned}\right\} \quad k_{diaphragm} = 302\ kN/mm$$

This is in good correspondence with the test result. The largest diaphragm displacement occurs with a cracked diaphragm, so that gives a worst case scenario. Also, it is likely that due to shrinkage or during an earthquake cracking will occur, so for the modelling the following values for the modulus of elasticity and the modulus of rigidity are assumed:

$$E_{cracked} = 0.2E = 5600\ Mpa$$
$$G_{cracked} = 0.2G = 2240\ Mpa$$

Eurocode 5 [CEN, 2004c] states that as a simple approach a reduced stiffness value of 40% of the uncracked stiffness may be taken. The value of 0.2 (20%) is again a conservative approach since a more flexible diaphragm is more likely to show larger displacements and accelerations.
With these values it is possible to calculate the diaphragm stiffness for each of the five designs presented in Chapter 6.3. In a real building the floor mass, and thus the earthquake

forces generated by the floor are generally distributed along the floor. Also the assumption that the ends of the floor are clamped by the LLRS is not valid anymore. Figure 6.10 shows the idealisation of the floor diaphragm which is used for the numerical models. Eq. 6.12 and 6.13 are used to calculate the flexural and shear stiffness of the diaphragm.

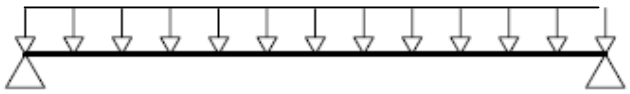

Figure 6.10 – Idealization of the floor diaphragm for numerical models

$$\delta = F/k = \frac{5}{384} \times \frac{Fl^3}{EI} \quad \rightarrow \quad k_{flex} = \frac{384}{5} \times \frac{EI}{l^3} \qquad \textit{Eq. 6.12}$$

$$\delta = F/k = \frac{ql^2}{8GA_s} \quad \rightarrow \quad k_{shear} = \frac{8GA_s}{l} \qquad \textit{Eq. 6.13}$$

An overview of the flexural and shear stiffness and the combined diaphragm stiffness is shown in Table 6.3. These values are used for the SDOF-2 model. The MDOF model uses the derived modulus of elasticity and modulus of rigidity as properties of the beam elements.

Table 6.3 – Overview diaphragm stiffness

Design	k_{flex} [kN/mm]	k_{shear} [kN/mm]	$k_{diaphragm}$ [kN/mm]	Flexural part [%]	Shear part [%]
A	67737	3136	2997	4	96
B	8467	1568	1323	16	84
C	2508	1045	738	29	71
D	743	697	360	48	52
E	313	523	196	63	38

6.5 Floor mass

The mass which needs to be taken into account is taken from the New Zealand standard [2004].

$$W_i = G_i + \Sigma \Psi_E Q_i$$

G_i and $\Psi_1 Q_i$ are summed between the mid-heights of adjacent storeys

G_i = the permanent action (self-weight or 'dead' action) at level *i*

Ψ_E = 0.6 is the earthquake imposed action (live load) combination factor for storage applications

Ψ_E = 0.3 is the earthquake imposed action (live load) combination factor for all other applications

Q_i = the imposed action for each occupancy class on level *i*, (refer AS/NZS 1170.1)

A previous design [Newcombe, 2008b] gives the following values:

$G = 2.4\ kN/m^2$
$Q = 3.0\ kN/m^2$
$W = G + \Psi * Q = 2.4 + 0.3 * 3.0 = 3.3 kN/m^2$

For each of the 5 designs the mass per length and the total mass are shown in Table 6.4. The difference in span would result in a difference in permanent weight. This difference is neglected in the design.

Table 6.4 – Overview floor mass

Design	Mass per length [kN/m]	Total mass [kN]
A	60	360
B	60	720
C	20	120
D	26	312
E	20	240

6.6 Design of the strength of the shear connectors

The earthquake causes an acceleration of the ground. The maximum value is the called the Peak Ground Acceleration (PGA). This movement results in an acceleration of each floor of the building. The majority of mass in a building is the weight of the floors. Non-structural elements, often sensitive components, are attached to the floor, which makes the Peak Floor Acceleration (PFA) an important design parameter [Reinoso *et al.*, 2005].

Different design codes give different values for the PFA as a function of the design PGA. A lower design value and an upper design value are chosen in order to simplify the analysis. The lower limit is derived from the maximum of the International Building Code (IBC) [International Code Council., 2003] where the assumption is made that the floor undergoes a peak acceleration (PFA) equal to the peak ground acceleration (PGA), so PFA / PGA = 1. This ratio is called the Floor Acceleration Magnification (FAM). The IBC codes upper limit is found to be unconservative by many researchers [Fleischman *et al.*, 2001a; Lee *et al.*, 2007], so a lower value is not considered. The upper limit is derived from the New Zealand standard [2004] and inferred as a maximum for researchers [Fleischman *et al.*, 2001a; Rivera, 2008] which results in a FAM of 3.

The PGA is evaluated according to the New Zealand standard for a site in Wellington city, with soil class C and a return period of 1/500 years. This results in a PGA of 0.70g or 6.9 m/s^2. Thus the lower limit of the PFA is 6.9 m/s^2 and the upper limit 20.6 m/s^2.

Using Newton's second law the upper and lower limit for the horizontal force generated by the floor for each design can be calculated assuming that the entire floor mass is accelerated. These values are shown in Table 6.5.

Table 6.5 – Overview connector forces

Design	Floor mass [ton]	Lower limit [kN]	Upper limit [kN]
A	36	247	742
B	72	494	1483
C	12	82	247
D	32	220	659
E	24	165	494

An EC5 design has been made to determine the strength of a timber-to-timber connection for a 10 mm diameter coach screw with a yield-strength of 1000 N/mm^2. Laboratory testing showed that there was not a significant difference in the strength of the different orientations of timber-to-timber connectors. Therefore only screws installed under a 90^o angle are considered for the strength of the connectors.

A Eurocode 5 calculation similar to the one in Appendix A.3 is made. The results are shown in Table 6.6. Evaluation of the test results showed that the rope effect cannot be taken fully into account for cyclic loading. Therefore a design strength of 12 kN is chosen.

Table 6.6 – Strength of screwed connection for 6 different failure modes

Failure mode	Strength without rope effect [kN]	Strength with rope effect [kN]
a	32.0	--
b	32.0	--
c	13.3	15.7
d	12.6	15.0
e	12.6	15.0
f	10.6	13.1

The number of connectors needed to resist the seismic loading is shown in Table 6.7. The numbers have been rounded off upwards to an even number, since the connectors need to be placed at both sides of the floor.

Table 6.7 – Overview number of connectors

Design	Lower limit [kN]	Upper limit [kN]	No. Connectors lower limit	No. Connectors upper limit
A	247	742	22	62
B	494	1483	42	124
C	82	247	8	22
D	220	659	20	56
E	165	494	14	42

6.7 Design of the stiffness of the shear connectors

The laboratory testing gave us the stiffness of 5 mm diameter connectors. The derivation below shows how this can be scaled for 10 mm diameter connectors.

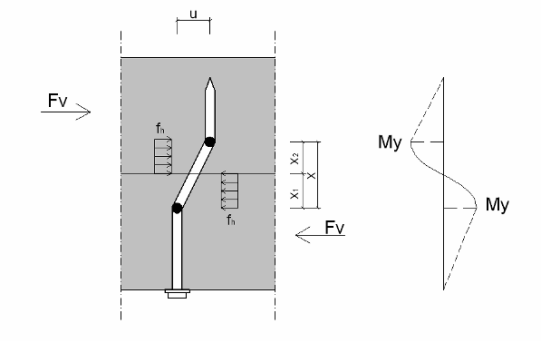

Figure 6.11 – Double yielding of fastener

In Figure 6.11 it holds that in case of two identical timber spices:

$$x_1 = x_2 = 0.5 \times x \qquad \textit{Eq. 6.14}$$

Further, the yield moment can be determined as:

$$M_y = F \times a = (f_h \times d \times x_1)(0.5 \times x_1) = 0.5 \times f_h \times d \times x_1^2 \qquad \textit{Eq. 6.15}$$

Eq. 6.15 can be rewritten for x_1.

$$x_1 = \sqrt{\frac{2M_y}{f_h \times d}} \qquad \textit{Eq. 6.16}$$

Eq. 6.14 and 6.16 result in Eq. 6.17.

$$x = 2 \times x_1 = 2 \times \sqrt{\frac{2M_y}{f_h \times d}} \qquad \textit{Eq. 6.17}$$

The yield moment depends on the diameter of the fastener as can be seen in Eq. 6.18.

$$My = 0.8 f_y \times \frac{d^3}{6} \qquad \textit{Eq. 6.18}$$

Eq. 6.16 and 6.18 together form Eq. 6.19.

$$x = 2 \times x_1 = 2 \times \sqrt{\frac{2 \times 0.8 \times f_y \times d^3}{6 \times f_h \times d}} = 2 \times \sqrt{\frac{1.6 \times f_y \times d^2}{6 f_h}} = 2 \times d \times \sqrt{\frac{1.6 f_y}{6 f_h}} \qquad \textit{Eq. 6.19}$$

Further it can be seen from Figure 6.11 that:

$$u \sim x \qquad \textit{Eq. 6.20}$$

From Eq. 6.19 and 6.20 follows Eq. 6.21.

$$u \sim d \qquad \textit{Eq. 6.21}$$

So there is a linear dependence between the displacement in the connection and the diameter of the fastener.

The same is valid for inclined timber-to-timber connections [Bejtka, 2002].

$$x_1 = \sqrt{\frac{2\beta}{1+\beta}} \times \sqrt{\frac{2M_y \times \cos^2 \alpha}{f_{h,1} \times d}} \rightarrow x \propto \sqrt{\frac{M_y}{d}} \propto \sqrt{\frac{d^3}{d}} \propto d \qquad \textit{Eq. 6.22}$$

And also for inclined timber-to-concrete connections [Kavaliauskas, 2007].

$$x = 2t \times \sqrt{\frac{M_y}{f_h \times d \times t^2}} \times \sin(\alpha) \rightarrow x \propto \sqrt{\frac{M_y}{d}} \propto \sqrt{\frac{d^3}{d}} \propto d \qquad \textit{Eq. 6.23}$$

The shear force for this failure mode (double yielding) is given Eq. 6.24.

$$F_v = 1.15 \times \sqrt{\frac{2\beta}{1+\beta}} \times \sqrt{2M_y \times f_h \times d} \propto \sqrt{d^3 \times d} = d^2 \qquad \textit{Eq. 6.24}$$

So there is a quadratic dependence between the shear force over a connection and the diameter of the fastener.

The stiffness of the connection can be calculated with Eq. 6.25.

$$k = \frac{F}{u} \propto \frac{d^2}{d} = d \qquad \textit{Eq. 6.25}$$

This shows that there is a linear dependence between the stiffness of the connection and the diameter of the fastener.

Laboratory testing showed that the stiffness of 10 ø 5mm fasteners was between 20 and 80 kN/mm (depending on the orientation), so 1 ø 5mm has a stiffness between 2 and 8 kN/mm. With the previous derivation it can be concluded that 1 ø 10mm fastener has a stiffness between 4 and 16 kN/mm. The different stiffness values for the five designs are shown in Table 6.8.

A comparison with EC5, Eq 6.26, shows that the derived stiffness of the 10mm diameter 90^o angle screw connection is lower then prescribed by EC5. This was also noticed by other researchers [Dias, 2005].

$$K_{ser} = \frac{\rho_m^{1.5} \times d}{23} = \frac{600^{1.5} \times 10}{23} = 6.4 kN/mm \qquad \textit{Eq 6.26}$$

Table 6.8 – Overview of upper and lower values for the connector stiffness

Design	No. Connectors lower limit	No. Connectors upper limit	Stiffness lower limit [kN/mm]	Stiffness upper limit [kN/mm]
A	22	62	88	992
B	42	124	168	1984
C	8	22	32	352
D	20	56	80	896
E	14	42	56	672

The five designs have each been modelled with a range of different stiffness values for the connectors. The period of natural vibration for the connectors (T_{conn}) has been calculated according to Eq. 6.27. The five different ranges of connector period turn out to be all between 0.02 and 0.20 seconds, which makes it a good parameter for comparison of the different designs.

$$T_{conn} = 2\pi \times \sqrt{\frac{M}{K_{conn}}} \qquad \textit{Eq. 6.27}$$

6.8 Overview of Design Parameters

Table 6.9 and 6.10 give an overview of the design parameters for each of the five designs.

Table 6.9 – Overview design parameters (1)

Design	Aspect ratio (λ)	A [m2]	A_s [m^2]	I [m4]	Mass per length [kN/m]	Total mass [kN]
A	0.33	1.26	1.05	34.02	60	360
B	0.66	1.26	1.05	34.02	60	720
C	1.00	0.42	0.35	1.26	20	120
D	1.50	0.56	0.47	2.99	26	312
E	2.00	0.42	0.35	1.26	20	240

Table 6.10 – Overview design parameters (2)

Design	$k_{diaphragm}$ [kN/mm]	$k_{connector}$ lower limit [kN/mm]	$k_{connector}$ upper limit [kN/mm]	T_{conn} lower limit [s]	T_{conn} upper limit [s]
A	2997	88	992	0.127	0.038
B	1323	168	1984	0.130	0.038
C	738	32	352	0.122	0.037
D	360	80	896	0.124	0.037
E	196	56	672	0.130	0.038

6.9 Results

Each of the 5 designs has been evaluated seven times with different values of the connector stiffness in Ruaumoko. Each time the model was subjected to 15 different earthquake records. Examples and explanation of the input for Ruaumoko can be found in Appendix B. The earthquake records are presented in Appendix C. The time step used for the analysis is 0.01 seconds.

In this chapter the process of acquiring the results from the analysis output and a summary of the results is shown. Design E with the MDOF model is used as an example, as can be seen in Figure 6.12. The results per design are added in Appendix D.

6.9.1 Interpretation of results

The response of a structure to 15 different earthquake records varies widely. Therefore the statistical variability needs to be considered in order to compare the different designs. For each design the Median and the 84th percentile (or +Sigma) values have been calculated from the data sets of the 15 earthquakes. The Median and +Sigma have been chosen over the Average and Standard Deviation because they are less sensitive to extreme values in a data range, which might occur if one of the structures collapses.

The Median value is 'the exponent of the mean of the natural log values' of the data set, as shown in Eq. 6.25. The 84th percentile (Eq. 6.27) is the Median multiplied by the exponent of the dispersion (Eq. 6.26), where the dispersion is determined as the standard deviation of the natural log values of the data set [Chopra, 2008].

$$median = e^{\frac{1}{N}*\sum_{i=1}^{N}\ln(x_i)} \qquad \textit{Eq. 6.25}$$

$$dispersion = \sqrt{\frac{1}{N-1}*\sum_{i=1}^{N}[\ln(x_i)-\ln(median)]^2} \qquad \textit{Eq. 6.26}$$

$$+sigma = median * e^{dispersion} \qquad \textit{Eq. 6.27}$$

6.9.2 Floor displacements

The floor displacement can be split up in two parts, the displacement in the connectors and the displacement in the diaphragm itself. The displacement over the connectors is equal to the displacement of Node 2 (or Node 10) of the model. The displacement of the diaphragm equals the displacement of Node 6 in the model minus the displacement of Node 2. The total floor displacement is the combined displacement of the connectors and the diaphragm, so that equals the displacement of Node 6. All these displacements are taken relative to the displacement of the ground (Node 1 or Node 11).

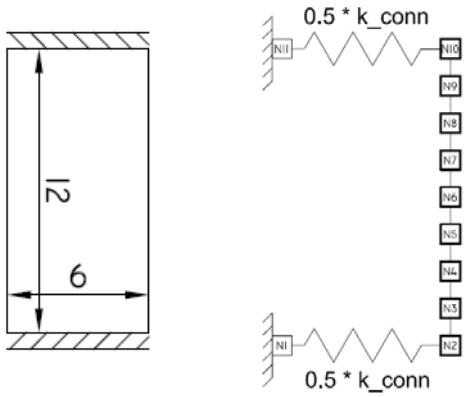

Figure 6.12 – Comparing Design E with the complex model

The results of the 15 different earthquakes have been evaluated as explained in Chapter 6.9.1. Figure 6.13 shows the Median results of the connector, diaphragm and floor displacement and the +Sigma results for the floor displacement. In the results of the analysis, which are shown in Appendix D, only the Median and +Sigma displacements of the floor are shown for the three different models.

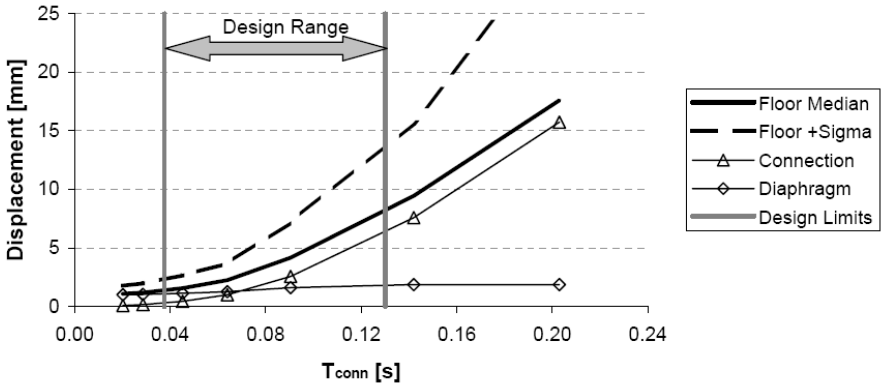

Figure 6.13 – Displacements of Design E calculated with the complex model

From Chapter 6.7 follows an upper limit for the stiffness of the connectors, namely having inclined screws and a FAM factor of 3. This upper limit for the stiffness gives a lower limit for the period of the connectors. Also a lower limit for the stiffness, and thus an upper limit for the period, of the connectors is derived for straight screws and a FAM factor of 1. These limits are the design limits, which are shown by the grey lines on the graph in Figure 6.13.

The design range, which falls between those limits, can be split up in different sections, as shown in Figure 6.14. Inclined screws give a stiff connection (so a low period), putting them on the left side in the design range. The opposite is the case for the straight screws. The FAM factor of 1 results in a low design force and thus a low number of connectors. Hence the low stiffness and the high period, which puts them on the right side in the design range.

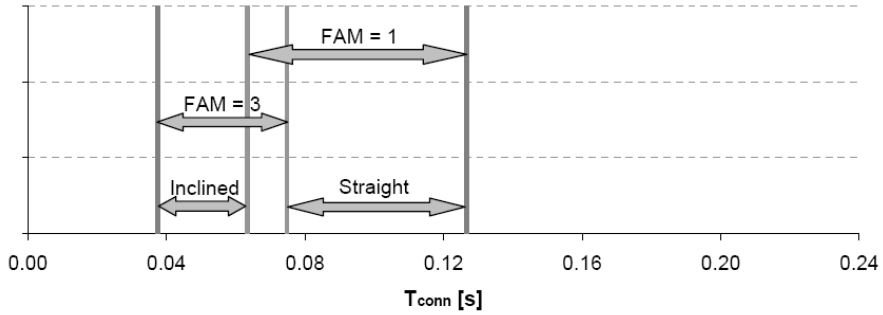

Figure 6.14 – Specification of the design range

The displacement of the floor is compared for the three different models shown in Figure 6.2. This is done by dividing the displacement according to MDOF model by the displacement according to the SDOF models. An example of such a comparison can be seen in Figure 6.15. This figure shows that the SDOF-2 model captures the response of the MDOF model really well; the maximum difference in displacement is only 8%. The SDOF-1 model however varies significantly from the MDOF model for the stiff connectors. The displacement of the diaphragm stays nearly constant over the full design range, but the displacement of the connector increases with an increasing period. Therefore the influence of the diaphragm displacement is the largest at a small period.

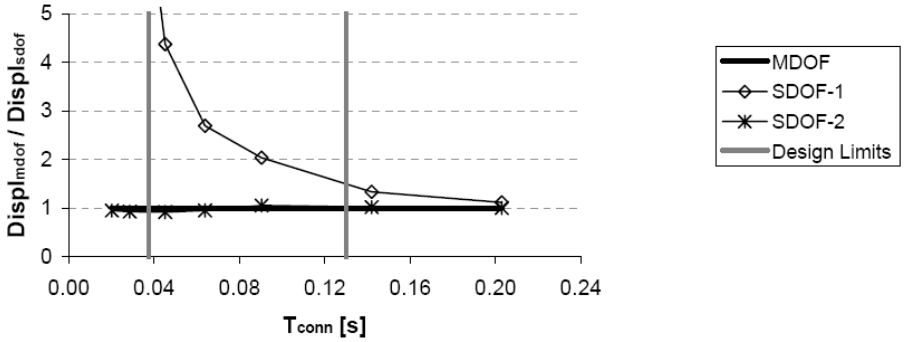

Figure 6.15 – Comparison of the floor displacement between the MDOF model and the SDOF models

6.9.3 Floor accelerations

In addition to the displacements, the accelerations of the floor have also been evaluated. The PFA is expressed as the number of units of gravity ('g') felt by the floor. Figure 6.16 shows the distribution of the maximum PFA, of one earthquake (record 1 in this case), over the 9 different nodes of the MDOF model. It can be seen that the middle of the floor has the largest PFA. It also shows that it is reasonable to make the simplification that the whole floor undergoes the same acceleration, since there is only a 5% difference between the outer nodes and the middle node.

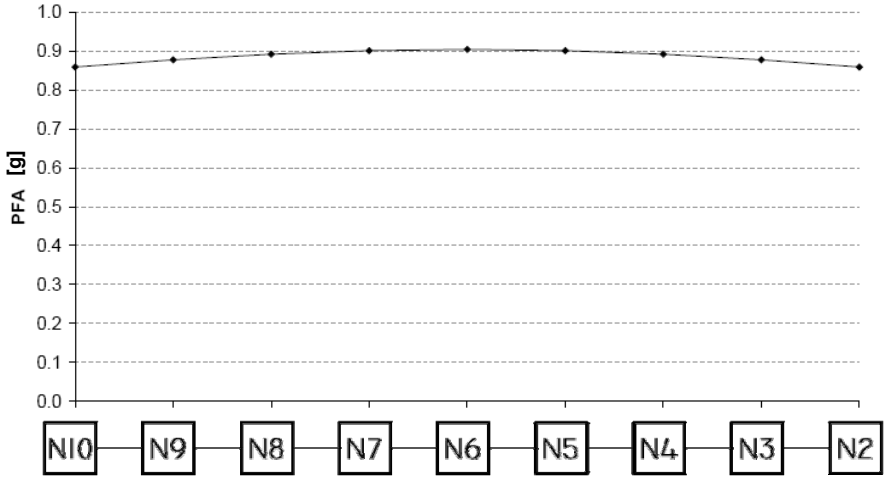

Figure 6.16 – PFA distribution over the floor

The maximum PFA can be evaluated for every earthquake. The maximum values for the 15 earthquakes are used to calculate the The Median and +Sigma values. The PFA/PGA ratios are calculated for each of the seven different values of connector periods and are shown in Figure 6.17. Also shown are the ratios 1 (IBC) and 3 (NZ1170.5), as they are used as the lower and upper limit for the connector design.

In theory, inelastic behaviour will occur if the PFA exceeds the PGA. However, this is conservatively ignored (by doing a linear elastic analysis) in this part of the study because the inelastic behaviour will reduce the diaphragm response.

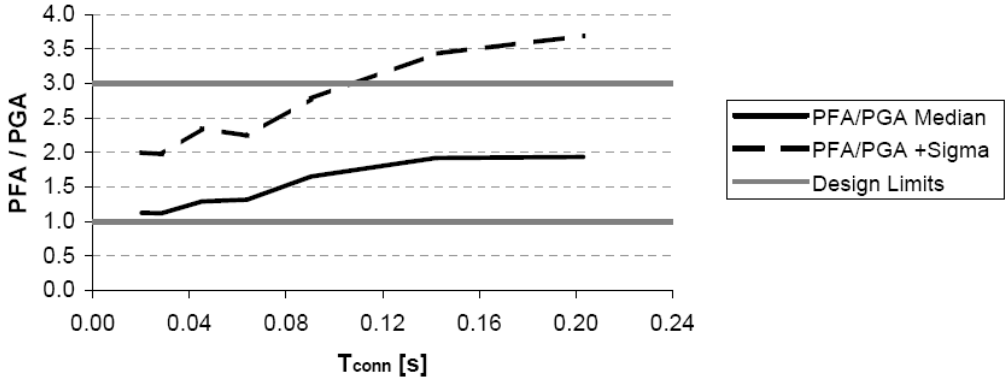

Figure 6.17 – The PFA/PGA ratio

It can be seen that the PFA/PGA increases as the period of the connection increases. This higher floor acceleration is due to an increase in the acceleration spectrum, as can be seen in Figure 6.18. The insert shows the period range in which the connector design is situated.

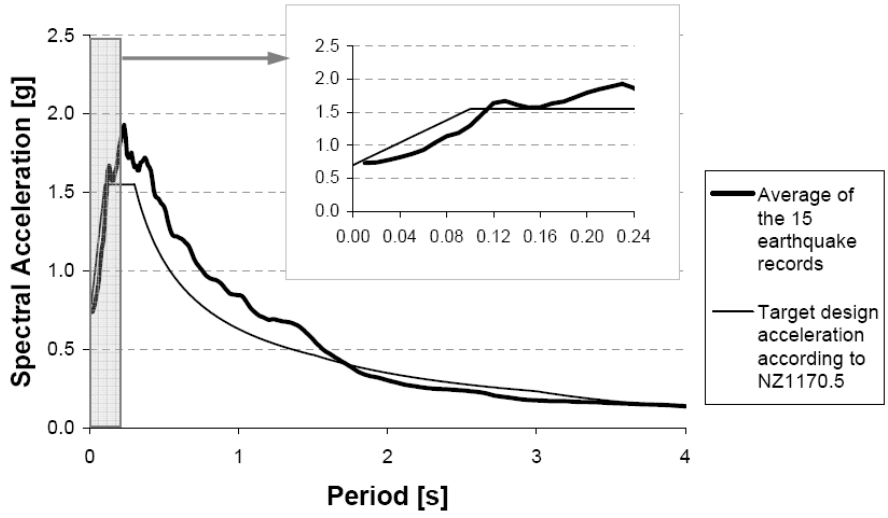

Figure 6.18 – Spectral acceleration graph

6.10 Comparison of the results

First the comparison is made between the MDOF model and the SDOF-1 model, which only models the connectors and not the diaphragm. Figure 6.19 shows that this model only gives a good result ($Displ_{mdof}$ / $Displ_{sdof\text{-}1} \approx 1$) for Design C and Design A, which both have a span of only 6 meters. The displacement of Design B (λ=0.66) is surprisingly far off compared to Design C (λ=1). This would suggest that the span of the floor is more important than the aspect ratio, something which is also noted by Nakaki [2000].

The model is the most accurate for higher periods of the connectors. This is because a high period means a low stiffness of the connectors. The low stiffness results in a large displacement of the connectors. Therefore the influence of the diaphragm displacement on the total floor displacement reduces.

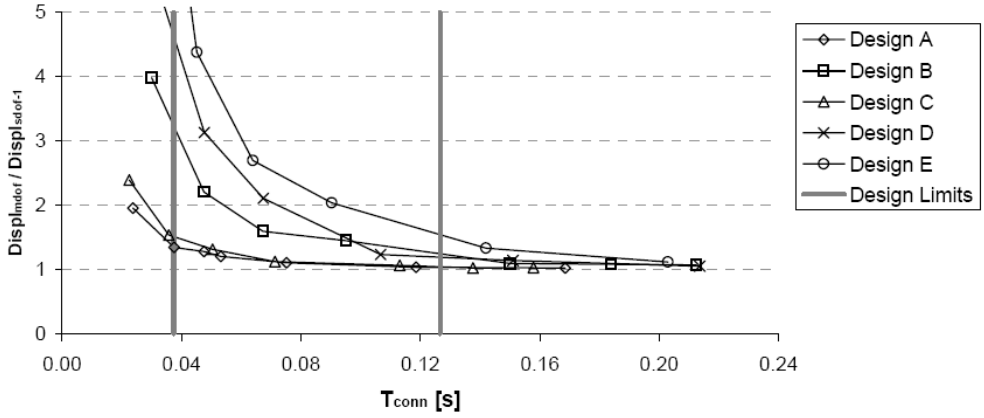

Figure 6.19 – Comparison of floor displacements of the MDOF model and SDOF-1 model

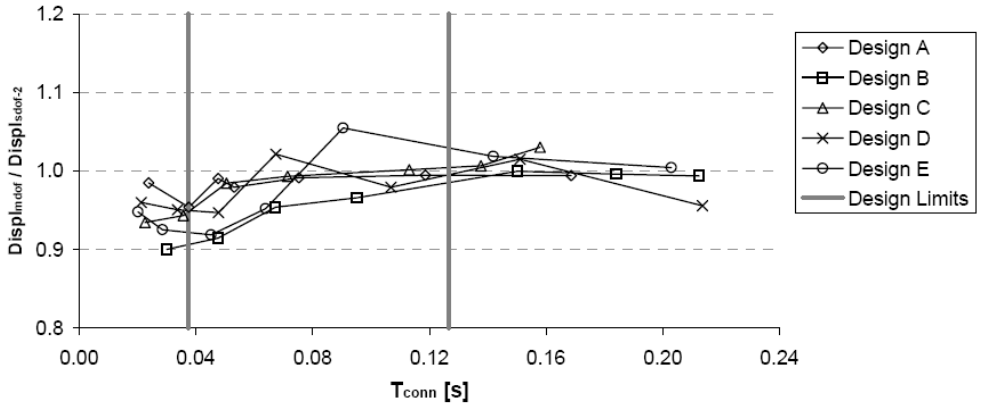

Figure 6.20 – Comparison of floor displacements of the MDOF model and SDOF-2 model

The same comparison can be made for the MDOF model and the SDOF-2 model, which models both, the connectors and the diaphragm, as a single spring. Figure 6.20 shows that

there is a good agreement with the MDOF model over the complete range of connector stiffness; the maximum error is only 9%. Therefore it is valid to conclude that the diaphragm can be modelled as a linear spring, with the stiffness as described in Chapter 6.7. There are no major higher order effects introduced by the movement of the diaphragm. This model has been shown to be sufficient for all the designs considered, but it means that the flexural and shear stiffness of the diaphragm need to be calculated.

It should be noted that even though the SDOF-1 model does not match the results from the MDOF model very well, the actual differences in displacements is only a couple of millimetres. Figure 6.21 shows the diaphragm displacement as calculated with the MDOF model. It can be seen that for all the models the diaphragm displacement stays below 2 mm. Therefore in the next step of the analysis, when the LLRS is added, it is possible that the SDOF-1 model may be sufficient to capture the overall response.

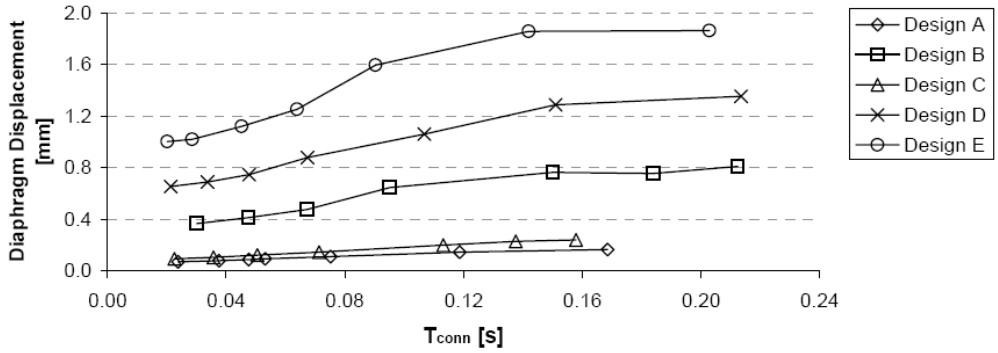

Figure 6.21 – Diaphragm displacement according to the MDOF model

Figure 6.22 and Figure 6.23 indicate that the peak floor accelerations have a similar trend as the floor displacements. The SDOF-1 model predicts the accelerations well for Design A and C, but gives up to a 60% difference for Design E. The SDOF-2 model gives a good prediction over the complete range of connector stiffness; the maximum error is 17%.

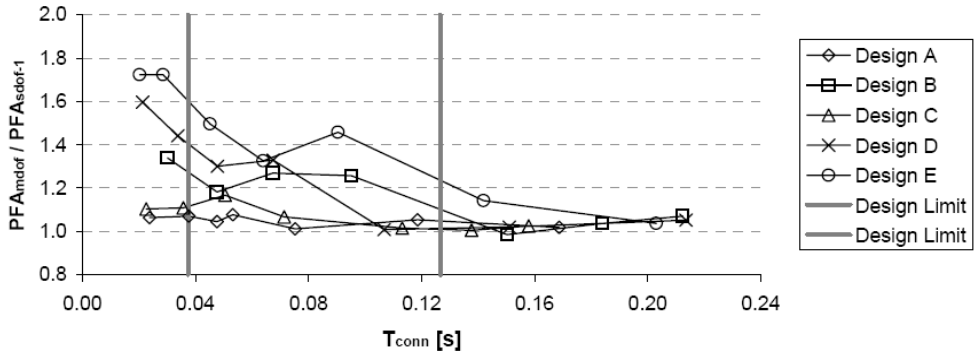

Figure 6.22 – Comparison of peak floor acceleration between the MDOF model and SDOF-1 model

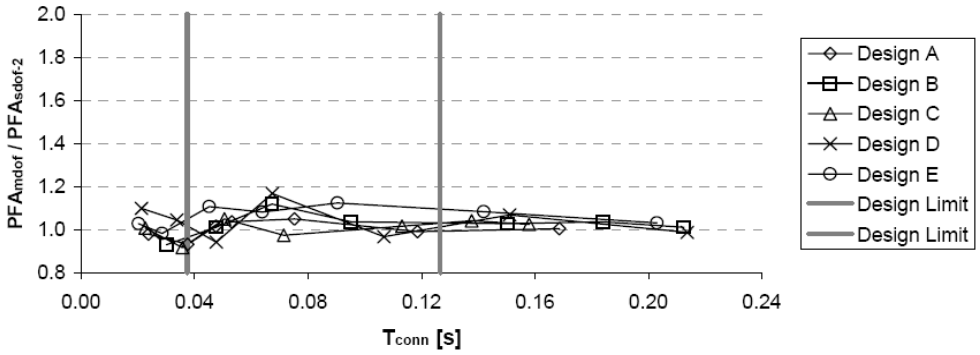

Figure 6.23 – Comparison of peak floor acceleration between MDOF model and SDOF-2 model

The ratio of the PFA over the PGA is shown for the 5 designs in Figure 6.24. This graph shows the Median and +Sigma values from the analysis with the MDOF model. The other two models give a similar graph. It can be seen that the lower design limit, which is the upper design limit according to IBC, would only be valid for a rigid diaphragm. A flexible diaphragm is likely to show a larger acceleration. Therefore, designing according to the IBC would significantly underestimate the diaphragm accelerations and result in inelastic deformation in the floor diaphragm. The upper design limit of PFA/PGA ratio of 3 is a safe upper limit for connections with a period of up to 0.13 seconds. The design limit for the period of the connectors is 0.13 seconds.

Design E, with the most flexible diaphragm, has a larger PFA then Design A, with the stiffest diaphragm. But there is no clear relationship between the aspect ratio and the peak floor acceleration.

Designs with straight connectors are more flexible and have a higher connection period. Therefore they introduce higher accelerations in the floor diaphragm. A stiffer connection, with inclined screws, lowers the connection period and thus lowers the PFA.

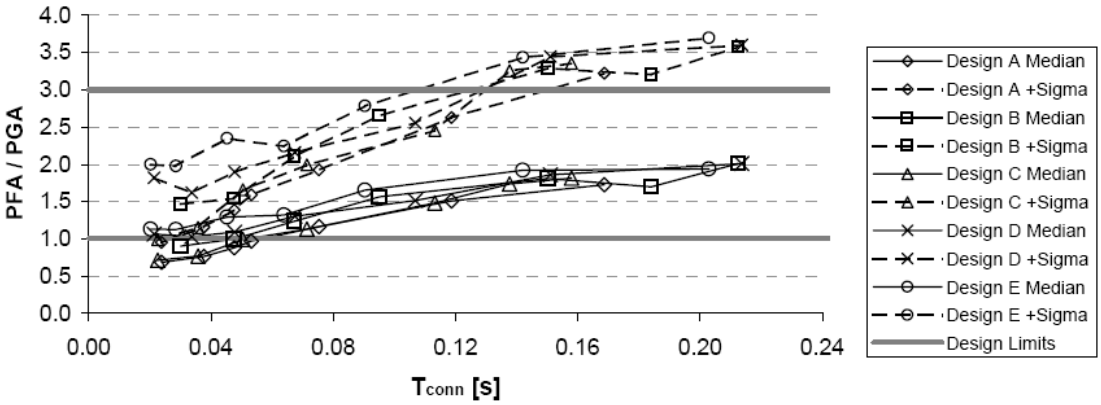

Figure 6.24 – PFA / PGA according to the MDOF model

6.11 Summary

The floor flexibility consists of three different parts, the deformation of the connectors, the shear deformation in the diaphragm and the flexural deformation in the diaphragm. The numerical analysis showed that it is not necessary to model the diaphragms as several beam elements. The simplification to model it as a spring element is justified.

The analysis did not show a clear relationship between the aspect ratio of the floor and the seismic response. The difference was clearer when comparing the different spans of the floor. The numerical analysis showed that for short spans (6 meter) over 80% of the displacements take place in the connectors. Therefore, with those short spans, the influence of the diaphragm can be neglected. It is also shown that neglecting the diaphragm flexibility does not significantly influence the peak floor accelerations.

For larger spans (over 6 meter) and especially spans with a high aspect ratio, there is a significant (over 20%) influence of the diaphragm flexibility on the floor displacements and the floor accelerations. The diaphragm needs to be included in the model, which can be done as a spring. It must be noted that although the influence is significant, the absolute displacements in the diaphragm stay below 2 millimeters.

The floor accelerations can be assumed constant along the length of the diaphragm. The flexible floor can lead to accelerations of up to 3 times the PGA. This indicates that a rigid floor diaphragm assumption in a design can severely underestimate the floor accelerations. A stiffer connection (e.g. inclined screws) between the LLRS and the floor results in lower floor accelerations then less stiff connections.

7 Numerical analysis of a single storey building

In the previous chapter several models of the floor flexibility were developed. The next step in the analysis is to add the LLRS to the floor and to investigate the influence of the floor flexibility on the overall response of a single storey building. A displacement based design has been made to estimate the stiffness of the LLRS. Again, Ruaumoko has been used for the analysis with the same 15 earthquake records. The results from the analyses are discussed in the end of this chapter.

7.1 Introduction

This second part of the numerical analysis focuses on a single storey building. This is done to get a better understanding of the interaction between the floor diaphragm and the LLRS. With this model it will be possible to determine when a floor can be assumed rigid and when the flexibility should be taken into account.

7.2 Numerical Model

The three models made in the previous chapter are used again, but with an extra spring added to model the LLRS. A forth model is made which only models the LLRS. This is shown in Figure 7.1.

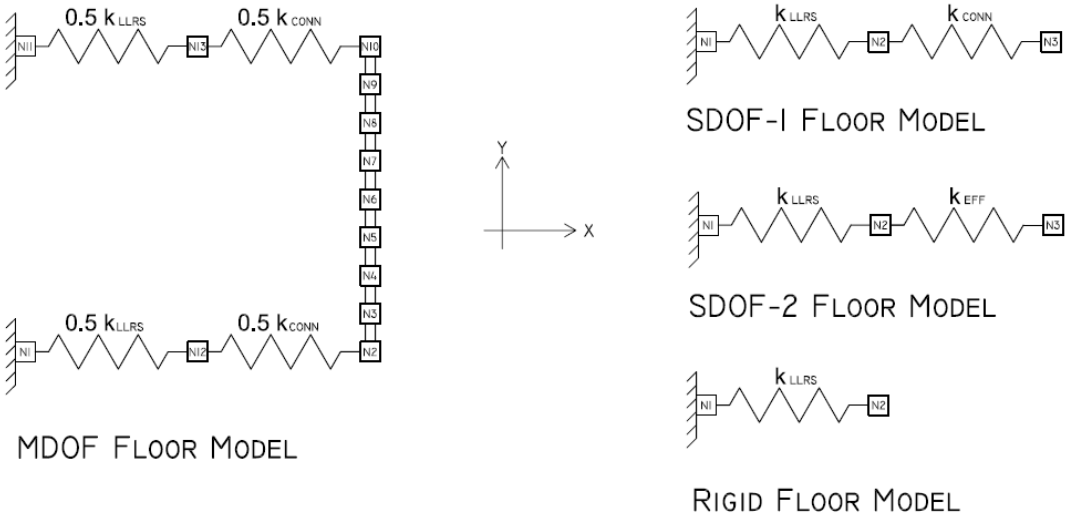

Figure 7.1 – The four numerical models

7.3 Design Parameters

The previous chapter showed that the influence of the floor stiffness was the biggest for Design E (λ=2). Therefore only this design has been considered for the modelling of the single-storey building.

Two different LLRS are analysed, a frame solution and a wall solution. They represent the boundaries of the range in which a possible real solution will be situated.

7.4 Stiffness of the LLRS

A displacement based design (DBD) [Priestley *et al.*, 2007] has been made in order to determine the stiffness of the LLRS which is needed for the numerical analysis.

Firstly, a DBD is presented for a single storey building where a frame is used for the LLRS as shown in Figure 7.2.

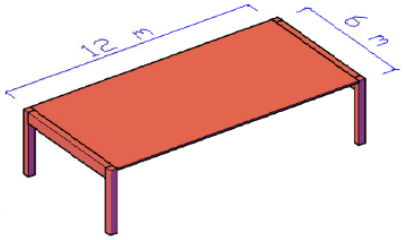

Figure 7.2 – Single storey building with frame

Step 1. *Determine the design displacement, the effective mass and the effective height (Figure 7.3).*

The target inter-storey drift level for a timber frame structure is 2%. The New Zealand standard [2004] gives an inter-storey drift limit of 2.5% for the ultimate limit state. With a storey height of 3.2 meter, this gives a target displacement, Δd = 64 mm.

The mass of the floor is its weight times the area. The analysed structure has a floor depth of 6 meter and a span of 12 meter, giving a total area of 72m^2. The weight per square meter is 3.3 kN/m^2, resulting in a total mass of 240 kN or 24.5 ton. The weight of the frame is estimated at 10% of the weight of the floor, so 24 kN or 2.4 ton. Since it is only a single storey building, its effective mass, m_e, equals its total mass, so 26.9 ton.

$$\Delta_d = \sum_{i=1}^{n}\left(m_i\Delta_i^{\,2}\right) \Big/ \sum_{i=1}^{n}\left(m_i\Delta_i\right)$$

$$m_e = \sum_{i=1}^{n}\left(m_i\Delta_i\right) \Big/ \Delta_d$$

$$H_e = \sum_{i=1}^{n}\left(m_i\Delta_i H_i\right) \Big/ \sum_{i=1}^{n}\left(m_i\Delta_i\right)$$

Figure 7.3 – Equations for the target displacement, effective mass and effective height

The effective height, H_e, is approximately equal to the total height for the single storey building, so H_e = 3.2 meter.

Step 2. *Calculate the equivalent viscous damping.*

The equivalent viscous damping, ζ_{eq}, consists of two parts, the elastic damping, ζ_{el}, and the hysteretic damping, ζ_{hyst}. The elastic damping is assumed 2% and the hysteretic damping is assumed 20% [Newcombe, 2008b]. This high hysteretic damping gives a higher period and thus a lower stiffness. This lower stiffness creates the worst case lower design limit.
So $\zeta_{eq} = 22\%$.

Step 3. *Determine the effective period from the reduced design displacement spectrum.*

The design spectrum needs to be scaled by a scaling factor R_{eq} as defined in Eq. 7.1.

$$R_{eq} = \left(\frac{7}{2+\zeta_{eq}} \right)^{0.5} = \left(\frac{7}{2+22} \right)^{0.5} = 0.54 \qquad \textit{Eq. 7.1}$$

The scaled displacement spectrum can be seen in Figure 7.4. The effective period, T_e, can be determined as 1.0 seconds.

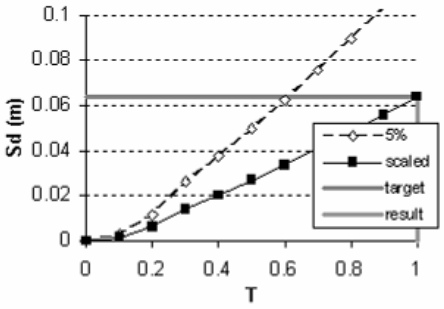

Figure 7.4 – The 5% and the scaled displacement spectrum

Step 4. *Obtain the equivalent lateral stiffness.*

The equivalent lateral stiffness, K_e, is given by Eq. 7.2.

$$K_e = \frac{4\pi^2 \times m_e}{T_e^2} = \frac{4\pi^2 \times 26.9}{1.00^2} = 1058 kN/m \qquad \textit{Eq. 7.2}$$

Step 5. *Determine the base shear.*

The base shear, V_b, is given by Eq. 7.3

$$V_b = K_e \times \Delta_d = 1058 \times 0.064 = 68 kN \qquad \textit{Eq. 7.3}$$

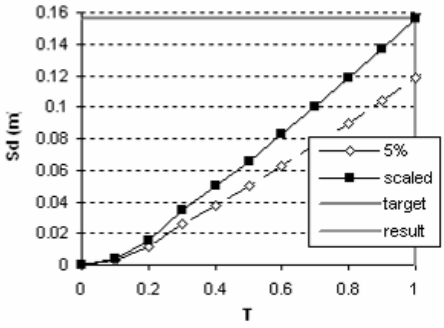

Figure 7.5 – The 5% and the scaled displacement spectrum

Step 6. *Distribute the base shear up the structure.*

Since there is only a single-storey, the entire shear force is distributed to the one floor.
So $F_1 = 68$ kN.

In Ruaumoko the hysteretic damping is conservately ignored since it will reduce the seismic response. In order to be able to compare the results of the numerical analysis with the DBD the target displacement needs to be back calculated according to the displacement spectrum belonging to 2% damping (instead of 22%), as shown in Figure 7.5. This calculation gives a design displacement of 156 mm. The corresponding base shear is 165 kN.

The same DBD calculation is done for a wall structure. The steps are summarized below.

Step 1.
The target inter-storey drift level for a timber wall structure is 1%, so $\Delta d = 32$ mm
The mass of the wall is assumed to be 20% of the mass of the floor, so $m_e = 29.4$ ton
$H_e = 3.2$ meter.

Step 2.
$\zeta_{eq} = 2\%$. No hysteretic damping is assumed here, which means a lower period and thus a higher stiffness. This is done to get the upper design limit.

Step 3.
$R_{eq} = 1.32$
$T_e = 0.29$ *seconds.*

Step 4.
$K_e = 14157 kN/m$

Step 5.
$V_b = 453 kN$

Step 6.
$F_1 = 453$ *kN*

7.5 Results

A similar analysis as for the floor system (Chapter 6) has been performed for the single-storey building. The results are split in two parts. First the results from the single storey building with a frame as LLRS are presented and secondly the results from the model with the wall as LLRS.

7.5.1 Frame

The displacement can be split up into three parts, the displacement of the LLRS, the displacement of the connection and the displacement of the diaphragm. Figure 7.6 shows these displacement values for the MDOF floor model. It can clearly be seen that the displacement of the LLRS is much larger then the other components.

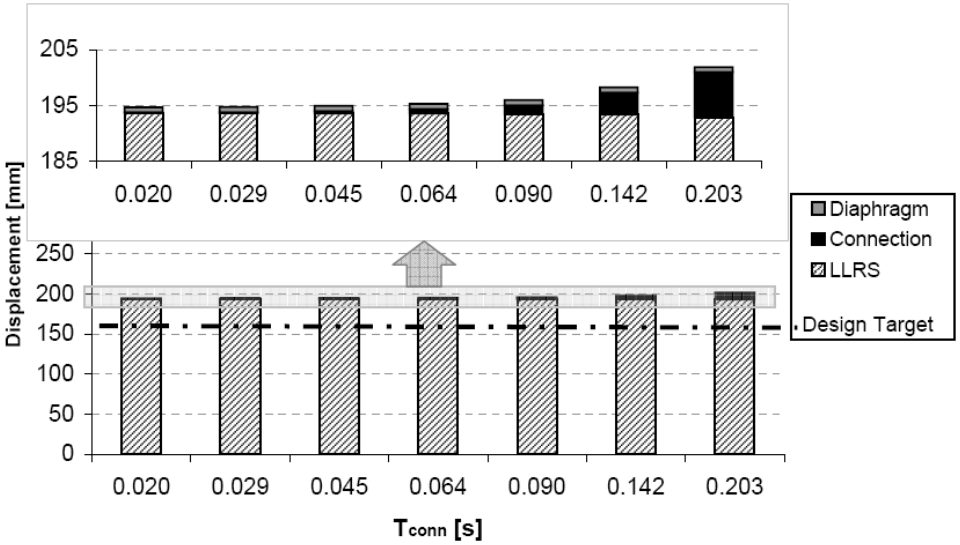

Figure 7.6 – Displacements of single storey building with frame as LLRS according to the complex model

Figure 7.7 gives the Median and +Sigma displacement for all the four models. Also the calculated target displacement from the DBD is shown. The rigid floor model is only calculated once, since it does not model the connectors. Therefore there is no actual period of the connection. Hence, the displacement of the rigid floor model is constant over the entire range of connector period.

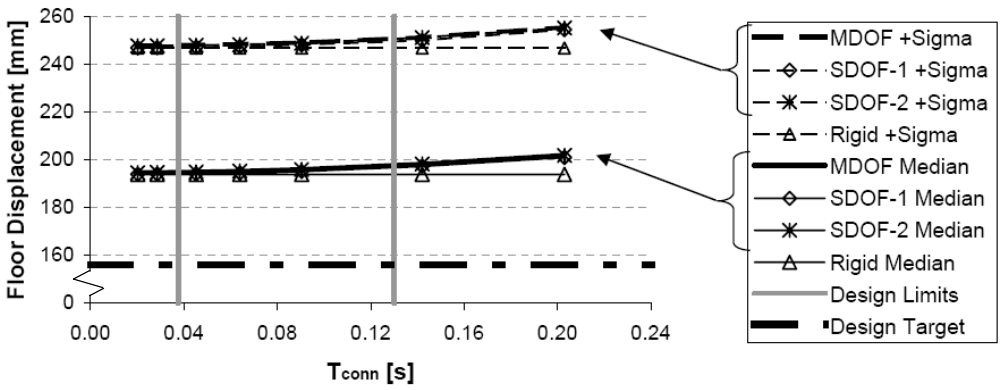

Figure 7.7 – Comparison of floor displacements of single storey building with frame as LLRS

Figure 7.7 shows that the displacements of the MDOF, the SDOF-1 and the SDOF-2 floor model are nearly the same. This can also be seen from Figure 7.8, where the ratio between these three models is nearly equal to 1. The rigid floor model is giving very good results at lower periods of the connectors, due to the limited influence of the connector displacement. For the higher periods of the connectors the rigid floor model is in the design range maximum 2% off.

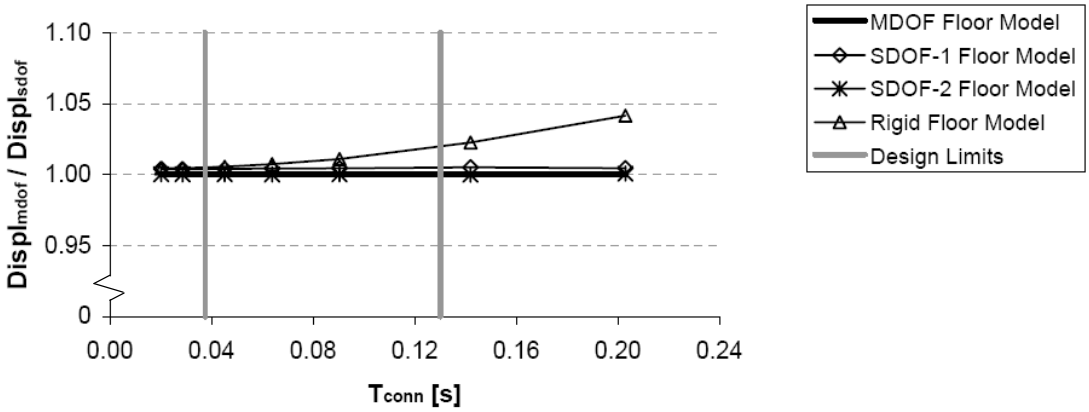

Figure 7.8 – Further comparison of displacements of single storey building with frame as LLRS

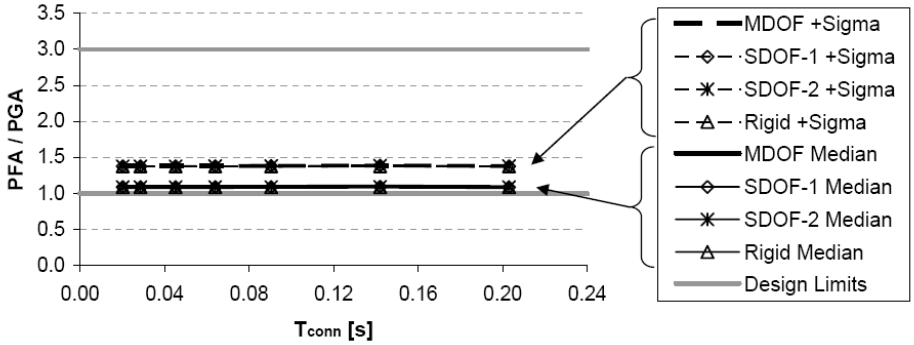

Figure 7.9 – Comparison of floor accelerations of single storey building with frame as LLRS

The floor accelerations are nearly constant for all the different values of connector stiffness, as can be seen in Figure 7.9. This means that the connector stiffness does not influence the floor accelerations for a single storey building with a frame as LLRS. This can be explained by looking at the period of the structure, simplified as a SDOF. The period of the LLRS is approximate 1.0 seconds, as calculated in the DBD. The equivalent stiffness of the LLRS and the connectors combined varies between 0.95 and 0.97 seconds as can be see in Eq. 7.5 and 7.6.

$$k_{eff} = \frac{1}{\frac{1}{k_{LLRS}} + \frac{1}{k_{conn}}} = \frac{1}{\frac{1}{1.053} + \frac{1}{23}} = 1.007 kN/mm \rightarrow T_{eff} = 0.97s \qquad \textit{Eq. 7.5}$$

$$k_{eff} = \frac{1}{\frac{1}{k_{LLRS}} + \frac{1}{k_{conn}}} = \frac{1}{\frac{1}{1.053} + \frac{1}{2320}} = 1.052 kN/mm \rightarrow T_{eff} = 0.95s \qquad \textit{Eq. 7.6}$$

This shows that the connectors hardly influence the period of the structure, and thus do not influence the floor accelerations.

The Median shear force in the LLRS is shown in Figure 7.10. The force is nearly constant since the floor accelerations are also constant. The figure shows that the MDOF floor model gives a smaller shear force in the LLRS then the SDOF floor models and the rigid floor model. The shear force is higher than the design force according to the DBD due to the PFA being higher than the PGA

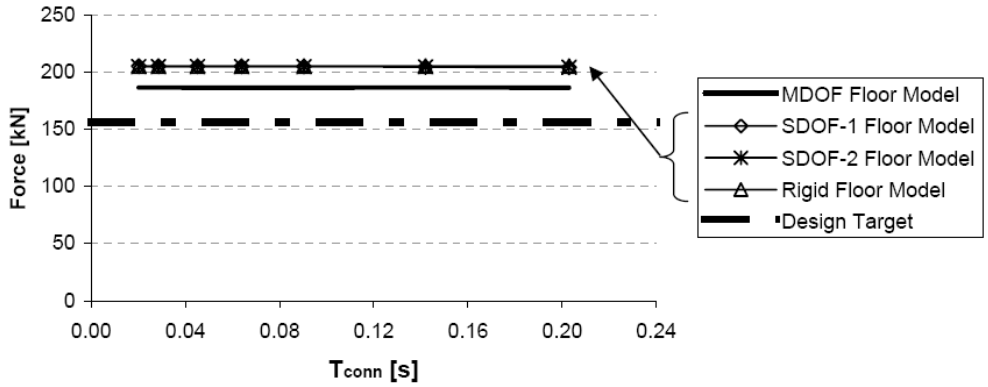

Figure 7.10 – Comparison of Median shear force of single storey building with frame as LLRS

7.5.2 Wall

The design with the wall as LLRS is much stiffer than the design with the frame. Therefore the displacement of the LLRS is much less and the influence of the flexible floor is larger. This can be seen in Figure 7.11 and Figure 7.12. Other researchers [Nakaki, 2000] also came to this conclusion when looking at precast concrete structures.

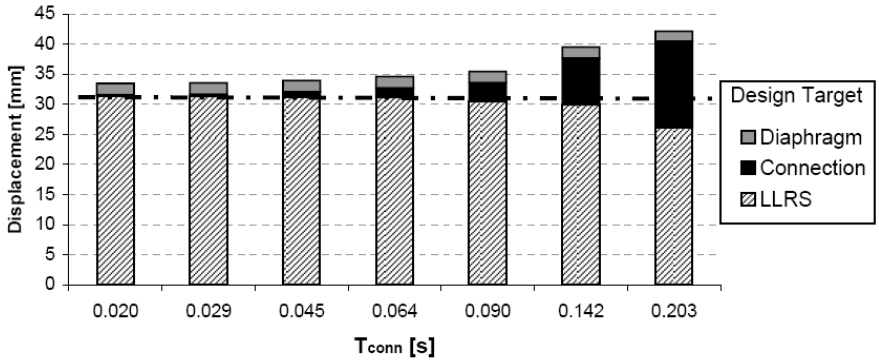

Figure 7.11 – Displacements of single storey building with wall as LLRS according to the complex model

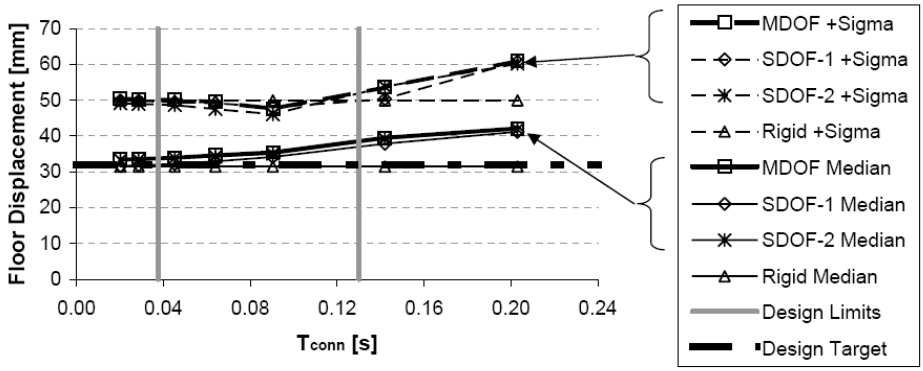

Figure 7.12 – Comparison of floor displacements of single storey building with wall as LLRS

Figure 7.12 and Figure 7.13 show that the SDOF floor models describe the displacements accurately in comparison to the MDOF model. The rigid floor model shows an error of up to 23%.

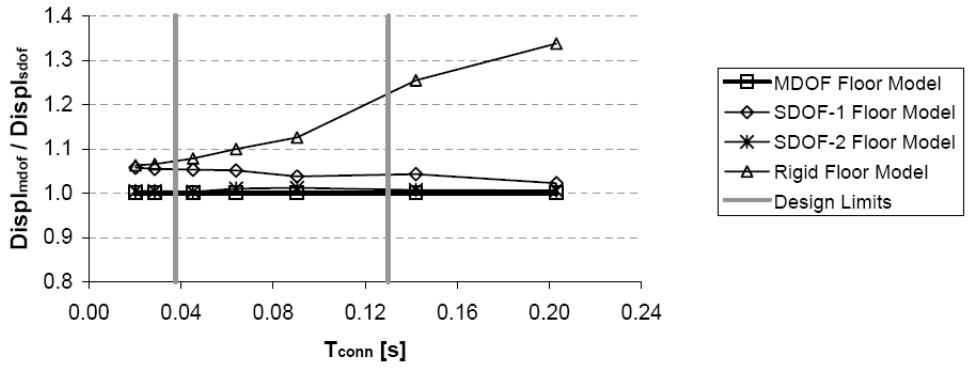

Figure 7.13 – Further comparison of displacements of single storey building with wall as LLRS

The MDOF model gives the floor displacements and the rigid model gives the LLRS displacement, as shown in Figure 7.14. These values can be used to determine if the diaphragm can model assumed stiff according to different building codes as described in Chapter 2.4.1. In order to make the assumption that the diaphragm is rigid the New Zealand standard and the IBC state that $u_{floor} \leq u_{llrs}$. This is the case for the all the values of T_{conn} as can be seen in Figure 7.14. The Eurocode states that $u_{floor} \leq 10\% * u_{llrs}$, it can be seen that this is only the case for $T_{conn} < 0.055$ seconds. Thus according to the Eurocode the flexibility of the floor should be taken into account for the design of this structure for $T_{conn} > 0.055$ seconds. This fits well with the results of Figure 7.13, which show that the rigid floor model gives more than a 10% difference with the MDOF model.

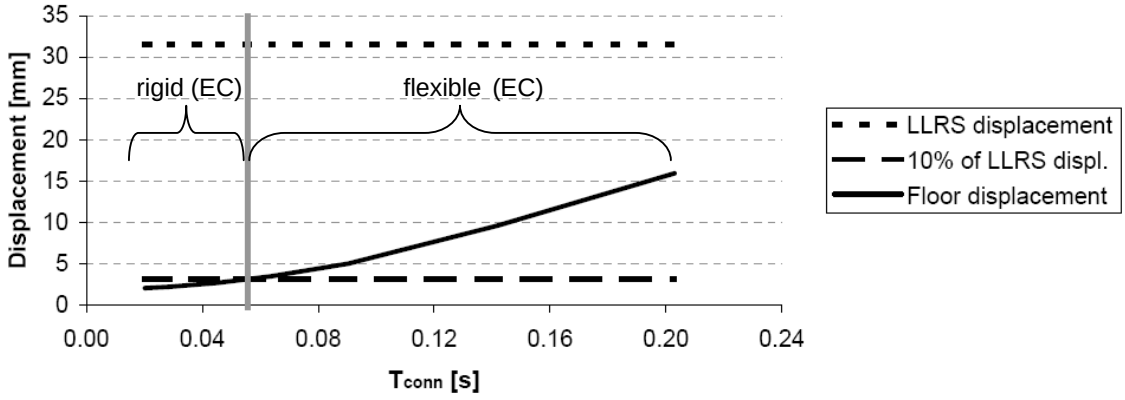

Figure 7.14 – Comparison diaphragm flexibility with different code requirements

The accelerations are shown in Figure 7.15. Again, the SDOF floor models are accurate, but the rigid floor model is not. The accelerations are decreasing with the increasing period. This can be explained by looking at the effective period of the total structure.

$$k_{eff} = \frac{1}{\frac{1}{k_{LLRS}} + \frac{1}{k_{conn}}} = \frac{1}{\frac{1}{14.2} + \frac{1}{23}} = 8.8kN/mm \rightarrow T_{eff} = 0.33s$$

$$k_{eff} = \frac{1}{\frac{1}{k_{LLRS}} + \frac{1}{k_{conn}}} = \frac{1}{\frac{1}{14.2} + \frac{1}{2320}} = 14.1kN/mm \rightarrow T_{eff} = 0.26s$$

This time the connector stiffness is influencing the effective period of the structure. A comparison with the spectral acceleration spectra, as shown in Figure 7.16 shows the period range of the wall structure. The decline in the acceleration is exactly in the period range of the structure.

Figure 7.15 shows that the Median PFA is twice the PGA. This is nearly double that of the frame structure. The spectral acceleration graph, Figure 7.16, shows that for a structure with a period of around 1 second (the frame structure), the design acceleration will be nearly half of the design acceleration for a structure with a period of 0.3 seconds. A rigid floor assumption,

in which case the connectors will be designed for a maximum of one PGA, will severely underestimate the floor accelerations. It can be seen that a design of the connectors for a FAM of 3 is much more realistic.

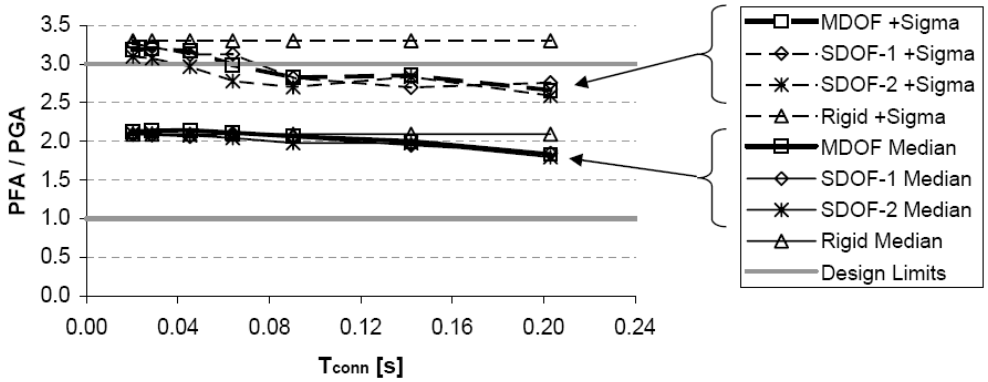

Figure 7.15 – Comparison of floor accelerations of single storey building with wall as LLRS

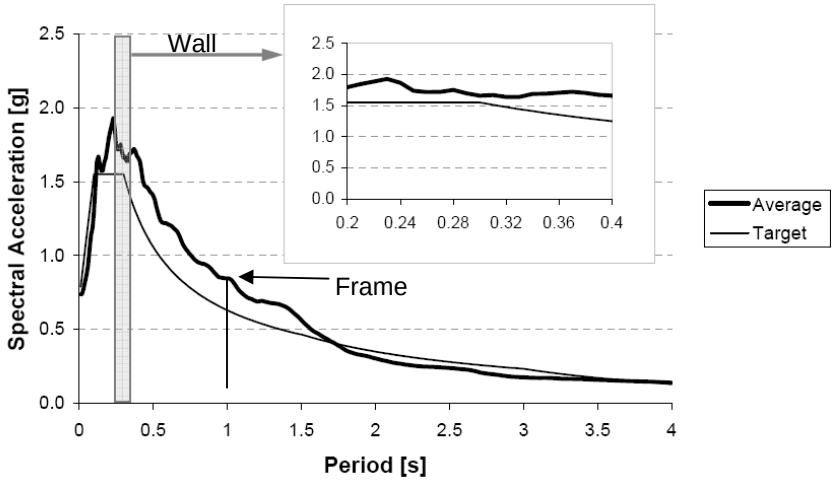

Figure 7.16 – Spectral acceleration graph

Figure 7.17 shows the median shear forces. They show an analogous result as the floor accelerations. The design target, *F = 453kN*, corresponds well with the median shear forces.

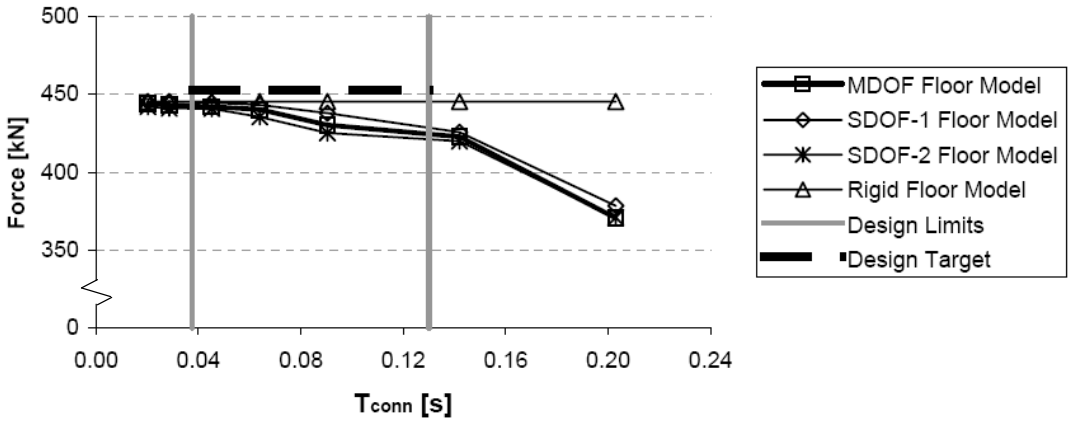

Figure 7.17 – Comparison of median shear force of single storey building with wall as LLRS

7.6 Summary

This chapter showed that for a single storey structure with a low stiffness of the LLRS, like a frame, the influence of the diaphragm flexibility on the seismic design is negligible. The floor diaphragm and the connectors are much stiffer than the LLRS and thus hardly influence displacements, accelerations and shear forces.

For a single storey with a stiff LLRS, like a wall, there is a significant influence of the floor flexibility. For very stiff connectors (inclined screws and FAM = 3) the floor diaphragm can be assumed rigid, as is also stated in the Eurocode. For all other connectors, the flexibility of the floor needs to be taken into account. Only taking the flexibility of the connectors into account is sufficient for an accurate result. Neglecting the floor flexibility can lead to an underestimation of the displacements of up to 23%. This increased displacement can lead to higher demands on gravity columns. It also leads to an underestimation of the floor accelerations, which can be up to twice the PGA (median results) and three times the PGA (+Sigma results).

The Eurocode definition of a flexible diaphragm is much stricter, but seems to be more accurate than the definition provided in the New Zealand standard or the IBC.

8 Numerical analysis of a multi-storey building

The last step in the numerical analysis is to model a multi-storey building. This chapter describes the model and the results of the analysis. A short overview of the displacement based design is given, since it is used for the Ruaumoko model and to determine the strength of the connectors.

8.1 Introduction

A six storey post-tensioned building, shown in Figure 8.1, has been analysed in order to investigate the difference in seismic response between a model with flexible floor diaphragms and a model with a rigid floor diaphragm.

The analysis has been run three times, for a 1/50, 1/500 and a 1/2500 year earthquake. The design spectrum scale factor, according to the New Zealand Standard [2004], is 0.5, 1.0 and 1.8 respectively.

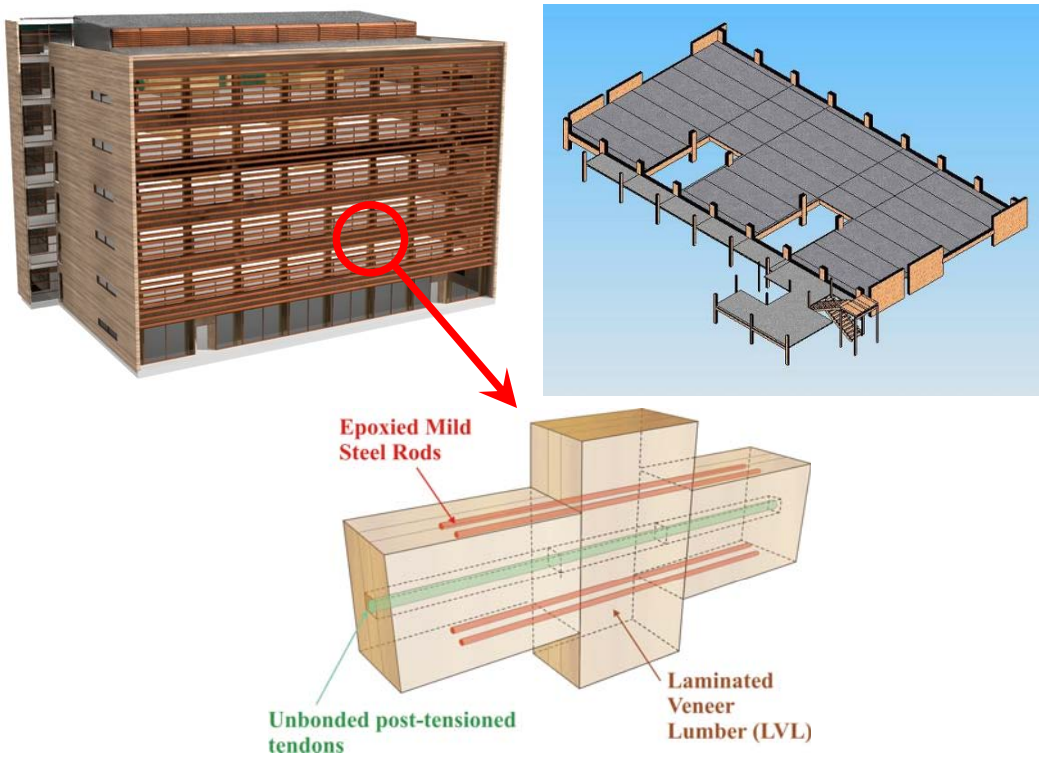

Figure 8.1 – 6 Storey building, artist impression, typical floor plan and connection detail [Newcombe, 2008a; Smith, 2008]

8.2 Displacement Based Design

A displacement based design (DBD) has been performed [Newcombe, 2008b] for a six storey frame building for a 1/500 year earthquake. The calculations showed that the building has an effective period of 2.4 seconds at a design drift of 2%. This results in a design acceleration of 0.188g, as is shown in Figure 8.2. The other parameters and results of the DBD are shown in Table 8.1. The results from this design have been used to determine the strength of the connectors in the analysis.

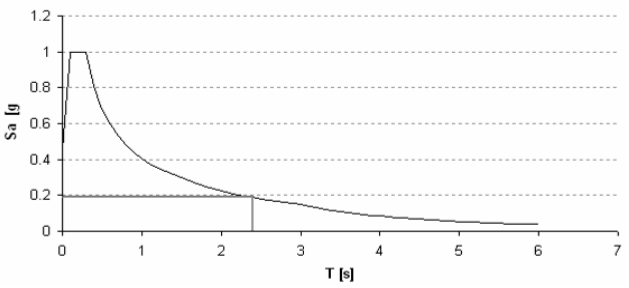

Figure 8.2 – Spectral acceleration for DBD

Table 8.1 – Results DBD for 6 storey building

Storey	Height [m]	Mass (per frame) [kN]	Displacement [m]	Horizontal force (per frame) [kN]	Shear force (per frame) [kN]	Moments (per frame) [kNm]	Drift [%]
6	22.8	1229	0.36	482	482	1583	1.13%
5	19.0	1300	0.31	311	793	1302	1.30%
4	15.2	1300	0.27	262	1054	1733	1.48%
3	11.4	1300	0.21	206	1260	2071	1.65%
2	7.6	1300	0.15	144	1404	2308	1.83%
1	3.8	1300	0.08	75	1480	2432	2.00%
0	0.0	-	0.00	-	1480	3382	-

8.3 Numerical Model

The building is 6 storeys with an interstorey height of 3.8 meter and 5 bays of 7 meters long. Figure 8.3 shows how the mass of the building is modelled for the rigid floor model and for the flexible floor model. All the nodes on a floor are constrained to the same displacement in the horizontal direction, except for the nodes with the floor mass in the flexible model.

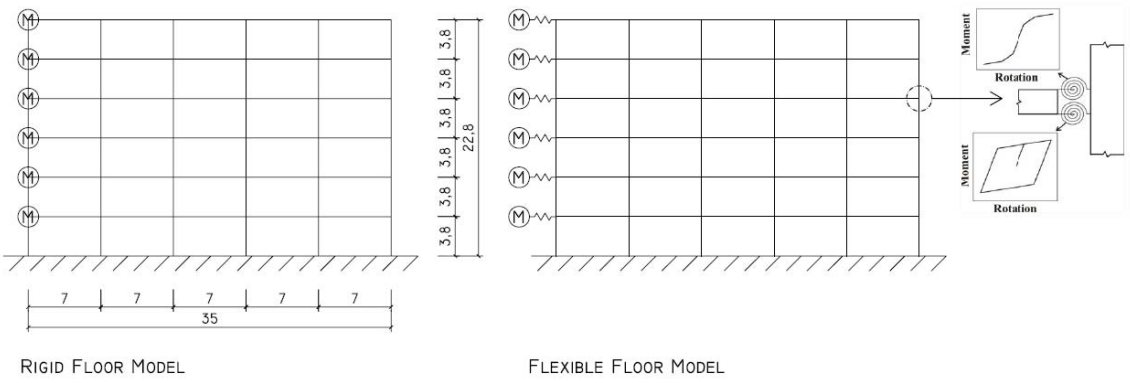

Figure 8.3 – 6 Storey building model with rigid floor and flexible floor assumption

The frame represents a 2D model of one of the frames of the building shown in Figure 8.1. The building is a prototype design for the newly developed building system. Post-tensioning, together with energy dissipaters, create a 'hybrid' system which results in energy dissipating connections with self-centring capacity. This is incorporated in the model using rotational springs at the connections, as shown in Figure 8.3. Some typical sections are shown in Figure 8.4. The model uses a constant damping of 2% for the first and third mode shape. Gravity loads are applied to every node of the frame.

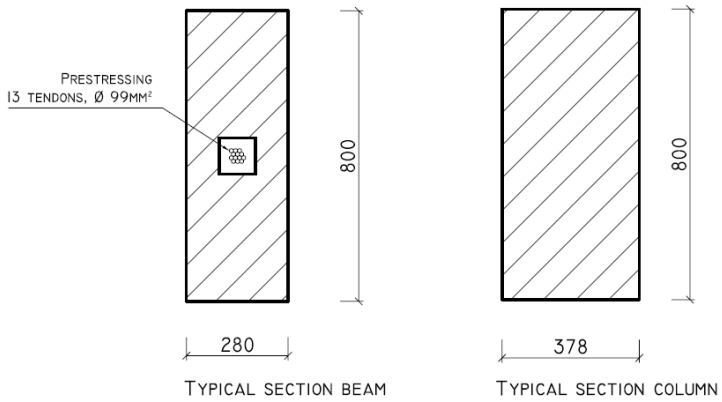

Figure 8.4 – Typical sections of beams and columns

8.4 Design Parameters

For this study, the main design parameters are the properties of the spring element which models the floor deformations. As shown in Chapter 7, the floor system for a frame building can be modelled with just the stiffness of the connectors to get a good prediction of the results. This time the spring is not a linear element, but the hysteresis data from the laboratory testing of the straight timber-to-timber screws (Test 3) has been used.

The required strength of the connectors is determined using the upper limit of the IBC, which is 1 PGA. This results in a horizontal force of 482 kN. This is then amplified by an overstrength factor of 1.3 as described in several building codes (Chapter 2.4.2.) and by Gardiner *et al.* [2008]. The result is a design force of $F_d = 625$ *kN*.

The hysteresis loops have been scaled according to the principles derived in Chapter 6.6 and 6.7. The hysteresis loops and the backbone curve are shown in Figure 8.5. The initial stiffness is 342000 kN/m, the yield displacement is 2 mm and the displacement at the ultimate force is 10 mm. This hysteresis data has been used for all three different earthquake intensities.

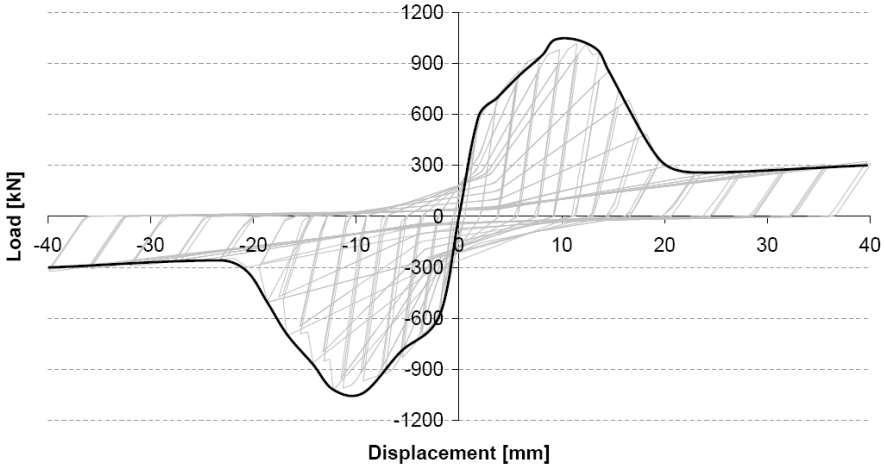

Figure 8.5 – Hysteresis loops used to model the properties of the connectors

8.5 Results

The analysis has been run under the same 15 earthquakes as the other analysis. This time the analysis has been done with a time step of 0.001 seconds. The results are presented as the Median and +Sigma values. A complete overview of the results can be found in Appendix E.

8.5.1 – Drifts and displacements

The analysis gives the displacement of every point of the structure at every time step of the analysis. The maximum displacement at the floor closest to the effective height (which is around the 4th floor) has been selected, and the corresponding displacement profile, see Figure 8.6, is extracted for every earthquake. The inter-storey drift levels are used to show the deflection per floor. They are defined as the inter-storey deflection divided by the storey height, as shown in Figure 8.6. The absolute maximum drift levels of each storey of the frame are extracted from the analysis results. These maxima do not have to occur at the same time and thus may not be at the maximum displacement.

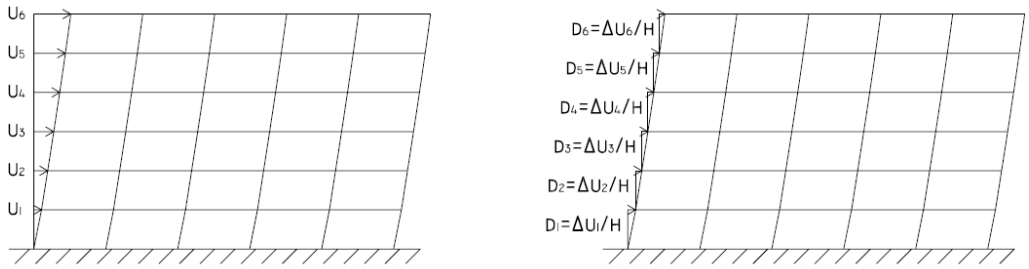

Figure 8.6 – Derivation of the deflections (u) and inter-storey drift levels (D) for the 6 storey building

Figure 8.7 shows the Median frame deflections of the two models at the three different limit states. It can be seen that the different modelling of the floor (rigid or flexible) hardly influences the displacement profile. The displacement according to the DBD fits well with the 1/500 year event displacements; the maximum difference is only 20 mm.

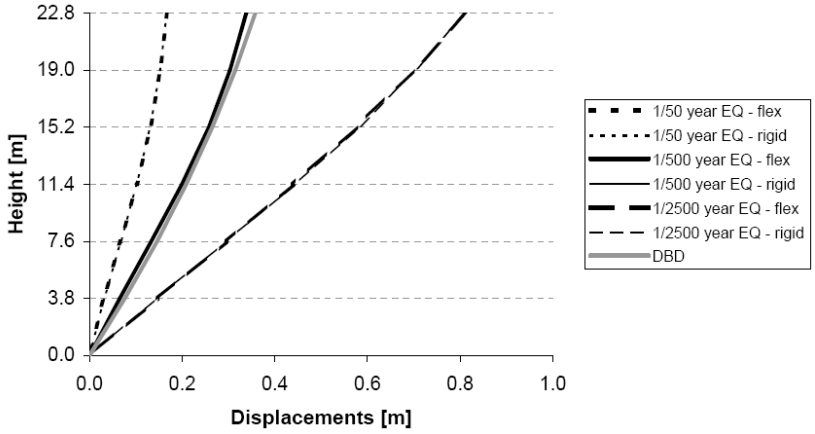

Figure 8.7 – Frame deflections at three different earthquake intensities for the 6 storey building

Figure 8.8 shows the displacement of the six stories over the duration of the earthquake. The displacements are from the third earthquake record and scaled for the 1/500 year event. The insert shows the peak displacements.

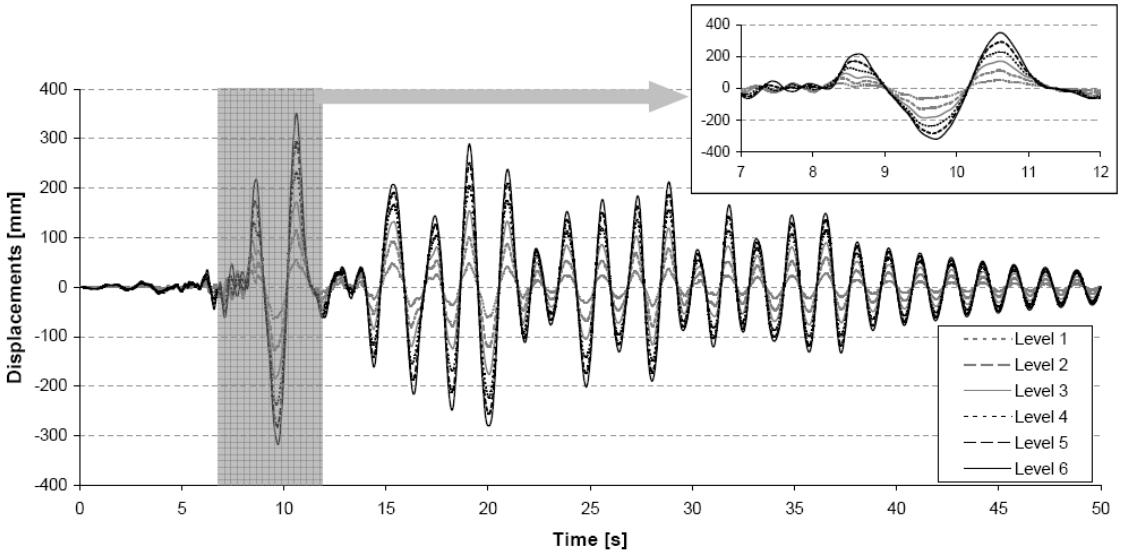

Figure 8.8 – Frame deflections of the 6 stories under the third earthquake record

The maximum drift levels are shown in Figure 8.9. They show an increasing difference between the rigid and flexible floor levels for the stronger earthquakes. The flexible floor reduces the maximum drift as the level of inelasticity increases. This is because more energy is absorbed by the inelastic deformation of the floor.

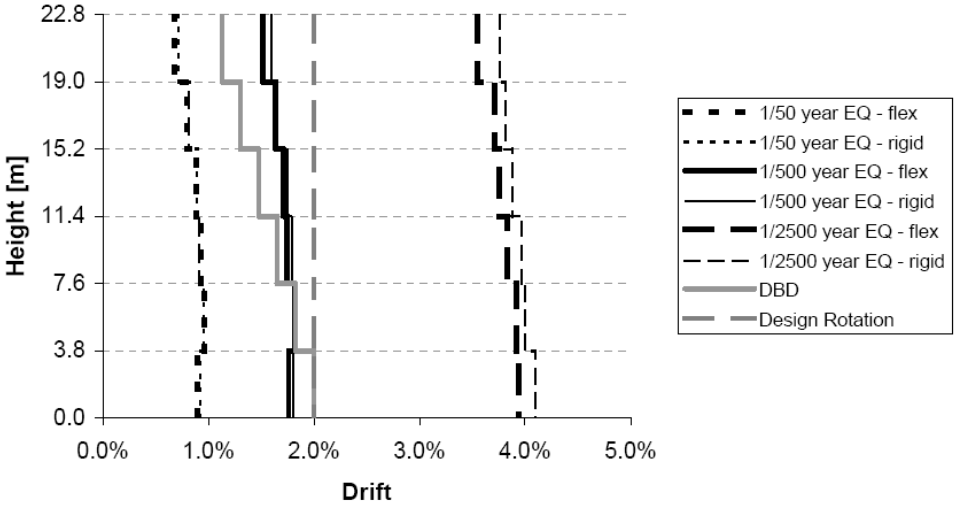

Figure 8.9 –Inter-storey drifts at three limit states for the 6 storey building

The displacement based design, which is for a 1/500 year event, gives a good prediction of the drifts at the lower levels. At the higher levels the drifts are underestimated since the displacement based design does not take higher modes of vibration into account. These higher

mode effects cause additional drifts mainly at the top levels of up to 0.4%. It is not expected that the DBD drift profile will match the 1/500 year EQ results, but rather that a uniform rotational demand (of 2% in this case) is achieved up the height of the structure [Priestley *et al.*, 2007].

The scaling of the 1/500 year earthquakes is twice that of the 1/50 year earthquakes. The drift levels are scaled accordingly since the response is mostly elastic. The 1/2500 year earthquakes are 1.8 times the 1/500 year earthquakes. But the drift levels are increasing by a factor of 2.2. This is due to the inelastic behaviour which occurs during the 1/2500 year earthquakes, which reduces the effective stiffness of the frame system and thus increases the displacements.

8.5.2 – Interstorey shear forces and moments

The shear forces and moments are evaluated for every storey. They are summed at each instant for the 6 columns, as shown in Figure 8.10, and then the maxim value is taken. This can be represented by Equation 8.1 and 8.2.

$$V = MAX\left[V(t)\right], \text{ where } V(t) = \sum_{i=1}^{6} V_i(t) \qquad \textit{Eq. 8.1}$$

$$M = MAX\left[M(t)\right], \text{ where } M(t) = \sum_{i=1}^{6} M_i(t) \qquad \textit{Eq. 8.2}$$

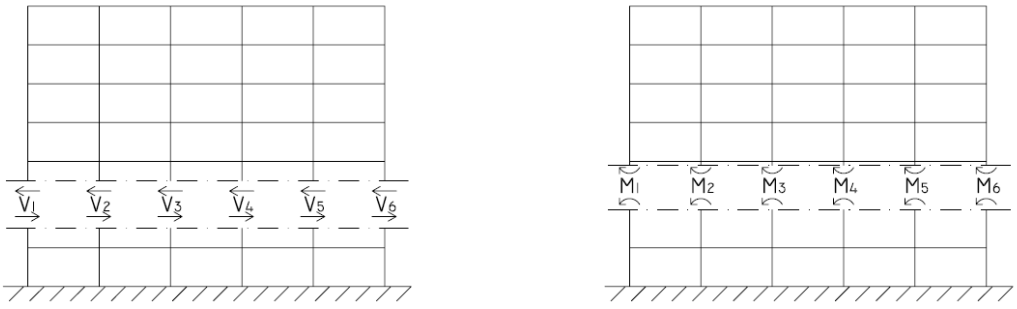

Figure 8.10 –Derivation of the shear force and bending moments for the 6 storey building

The shear force per floor is constant since there is no horizontal loading on the structure between the storeys. The moments are linear across the height of the storey. Therefore the moments are evaluated at the top and bottom of each column. Figure 8.11 shows the shear force distribution over the height of the building. Figure 8.12 shows the moment distribution over the height of the building. The forces and moments of the flexible floor model show the same trend as the drifts, nearly the same at low earthquake intensity and lower at higher intensity earthquakes.

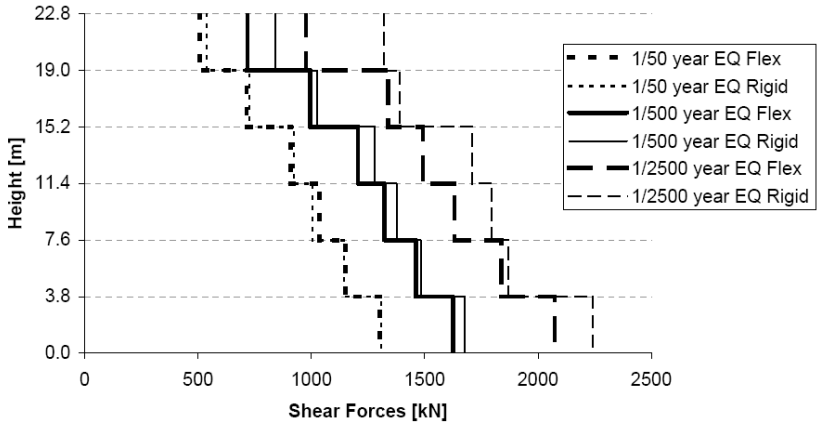

Figure 8.11 – Comparison of shear forces for the 6 storey building

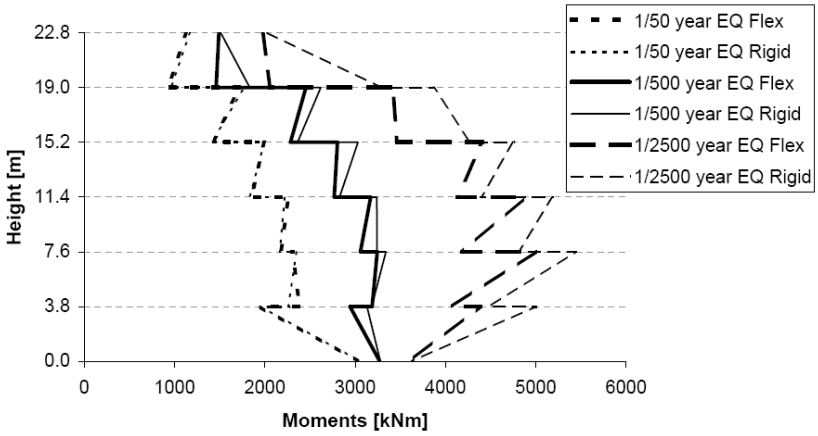

Figure 8.12 – Comparison of bending moments for the 6 storey building

8.5.3 – Floor Accelerations

The peak floor acceleration is a key engineering design parameter for the response of a multi-storey structure to an earthquake. The floor acceleration is strongly dependent on the earthquake intensity. However, it is unclear in this case which intensity measure is most appropriate to show the amplification of the floor acceleration.

It is chosen here to represent the floor accelerations as the ratio of the PFA over the PGA of the corresponding earthquake. This is the most appropriate for (near) rigid diaphragms [Bradley *et al.*, 2008]. This makes that the floor accelerations are all relative to the actual ground acceleration, and thus 1 at ground level, as is shown in Figure 8.13. This figure shows that the 1/50 year event generates relatively large accelerations in the structure, while for the 1/2500 year event the accelerations are mainly less than the ground acceleration. Hence, inelasticity in the floor connectors (see the next paragraph) results in a reduction of the floor accelerations.

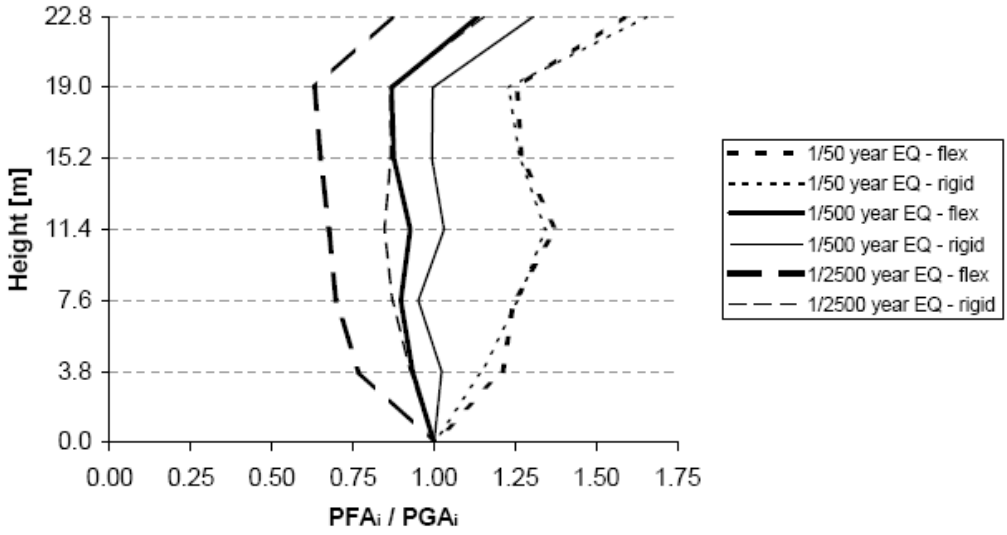

Figure 8.13 – Peak floor acceleration over the peak ground acceleration for the 6 storey building

8.5.4 – Connectors

The flexible model allows investigating of the forces and displacement over the connectors between the floor diaphragm and the LLRS. Figure 8.14 shows the displacement over the connectors in the top floor under the third earthquake, scaled for a 1/500 year event. The connector displacements exceed 2mm, which is the yield limit, but it stays well within the 10 mm, so there is no failure of the connectors. This can also be seen from the hysteresis loops belonging to the connection, which is shown in Figure 8.15.

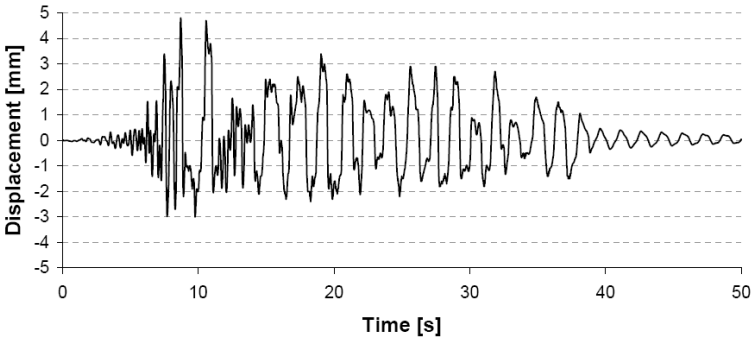

Figure 8.14 – Connector displacement at top floor under the third earthquake record

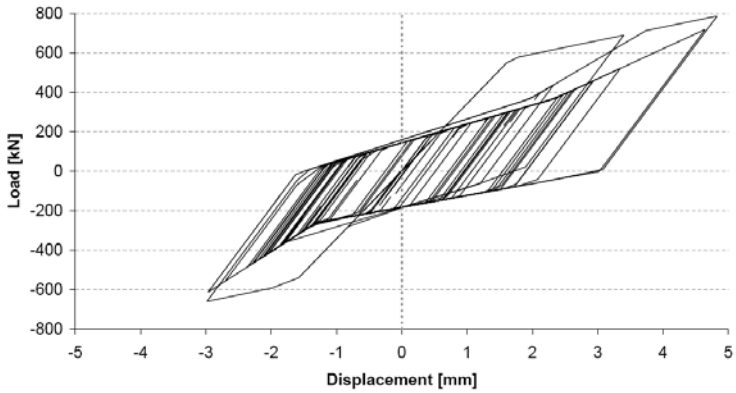

Figure 8.15 – Hysteresis loops of the connector at top level under the third earthquake record

The maximum displacement and corresponding force at each level under each earthquake are examined and plotted in Figure 8.16 to 8.18. It can be seen that under the 1/50 year earthquake the force in the connectors is below the design value of $F_d = 625kN$. This results in an elastic response, which explains why the displacements, drifts, accelerations, shear forces and moments are the same as for the rigid model. Under the 1/500 year earthquake the force in the connectors is larger then the yield force, but not as high as the ultimate force. So the structure stays intact, but has damage in the connectors. During the 1/2500 year earthquake the ultimate force is exceeded in some floors. Ten floors showed displacements over 40mm, which is not shown on the graph. This means that the connectors are broken and possible collapse of the structure occurs.

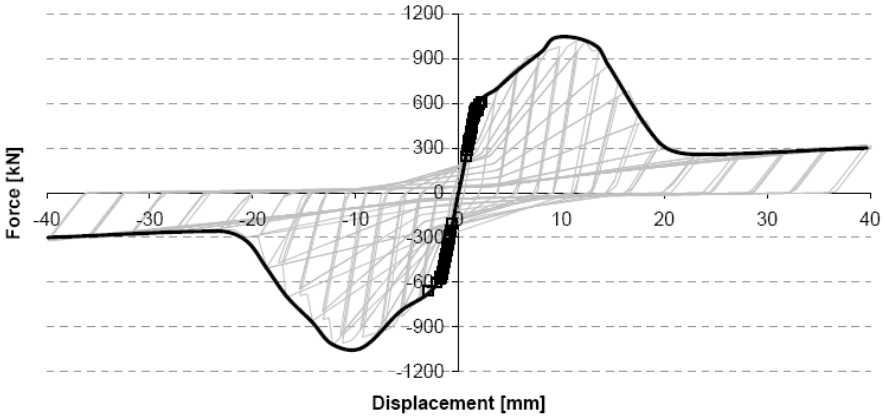

Figure 8.16 – Connector displacement vs. Connector Force for 1/50 year earthquake

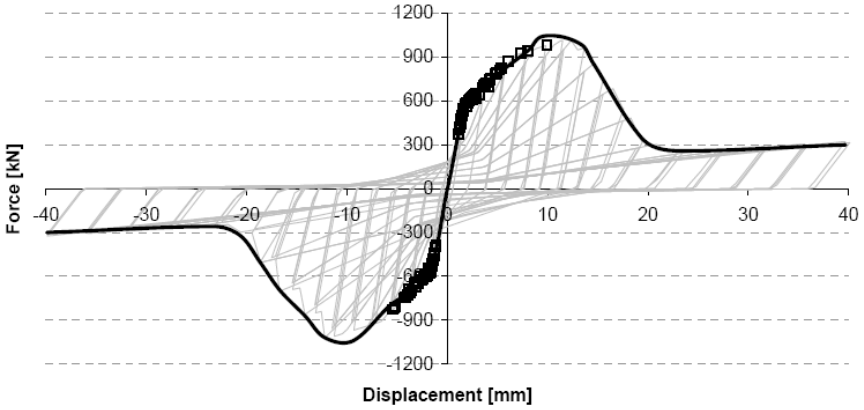

Figure 8.17 – Connector displacement vs. Connector Force for 1/500 year earthquake

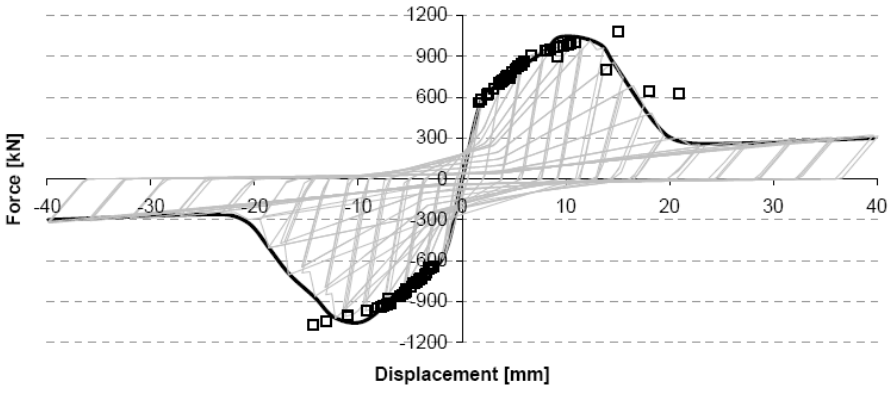

Figure 8.18 – Connector displacement vs. Connector Force for 1/2500 year earthquake

8.5.5 - Acceleration Response Spectra

The design ground acceleration spectrum is used to determine the seismic response of a SDOF representation of a structure. In the previous chapters it was concluded that the floor flexibility could be idealized as a spring, with the stiffness of the connectors, attached to a single mass which represents the mass of the floor. This idealization gives a SDOF system. Therefore the response of the flexible floor can be evaluated with the help of a floor acceleration spectrum. The difference with the design ground acceleration spectrum is that the floor is not directly connected to the ground. So the floor does not experience the ground motion, but a motion which is filtered by the structure. This motion varies on each level of the structure.

Figure 8.19 shows three graphs show the spectral acceleration at each level in the structure. Also shown are several periods, which are listed in Table 8.2. The first, second and third natural periods of the structure follow from the numerical analysis. The period of the connectors is calculated with Eq. 6.27 where M is the mass of one floor and K_{conn} is the initial stiffness of the connectors.

Table 8.2 – Overview of periods

Description	Period [s]
First natural period	1.53
Second natural period	0.50
Third natural period	0.26
Connector period	0.12

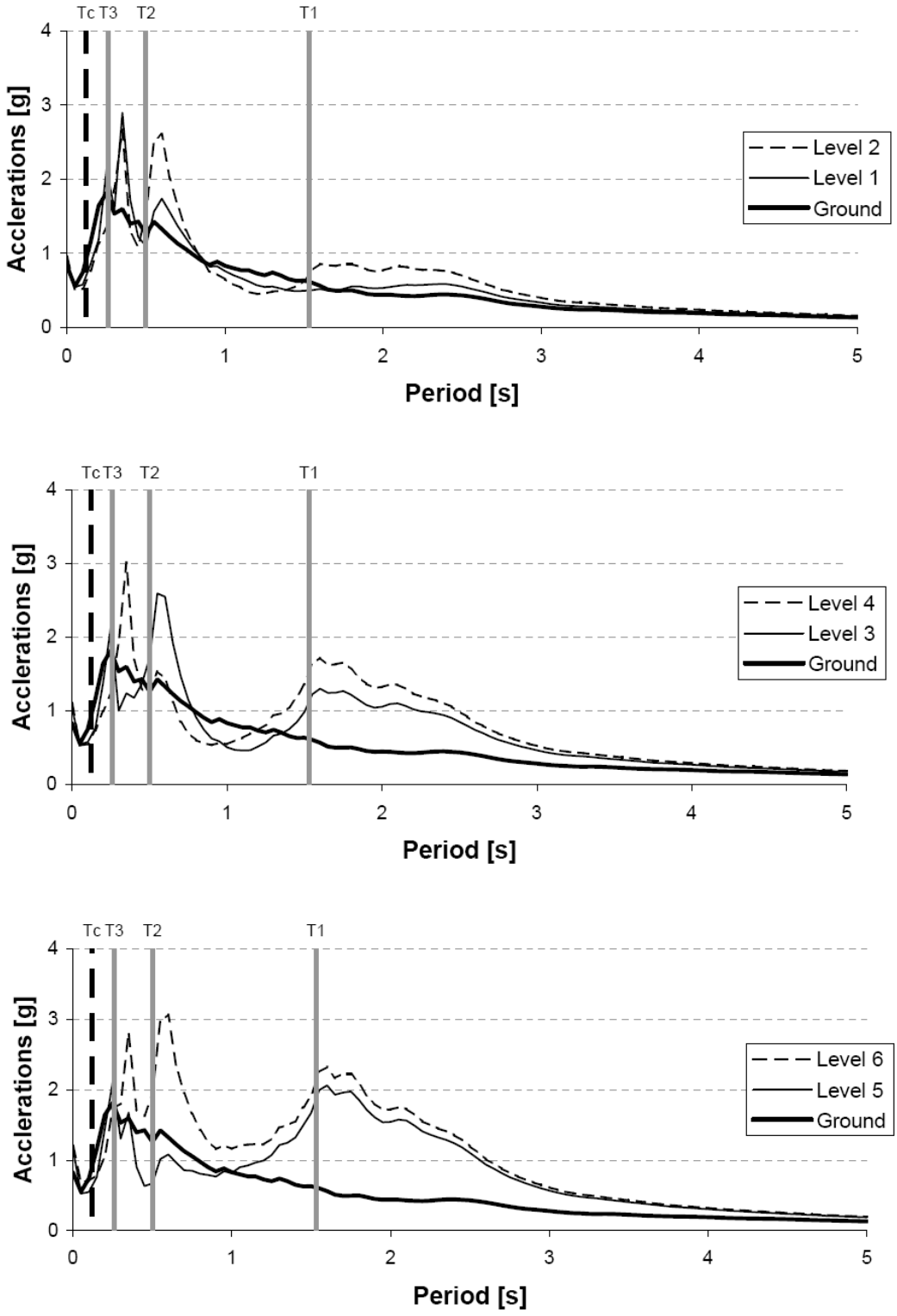

Figure 8.19 – Floor acceleration spectra at the levels 1 & 2, 3 & 4 and 5 & 6 of the building

The first three normal modes of vibration are shown in Figure 8.20. The mode shapes have been multiplied by the percentage of the effective mass that is associated with each mode shape. These percentages are 82%, 11% and 4% respectively. It can be seen that the first mode is dominant and that the influence of the third mode is only minor.

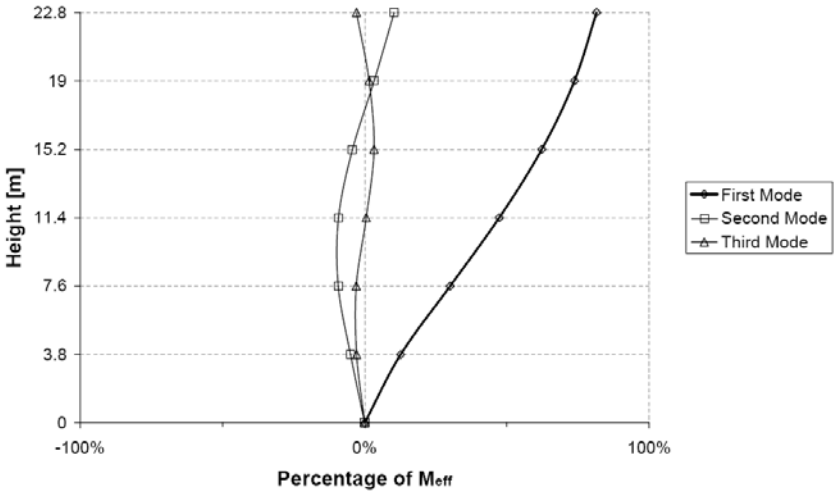

Figure 8.20 – Three normal modes of vibration

The first natural period of the structure is 1.53 seconds. The graphs in Figure 8.19 show a distinct spike in the spectral acceleration near this period. Another distinct spike can be seen close to the second natural period of 0.50 seconds and close to the third natural period of 0.26 seconds. Figure 8.21 shows the peak values of these two spikes divided by the ground acceleration for each level. It can be seen that these spikes correspond with the first, second and third mode of vibration. The second period response seconds shows little amplification at the 4th and 5th level, which is characteristic for the second mode of response. The peak value of 4 means that a SDOF system with a period of 1.6 seconds, attached to the sixth floor, has an acceleration of 4 times the ground design acceleration for the same SDOF system. However, it is demonstrated in Chapter 6, that the period of the connectors is much less.

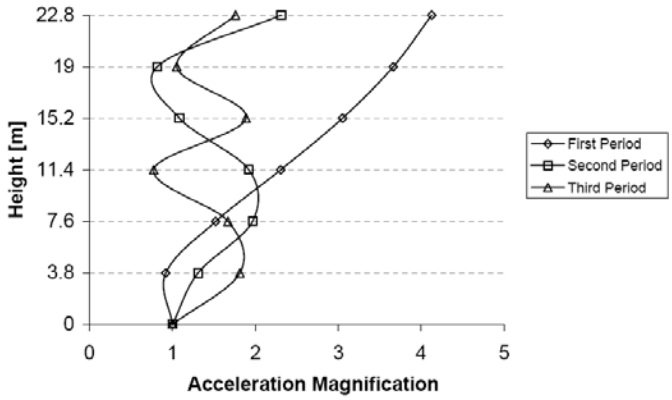

Figure 8.21 – Floor acceleration magnifications

The spectral acceleration graphs give the response of a SDOF system which would be attached to the frame of the structure at each level. This is exactly how the floor has been idealised as shown in Chapter 7. The period of the connectors, which represent the floor, is also shown in Figure 8.20. It can be seen that there are no major differences in the spectral acceleration of the floor motion at the period of the connectors. Therefore the floor connectors can be designed according to the design spectral acceleration of the ground motion with minor inaccuracies.

In general it can be concluded that the design spectral acceleration can be used for the design as long as the period of the floor is not near the first, second or third period of the structure. This can also be seen in Figure 7.15 and 7.16, where the floor accelerations follow the ground accelerations. Therefore, although it is appropriate to design the floor diaphragm according to the design acceleration spectrum for the ground motion for frames, it may not be the case for walls. The increased stiffness, and thus lower period, of inclined screws might make a difference for the seismic response of multi-storey wall structures. More investigation is needed in that area.

8.6 Summary

From the previous analysis it can be concluded that the influence of the floor flexibility on the seismic response of a multi-storey post-tensioned timber building with a frame as LLRS is small. The extra displacement in the floors is negligible compared to the displacement in the LLRS. Only under major earthquakes, where the connectors between the floor diaphragm and the LLRS show a ductile behaviour, there is a reduction in the seismic response. This means that neglecting the influence of the diaphragm stiffness is a conservative approach.

The median floor accelerations can be up to a factor 1.5 higher then the PGA. The top floor of the structure shows a severe increase in accelerations. The influence of the floor flexibility is only apparent if the connectors start yielding, which is the case for the 1/500 and 1/2500 year earthquake. The inelasticity in the floor connectors reduces the floor accelerations. The factor of 1.5 times the PGA is lower compared to the factor of 2, which was found for the wall structure in Chapter 7.5.2.

The inelastic modelling in this chapter results in a lower seismic response than the elastic modelling. This was expected since the inelasticity leads to energy dissipation which decreases the seismic response.

The design of the connectors between the LLRS and the floor can be done with the help of the design spectral acceleration, as long as the period of the floor is not near the first, second or third period of the structure. This is the case for the six storey frame structure which has been used in this chapter. But it is questionable whether this is the case for a structure with a wall as LLRS. In that case the stiffness of the connectors can make a difference.

9 Conclusions

The influence of the floor flexibility on the seismic response of post-tensioned timber buildings, in most cases, is small. In these cases, assuming a rigid diaphragm is a conservative design approach as floor flexibility reduces the displacement demands on a building. However, for structures with a stiff LLRS (like walls) and flexible floors there can be a significant amplification of building displacements. For these designs, it is sufficient to model the uni-direction floor response as SDOF system with the stiffness of the diaphragm connectors. Including the flexibility of the floor diaphragm is not required. Table 9.1 gives an overview of the different analyses which have been performed in this report and how the floor flexibility can be modelled under different options.

The experimental testing showed that the stiffness of connections between the diaphragm and the LLRS with inclined screws, 80 kN/mm, were approximately four times stiffer than connections with straight screws, 20 kN/mm. The strength of the timber-to-concrete connection with inclined screws was nearly double the strength of the same connection with straight screws. This difference was not observed for the timber-to-timber connections. The experimental testing showed that the rope effect can not be taken fully into account for the estimation of the strength of the connectors under cyclic loading.

It is recommended that the design spectral acceleration is used for the design of the connectors between the floor diaphragm and the LLRS. This predicts the floor accelerations more accurately than a design using the PGA. Only the stiffness of the connectors needs to be taken into account for the determination of the period of vibration of the floor system.

If a detailed analysis of the floor unit is needed, then for short spans the floor flexibility can be described using just the stiffness of the connectors. For long spans (> 6m), a spring with the combined stiffness of the connectors and diaphragm can be used.

Table 9.1 – Overview of how the floor flexibility can be modelled

Type of analysis	**Options**	**Modelling of floor flexibility**
Multi-storey (6) building	- LLRS = frame	Rigid floor
	- LLRS = wall - inclined screws	Rigid floor (*)
	- straight screws	Connectors (*)
Single-storey building	- LLRS = frame	Rigid floor
	- LLRS = wall - inclined screws	Rigid floor
	- straight screws	Connectors
Detailed floor analysis	- small span (< 6m)	Connectors
	- large span (> 6m)	Connectors and floor diaphragm

** = more research needed in this area*

10 Recommendations for further research

The use of inclined screws in timber-to-timber and timber-to-concrete connections seems very promising due to the high initial stiffness. But very little information is available about the behaviour of such a joint under cyclic loading. More research could result in a better understanding of the strength and stiffness of the fasteners in tension and compression. It is likely that if fully threaded screws are used, inclined screws will also activate in compression.

Only a 2D numerical analysis of a 6 storey building with frames as LLRS was performed. A 2D analysis of a 6 storey structure with walls as LLRS is needed to evaluate the possible amplification which can occur when the period of the second mode of vibration is close to the period of the connectors. A 3D numerical analysis of different multi-storey timber buildings could be made to validate the conclusions made in this report.

11 References

ACI Committee 318 [2005]. "Building code requirements for structural concrete and commentary (ACI 318M-05)". American Concrete Institute, Farmington Hills, Mich., 436.

ASTM [2003]. "Standard Test Method for Determining Bending Yield Moment of Nails". F1575-03, ASTM International.

Bejtka, I., Blaß H. J. [2002]. "Joints with inclined screws". *CIB Working commision W18 - Timber structures*, Vol. Meeting 35, Kyoto, Japan.

Bradley, B. A., Dhakal, R. P., Curbinovski, M., and MacRae, G. A. [2008]. "Prediction of spatially distributed seismic demands in structures". 14th World Conference on Earthquake Engineering, Beijing, China.

Brignola, A., Podestà, S., and Pampanin, S. [2008a]. "In-plane stiffness of wooden floor". NZSEE Conference, Wairakei, New Zealand.

Brignola, A., Podestà, S., and Pampanin, S. 2008b. In-plane stiffness of wooden floors. *New Zealand Society of Earthquake Engineering Conference*, Wairaki, New Zealand.

Buchanan, A. H. [2007]. "Timber Design Guide", New Zealand Timber Industry Federation, Wellington, N.Z.

Buchanan, A. H., Deam, B. L., Fragiacomo, M., Pampanin, S., and Palermo, A. [2008]. "Multi-Storey Prestressed Timber Buildings in New Zealand". *Structural Engineering International*, Vol. 18, 166-173.

Carr, A. J. [2008]. "Ruaumoko". University of Canterbury, Christchurch, New Zealand.

CEN [2001]. "Timber structures - Test methods - Cyclic testing of joints made with mechanical fasteners". EN 12512, Brussels, Belgium, 13.

CEN [2004a]. "Eurocode 2 : Design of concrete structures - Part 1-1: General rules and rules for buildings". EN1991-1-1:2004 (E), European Committee for Standardization, Brussels, Belgium, 225.

CEN [2004b]. "Eurocode 5 : Design of timber structures - Part 1-1: General - Common rules and rules for buildings". EN1995-1-1:2004 (E), European Committee for Standardization, Brussels, Belgium, ii, 123.

CEN [2004c]. "Eurocode 5 : Design of timber structures - Part 2: Bridges". EN1995-2:2004 (E), European Committee for Standardization, Brussels, Belgium, 29.

CEN [2004d]. "Eurocode 8 : Design of structures for earthquake resistance - Part 1: General rules, seismic actions and rules for buildings". EN1998-1:2004 (E), European Committee for Standardization, Brussels, Belgium, 229.

CEN [2006]. "Timber structures - Calculation of characteristic 5-percentile values and acceptance criteria for a sample". EN 14358, Brussels, Belgium, 8.

Chopra, A. K. [2008]. "Dynamics of structures : theory and applications to earthquake engineering", Prentice Hall, Upper Saddle River, NJ.

Deam, B. L., Fragiacomo, M., Buchanan, A. H. [2007]. "Connections for composite concrete slab and LVL flooring systems". *Materials and Structures (2008)*, Vol. 41, 495-507.

Dias, A. M. P. G. [2005]. "Mechanical behaviour of timber-concrete joints," PhD Thesis, Faculty of Civil Engineering and Geosciences, Delft University of Technology, Delft, The Netherlands.

FEMA 450 [2003]. "The 2003 NEHRP recommended provisions for seismic regulations of new buildings. Part 1: Provisions", Federal Emergancy Management Agency, Washington.

Fleischman, R. B., and Farrow, K. T. [2001a]. "Dynamic behavior of perimeter lateral-system structures with flexible diaphragms". *Earthquake Engineering & Structural Dynamics*, Vol. 30, 745-763.

Fleischman, R. B., and Farrow, K. T. [2001b]. "Dynamic behavior of perimeter lateral-system structures with flexible diaphragms". *Earthquake Engineering and Structural Dynamics*, Vol. 30, pp. 745-763.

Gardiner, D. R., Bull, D. K., and Carr, A. J. [2008]. "Internal forces of concrete floor diaphragms in multi-storey buildings". NZSEE Conference, Wairakei, New Zealand.

Hall, J. F. [1995]. "Northridge Earthquake of January 17, 1994, Reconnaissance Report, vol 1". *Publication 95-03*, Earthquake Spectra.

IBC [2003]. "International Building Code", International conference of building officials, Whitter, CA, 2003.

International Code Council. [2003]. "International building code", The Council, Falls Church, Va.

ISO [2007]. "Timber structures - Static and cyclic lateral load test method for shear walls". CD 21581, Geneva, Switzerland, 12.

Iverson, J. K., and Hawkins, N. M. [1994a]. "Performance of precast/prestressed concrete building structures during Northridge earthquake". *PCI journal*, Vol. 39, 38-55.

Iverson, J. K., and Hawkins, N. M. [1994b]. "Performance of precast/prestressed concrete building structures during Northridge earthquake". *PCI Journal*, Vol. 39, pp. 38-55.

Kavaliauskas, S., Kazimieras Kvedaras, A., Valiūnas, B. [2007]. "Mechanical behaviour of timber-to-concrete connections with inclined screws". *Journal of Civil Engineering and Management*, Vol. Vol XIII.

Le Heux, M. [2008]. "Floor Diaphragm Flexibility in Timber Buildings," Third Professional Year Project, Department of Civil Engineering, University of Canterbury, Christchurch, New Zealand.

Lee, H. J., Kuchma, D., and Aschheim, M. A. [2007]. "Strength-based design of flexible diaphragms in low-rise structures subjected to earthquake loading". *Engineering Structures*, Vol. 29, 1277-1295.

Linden, M. v. d. [1999]. "Timber-concrete composite floor systems," PhD Thesis, Faculty of Civil Engineering and Geosciences, Delft University Press, Delft, The Netherlands.

Lukaszewska, E., Johnsson, H., and Fragiacomo, M. [2007]. "Performance of connections for prefabricated timber–concrete composite floors". *Materials and Structures*, Vol. 41.

Nakaki, S. D. [2000]. "Design guidelines for precast and cast-in-place concrete diaphragms", Earthquake Engineering Research Institute, Oakland, California.

Newcombe, M. P. [2008a]. "Seismic Design of Post-Tensioned Timber Frames". 14th World Conference in Earthquake Engineering, Beijing, China.

Newcombe, M. P., Pampanin, S., Buchanan, A.H., and Palermo, A. [2008b]. "Seismic Design of Multi-storey Post-Tensioned Timber Buildings," Masters Thesis, University of Pavia, Pavia, Italy.

Palermo, A., Pampanin, S., and Buchanan, A. H. [2006]. "Experimental Investigations on LVL seismic resistant wall and frame subassemblies". First European Conference on Earthquake Engineering and Seismology, Geneva, Switzerland.

Priestley, M. J. N., Calvi, G. M., and Kowalsky, M. J. [2007]. "Displacement-based seismic design of structures", IUSS PRESS, Pavia, Italy.

Reinoso, E., and Miranda, E. [2005]. "Estimation of floor acceleration demands in high-rise buildings during earthquakes". *The Structural Design of Tall and Special Buildings*, Vol. 14.

Rivera, J. A. [2008]. "On the development of seismic design forces for flexible floor diaphragms in Reinforced concrete wall buildings," Ph.D. Thesis, University of Pavia, Italy.

Rodriguez, M. E., Restrepo, J. I., and Carr, A. J. [2002]. "Earthquake-induced floor horizontal accelerations in buildings". *Earthquake Engineering and Structural Dynamics*, Vol. 31, pp. 693-718.

Seibold, E. [2004]. "Feasibility Study for Composite Concrete/timber Floor Systems Using Laminated Veneer Lumber in New Zealand," Department of Civil Engineering, University of Canterbury, Christchurch, New Zealand.

Sika Ltd [2008]. "Sika® Grout GP", New Zealand.

Smith, T. [2008]. "Feasibility of Multi Storey Post Tensioned Timber Buildings: Detailing, Cost and Construction," Masters Thesis, Department of Civil Engineering, University of Canterbury, New Zealand.

Spooner, M. S. [2008]. "Quantifying the Dynamic Response of Flexible Floor Diaphragms," Third Professional Year Project, Department of Civil Engineering, University of Canterbury, Christchurch, New Zealand.

Standards New Zealand [1993]. "3063 - Timber structures standard". Standards New Zealand, Wellington, New Zealand.

Standards New Zealand [2004]. "1170.5 - Structural Design Actions Part 5: Earthquake Actions - New Zealand". Standards New Zealand, Wellington, New Zealand.

Standards New Zealand [2006]. "3061 - Concrete structures standard". Standards New Zealand, Wellington, New Zealand.

UBC [1997]. "Uniform Building Code", International conference of building officials, Whitter, CA, 1997

Yeoh, E. C., Fragiacomo, M., Buchanan, A. H., Crews, K., Haskell, J., and Deam, B. L. [2008]. "Development of semi-prefabricated timber-concrete composite floors in Australasia". 10th World Conference of Timber Engineering, Miyazaki, Japan.

Appendix A – Calculations connection strength

Test 1 - Strength evaluation according to EC5

Steel to timber connections failure modes c,d and e

Steel fastener properties

diameter $d := 5.43mm$

Yield strength $f_y := 396 \frac{N}{mm^2}$

Yield moment $M_{yRk} := 8460N \cdot mm$

Timber properties

thickness $t_1 := 45mm$

embedment strength $f_{hk} := 32 \frac{N}{mm^2}$

density $\rho := 600$

angle to the grain $\alpha := 90deg$

effective number of screws $n_{ef} := 1$

pointside penetration length $l_{ef} := t_1 - d = 40$

withdrawal capacity $f_{ax} := \frac{0.0036 \cdot \rho^{1.5}}{(\sin(\alpha))^2 + 1.5 \cdot (\cos(\alpha))^2} = 52.9 N/mm^2$

(EN1995-1-1 art. 8.7.2)

$F_{ax} := n_{ef} \cdot (\pi \cdot d \cdot l_{ef})^{0.8} \cdot f_{ax} = 9.8\,kN$

Calculation EN1995-1-1 art. 8.2.3

$F := \frac{F_{axRk}}{4} = 2.5 \cdot kN$

(mode c) $F_{vRk1} := f_{hk} \cdot t_1 \cdot d = 7.8 \cdot kN$

(mode d) $F_{vRk2} := f_{hk} \cdot t_1 \cdot d \cdot \left(\sqrt{2 + 4 \frac{M_{yRk}}{f_{hk} \cdot d \cdot t_1^2}} - 1 \right) = 3.5 \cdot kN$

$F_{vRk2b} := \begin{cases} F_{vRk2} \cdot 2 & \text{if } (F > F_{vRk2}) \\ (F_{vRk2} + F) & \text{otherwise} \end{cases}$ $F_{vRk2b} = 5.95 \cdot kN$ *(rope effect)*

(mode e) $F_{vRk3} := 2.3 \cdot \sqrt{M_{yRk} \cdot f_{hk} \cdot d} = 2.8 \cdot kN$

$F_{vRk3b} := \begin{cases} F_{vRk3} \cdot 2 & \text{if } (F > F_{vRk3}) \\ (F_{vRk3} + F) & \text{otherwise} \end{cases}$ $F_{vRk3b} = 5.2 \cdot kN$ *(rope effect)*

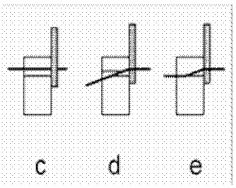

Overview

	Without rope effect	With rope effect
Mode c	$F_{vRk1} = 7.8 \cdot kN$	---
Mode d	$F_{vRk2} = 3.5 \cdot kN$	$F_{vRk2b} = 6.0 \cdot kN$
Mode e	$F_{vRk3} = 2.8 \cdot kN$	$F_{vRk3b} = 5.2 \cdot kN$

Test 2 - Strength evaluation for inclined screws *[Kavaliauskas et al.]*

Steel fastener properties

diameter $d := 4.96mm$

Yield strength $f_y := 1387 \frac{N}{mm^2}$

Yield moment $M_{yRk} := 22560N \cdot mm$

Timber properties

thickness $t := 35mm$ *(t is the depth of the screw perpendicular in the timber member)*

embedment strength $f_{hk} := 32 \frac{N}{mm^2}$

friction $\mu := 0.25$ *(assumed)*

density $\rho := 600$

angle to the grain $\alpha := 45deg$

withdrawal capacity $f_{ax} := \frac{0.0036 \rho^{1.5}}{(\sin(\alpha))^2 + 1.5 \cdot (\cos(\alpha))^2} = 42.3\ N/mm^2$

Calculation

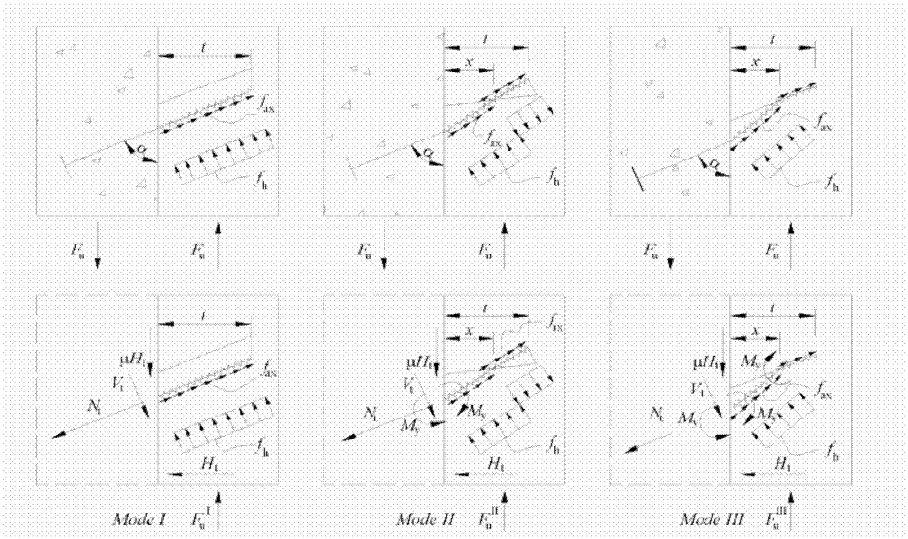

(mode 1) $F_{vRk1} := f_{ax} \cdot d \cdot t \cdot (\cot(\alpha) + \mu) + f_{hk} \cdot t \cdot d \cdot (1 - \mu \cdot \cot(\alpha)) = 13.3 \cdot kN$

(mode 2) $F_{vRk2} := f_{ax} \cdot d \cdot t \cdot (\cot(\alpha) + \mu) + (1 - \mu \cdot \cot(\alpha)) \cdot \left(\sqrt{2} \cdot \sqrt{\frac{M_{yRk}}{f_{hk} \cdot d \cdot t^2} + 1} - 1 \right) \cdot f_{hk} \cdot d \cdot t = 11.2 \cdot kN$

(mode 3) $F_{vRk3} := f_{ax} \cdot d \cdot t \cdot (\cos(\alpha) + \mu) + 2 \sqrt{M_{yRk} \cdot f_{hk} \cdot d} \cdot (\sin(\alpha) - \mu \cdot \cos(\alpha)) = 9.0 \cdot kN$

Test 3 - Strength evaluation according to EC5

Timber to timber connections failure modes a,b,c,d,e and f

Steel fastener properties

diameter $d := 5.18mm$

Yield strength $f_y := 1010\frac{N}{mm^2}$

Yield moment $M_{yRk} := 18720N\cdot mm$

Timber properties

thickness $t_1 := 77mm$ $t_2 := 48mm$

embedment strength $f_{hk1} := 32\frac{N}{mm^2}$

$f_{hk2} := 32\frac{N}{mm^2}$ $\beta := \frac{f_{hk1}}{f_{hk2}} = 1$

density $\rho := 600$

angle to the grain $\alpha := 90deg$

effective number of screws $n_{ef} := 1$

pointside penetration length $l_{ef} := t_2 - d = 43\cdot mm$

withdrawal capacity $f_{ax} := \frac{0.0036\rho^{1.5}}{(\sin(\alpha))^2 + 1.5\cdot(\cos(\alpha))^2} = 52.9\,N/mm^2$

(EN1995-1-1 art. 8.7.2)

$F_{ax} := n_{ef}\cdot(\pi\cdot d\cdot l_{ef})^{0.8}\cdot f_{ax} = 9.9\,kN$

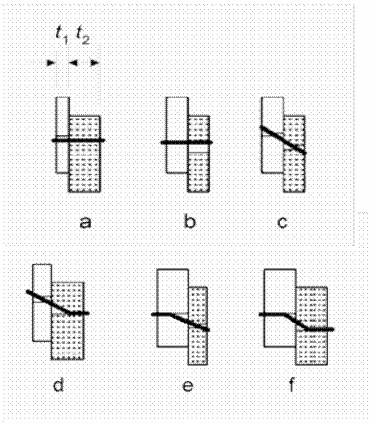

Calculation EN1995-1-1 art. 8.2.2

$F := \frac{F_{axRk}}{4} = 2.5\cdot kN$

(mode a) $F_{vRk1} := f_{hk1}\cdot t_1\cdot d = 12.8\cdot kN$

(mode b) $F_{vRk2} := f_{hk2}\cdot t_2\cdot d = 8.0\cdot kN$

(mode c) $F_{vRk3} := \frac{f_{hk1}\cdot t_1\cdot d}{1+\beta}\cdot\left[\sqrt{\beta + 2\cdot\beta^2\cdot\left[1 + \frac{t_2}{t_1} + \left(\frac{t_2}{t_1}\right)^2\right] + \beta^3\cdot\left(\frac{t_2}{t_1}\right)^2} - \beta\cdot\left(1 + \frac{t_2}{t_1}\right)\right] = 4.5\cdot kN$

$F_{vRk3b} := \begin{cases} F_{vRk3}\cdot 2 & \text{if } (F > F_{vRk3}) \\ (F_{vRk3} + F) & \text{otherwise} \end{cases}$ $F_{vRk3b} = 7.0\cdot kN$ *(rope effect)*

(mode d) $F_{vRk4} := 1.05\cdot\frac{f_{hk1}\cdot t_1\cdot d}{2+\beta}\cdot\left[\sqrt{2\cdot\beta\cdot(1+\beta) + \frac{4\cdot\beta\cdot(2+\beta)\cdot M_{yRk}}{f_{hk1}\cdot d\cdot t_1^2}} - \beta\right] = 4.7\cdot kN$

$F_{vRk4b} := \begin{cases} F_{vRk4}\cdot 2 & \text{if } (F > F_{vRk4}) \\ (F_{vRk4} + F) & \text{otherwise} \end{cases}$ $F_{vRk4b} = 7.2\cdot kN$ *(rope effect)*

(mode e) $F_{vRk5} := 1.05\cdot\frac{f_{hk1}\cdot t_2\cdot d}{2+\beta}\cdot\left[\sqrt{2\cdot\beta^2\cdot(1+\beta) + \frac{4\cdot\beta\cdot(1+2\cdot\beta)\cdot M_{yRk}}{f_{hk1}\cdot d\cdot t_2^2}} - \beta\right] = 3.18\cdot kN$

$F_{vRk5b} := \begin{cases} F_{vRk5}\cdot 2 & \text{if } (F > F_{vRk5}) \\ (F_{vRk5} + F) & \text{otherwise} \end{cases}$ $F_{vRk5b} = 5.7\cdot kN$ *(rope effect)*

(mode f) $F_{vRk6} := 1.15 \cdot \sqrt{\frac{2 \cdot \beta}{1 + \beta}} \cdot \sqrt{2 M_{yRk} \cdot f_{hk1} \cdot d} = 2.9 \cdot kN$

$$F_{vRk6b} := \begin{cases} F_{vRk6} \cdot 2 & \text{if } (F > F_{vRk6}) \\ (F_{vRk6} + F) & \text{otherwise} \end{cases} \qquad F_{vRk6b} = 5.3 \cdot kN \qquad \textit{(rope effect)}$$

Overview

	Without rope effect	With rope effect
Mode a	$F_{vRk1} = 12.8 \cdot kN$	---
Mode b	$F_{vRk2} = 8.0 \cdot kN$	---
Mode c	$F_{vRk3} = 4.5 \cdot kN$	$F_{vRk3b} = 7.0 \cdot kN$
Mode d	$F_{vRk4} = 4.7 \cdot kN$	$F_{vRk4b} = 7.2 \cdot kN$
Mode e	$F_{vRk5} = 3.2 \cdot kN$	$F_{vRk5b} = 5.7 \cdot kN$
Mode f	$F_{vRk6} = 2.9 \cdot kN$	$F_{vRk6b} = 5.3 \cdot kN$

Test 4 - Strength evaluation according to EC5

Timber to timber connections failure modes a,b,c,d,e and f

Steel fastener properties

diameter $d := 5.32mm$

Yield strength $f_y := 755\frac{N}{mm^2}$

Yield moment $M_{yRk} := 15150N \cdot mm$

Timber properties

thickness $t_1 := 77mm$ $t_2 := 48mm$

density $\rho := 600kg/m^3$

embedment strength $f_{hk} := 0.082 \cdot \rho \cdot d^{-0.3} = 29.8\ N/mm^2$

pointside penetration length $t_{pen} := t_2 - d = 42.7 \cdot mm$

$$\beta := \frac{f_{hk1}}{f_{hk2}} = 1$$

withdrawal capacity $f_{ax} := 0.00007 \cdot \rho^2 = 25.2N/mm^2$

(EN1995-1-1 art. 8.3.2)

$$F_{axRk} := f_{ax} \cdot d \cdot t_{pen} = 5.7 \cdot kN$$

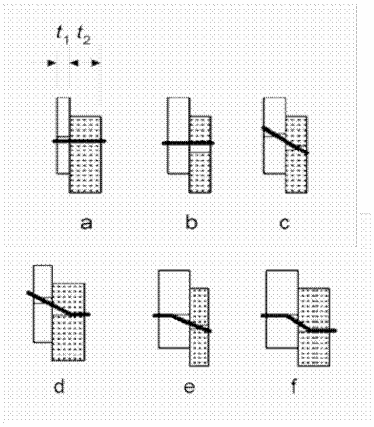

Calculation EN1995-1-1 art. 8.2.2

$$F := \frac{F_{axRk}}{4} = 1.4 \cdot kN$$

(mode a) $F_{vRk1} := f_{hk1} \cdot t_1 \cdot d = 12.2 \cdot kN$

(mode b) $F_{vRk2} := f_{hk2} \cdot t_2 \cdot d = 7.6 \cdot kN$

(mode c)

$$F_{vRk3} := \frac{f_{hk1} \cdot t_1 \cdot d}{1 + \beta} \cdot \left[\sqrt{\beta + 2 \cdot \beta^2 \cdot \left[1 + \frac{t_2}{t_1} + \left(\frac{t_2}{t_1} \right)^2 \right] + \beta^3 \cdot \left(\frac{t_2}{t_1} \right)^2} - \beta \cdot \left(1 + \frac{t_2}{t_1} \right) \right] = 4.3 \cdot kN$$

$$F_{vRk3b} := \begin{cases} F_{vRk3} \cdot 1.15 & \text{if } (F > 0.15 F_{vRk3}) \\ (F_{vRk3} + F) & \text{otherwise} \end{cases} \qquad F_{vRk3b} = 4.9 \cdot kN \quad \textit{(limited rope effect)}$$

$$F_{vRk3c} := \begin{cases} F_{vRk3} \cdot 2 & \text{if } (F > F_{vRk3}) \\ (F_{vRk3} + F) & \text{otherwise} \end{cases} \qquad F_{vRk3c} = 5.7 \cdot kN \quad \textit{(full rope effect)}$$

(mode d)

$$F_{vRk4} := 1.05 \cdot \frac{f_{hk1} \cdot t_1 \cdot d}{2 + \beta} \cdot \left[\sqrt{2 \cdot \beta \cdot (1 + \beta) + \frac{4 \cdot \beta \cdot (2 + \beta) \cdot M_{yRk}}{f_{hk1} \cdot d \cdot t_1^2}} - \beta \right] = 4.5 \cdot kN$$

$$F_{vRk4b} := \begin{cases} F_{vRk4} \cdot 1.15 & \text{if } (F > 0.15 F_{vRk4}) \\ (F_{vRk4} + F) & \text{otherwise} \end{cases} \qquad F_{vRk4b} = 5.1 \cdot kN \quad \textit{(limited rope effect)}$$

$$F_{vRk4c} := \begin{cases} F_{vRk4} \cdot 2 & \text{if } (F > F_{vRk4}) \\ (F_{vRk4} + F) & \text{otherwise} \end{cases} \qquad F_{vRk4c} = 5.9 \cdot kN \quad \textit{(full rope effect)}$$

(mode e)

$$F_{vRk5} := 1.05 \cdot \frac{f_{hk1} \cdot t_2 \cdot d}{2 + \beta} \cdot \left[\sqrt{2 \cdot \beta^2 \cdot (1 + \beta) + \frac{4 \cdot \beta \cdot (1 + 2 \cdot \beta) \cdot M_{yRk}}{f_{hk1} \cdot d \cdot t_2^{\,2}}} - \beta \right] = 3.0 \cdot kN$$

$$F_{vRk5b} := \begin{cases} F_{vRk5} \cdot 1.15 & \text{if } (F > 0.15 F_{vRk5}) \\ (F_{vRk5} + F) & \text{otherwise} \end{cases} \qquad F_{vRk5b} = 3.4 \cdot kN \qquad \textit{(limited rope effect)}$$

$$F_{vRk5c} := \begin{cases} F_{vRk5} \cdot 2 & \text{if } (F > F_{vRk5}) \\ (F_{vRk5} + F) & \text{otherwise} \end{cases} \qquad F_{vRk5c} = 4.4 \cdot kN \qquad \textit{(full rope effect)}$$

(mode f)

$$F_{vRk6} := 1.15 \cdot \sqrt{\frac{2 \cdot \beta}{1 + \beta}} \cdot \sqrt{2 M_{yRk} \cdot f_{hk1} \cdot d} = 2.5 \cdot kN$$

$$F_{vRk6b} := \begin{cases} F_{vRk6} \cdot 1.15 & \text{if } (F > 0.15 F_{vRk6}) \\ (F_{vRk6} + F) & \text{otherwise} \end{cases} \qquad F_{vRk6b} = 2.9 \cdot kN \qquad \textit{(limited rope effect)}$$

$$F_{vRk6c} := \begin{cases} F_{vRk6} \cdot 2 & \text{if } (F > F_{vRk6}) \\ (F_{vRk6} + F) & \text{otherwise} \end{cases} \qquad F_{vRk6c} = 4.0 \cdot kN \qquad \textit{(full rope effect)}$$

Overview

	Without rope effect	With 15% rope effect	With 100% rope effect
Mode a	$F_{vRk1} = 12.2 \cdot kN$	---	---
Mode b	$F_{vRk2} = 7.6 \cdot kN$	---	---
Mode c	$F_{vRk3} = 4.3 \cdot kN$	$F_{vRk3b} = 4.9 \cdot kN$	$F_{vRk3c} = 5.7 \cdot kN$
Mode d	$F_{vRk4} = 4.5 \cdot kN$	$F_{vRk4b} = 5.1 \cdot kN$	$F_{vRk4c} = 5.9 \cdot kN$
Mode e	$F_{vRk5} = 3.0 \cdot kN$	$F_{vRk5b} = 3.4 \cdot kN$	$F_{vRk5c} = 4.4 \cdot kN$
Mode f	$F_{vRk6} = 2.5 \cdot kN$	$F_{vRk6b} = 2.9 \cdot kN$	$F_{vRk6c} = 4.0 \cdot kN$

Test 5 - Strength evaluation for inclined screws *[Bejtka and Blass]*

Steel fastener properties

diameter $d := 4.98mm$

Yield strength $f_y := 1359\frac{N}{mm^2}$

Yield moment $M_{yRk} := 22380N\cdot mm$

Timber properties

thickness $t_1 := 77mm$ $t_2 := 30mm$ *(t is the depth of the screw perpendicular in the timber member)*

embedment strength $f_{hk1} := 32\frac{N}{mm^2}$

$f_{hk2} := 32\frac{N}{mm^2}$ $\beta := \frac{f_{hk1}}{f_{hk2}} = 1$

friction $\mu := 0.25$ *(assumed)*

density $\rho := 600$

angle to the grain $\alpha := 45deg$

withdrawal capacity $f_{ax} := \frac{0.0036\rho^{1.5}}{(\sin(\alpha))^2 + 1.5\cdot(\cos(\alpha))^2} = 42.3\,N/mm^2$

$f_{ax\_mod} := 0.7\cdot f_{ax} = 29.6N/mm^2$

(factor 0.7 is proposed by Bejtka and Blass)

$F_{ax} := f_{ax\_mod}\cdot d\cdot\frac{t_2}{\cos(\alpha)} = 6.3\cdot kN$

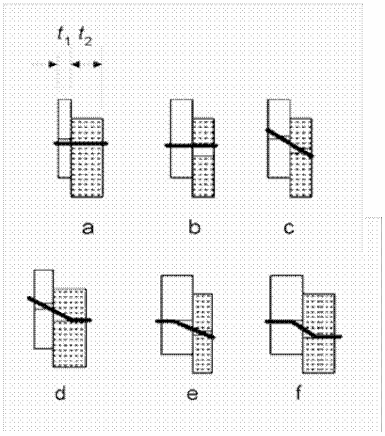

Calculation

Mode 1a,l compares to EC5 mode a
Mode 1a,r compares to EC5 mode b
Mode 1b compares to EC5 mode c
Mode 2a compares to EC5 mode d
Mode 2b compares to EC5 mode e
Mode 3 compares to EC5 mode f

(mode 1a,l) $F_{vRk1al} := F_{ax}\cdot\sin(\alpha) + f_{hk1}\cdot t_1\cdot d = 16.7\cdot kN$

(mode 1a,r) $F_{vRk1ar} := F_{ax}\cdot\sin(\alpha) + f_{hk2}\cdot t_2\cdot d = 9.2\cdot kN$

(mode 1b)

$$F_{vRk1b} := F_{ax}\cdot(\mu\cdot\cos(\alpha) + \sin(\alpha)) + \frac{f_{hk1}\cdot t_1\cdot d}{1+\beta}\cdot(1 - \mu\cdot\tan(\alpha))\cdot\left[\sqrt{\beta + 2\cdot\beta^2\cdot\left[1 + \frac{t_2}{t_1} + \left(\frac{t_2}{t_1}\right)^2\right] + \beta^3\cdot\left(\frac{t_2}{t_1}\right)^2} - \beta\cdot\left(1 + \frac{t_2}{t_1}\right)\right]$$

$F_{vRk1b} = 8.6\cdot kN$

(mode 2a)

$$F_{vRk2a} := F_{ax}\cdot(\mu\cdot\cos(\alpha) + \sin(\alpha)) + (1 - \mu\cdot\tan(\alpha))\cdot\frac{f_{hk1}\cdot t_1\cdot d}{2+\beta}\cdot\left[\sqrt{2\cdot\beta\cdot(1+\beta) + \frac{4\cdot\beta\cdot(2+\beta)\cdot M_{yRk}\cdot(\cos(\alpha))^2}{f_{hk1}\cdot d\cdot t_1^2}} - \beta\right]$$

$F_{vRk2a} = 8.7\cdot kN$

(mode 2b)

$$F_{vRk2b} := F_{ax}\cdot(\mu\cdot\cos(\alpha) + \sin(\alpha)) + (1 - \mu\cdot\tan(\alpha))\cdot\frac{f_{hk1}\cdot t_2\cdot d}{1+2\cdot\beta}\cdot\left[\sqrt{2\cdot\beta^2\cdot(1+\beta) + \frac{4\cdot\beta\cdot(1+2\beta)\cdot M_{yRk}\cdot(\cos(\alpha))^2}{f_{hk1}\cdot d\cdot t_2^2}} - \beta\right]$$

$F_{vRk2b} = 7\cdot kN$

(mode 3) $F_{vRk3} := F_{ax} \cdot (\mu \cdot \cos(\alpha) + \sin(\alpha)) + (1 - \mu \cdot \tan(\alpha)) \cdot \sqrt{\frac{2 \cdot \beta}{1 + \beta}} \cdot \sqrt{2 M_{yRk} \cdot f_{hk1} \cdot d \cdot (\cos(\alpha))^2} = 6.9 \cdot kN$

Overview

Mode 1,al	$F_{vRk1al} = 16.7 \cdot kN$
Mode 1,ar	$F_{vRk1ar} = 9.2 \cdot kN$
Mode 1b	$F_{vRk1b} = 8.6 \cdot kN$
Mode 2a	$F_{vRk2a} = 8.7 \cdot kN$
Mode 2b	$F_{vRk2b} = 7.0 \cdot kN$
Mode 3	$F_{vRk3} = 6.9 \cdot kN$

Appendix B – Ruaumoko Frame Files

First an overview of the main settings for the numerical analysis is given. Secondly, three files are shown which form the input for Ruaumoko. These files are modelling Design E, with the highest connector stiffness, under the first earthquake record.

B.1 – Program settings

Principle Analysis Options

IPANAL	2	Dynamic time-history using newmark constant average acceleration
IFMT	0	Binary post-processor file with extension .RES
IPLAS	1	In-elastic Time-history Analysis only
IPCONM	0	Lumped mass matrix used in Time-history
ICTYPE	6	Rayleigh Damping with Tangent damping matrix as Secant damping matrix
IPVERT	0	X-direction earthquake only
INLGEO	2	P-Delta effects included
IPNF	0	Modal analysis is carried out after the static analysis
IZERO	0	All zero output is omitted
ORTHO	0	Mode shape orthogonality check not carried out
IMODE	0	Householder QR eigenvalue algorithm used (Default)

Frame Control Parameters

NNP	11	Number of nodals points in the structure
NMEM	10	Number of members in the structure
NTYPE	2	Number of different cross-section in the section table
M	5	Number of mode shapes required to be printed in the modal analysis
MODE1	1	The mode number at which the first damping ratio is applied
MODE2	2	The mode number at which the second damping ratio is applied
GRAV	9.81	The acceleration of gravity
C1	2	The percentage of critical damping at mode MODE1
C2	2	The percentage of critical damping at mode MODE2
DT	0.01	The time-step
TIME	50	The length of time-history to be run
FACTOR	1.2	A scale factor applied to the time-history input

Output Intervals and Plotting Control Parameters

KP	0	Time-history output suppressed
KPA	10	Post-processor DYNAPLOT output every k time-steps
KPLOT	10	Plastic hinges plotted every k time-steps
JOUT	0	No used any longer, supply 0

DSTORT	1	No used any longer, supply 1
DFACT	1	Displacement multiplying scale factor for on-screen graphics
XMAX	1	Maximum X displacement for use in the on-screen graphics
YMAX	1	Maximum Y displacement for use in the on-screen graphics
NLEVEL	1	Number of levels for computed inter-storey drifts, i.e. number of storeys+1
NUP	2	Vertical axis for inter-storey drifts, 1=X axis or 2=Y axis.
IRESID	0	Residual displacements and forces not output
KDUMP	0	Mass and stiffness matrices output suppressed

Iteration Control and Wave Velocities

MAXIT	10	Maximum number of cycles of Newton-Raphson iteration per Time-step
MAXCIT	5	Maximum number of cycles of iteration/solution step for damping models
FTEST	0.0001	Norm of the out of balance force vector realtive to the incremental force vector for the Newton-Raphson or damping iteration. The value is the square of the iteration tolerance required.i.e. 0.0001 implies a tolerance of 1% in the residual vector.
WAVEX	0	Wave velocity of propogstion in the x-direction (if=0.0 taken as infinitive)
WAVEY	0	Wave velocity of propogstion in the y-direction (if=0.0 taken as infinitive)
THETA	0	Angle of earthquake X and Y directions to the structure X and Y directions
DXMAX	1.5	X displacement to terminate analysis
DYMAX	0	Y displacement to terminate analysis
D	0	Travelling wave dispersion factor, 0.0 implies no dispesion
OMEGA	0	Earthquake characteristic frequency (radians/second) used for dispersion
F	0	Scale factor for dispersion

B.2 – MDOF model

```
!  DESCRIPTION  OF  THE  ANALYSIS
   1 Storey  1 bay
!  Units  kN, m
!  PRINCIPAL  ANALYSIS  OPTIONS
!  IPANAL  IFMT  IPLAS  IPCONM  ICTYPE  IPVERT  INLGEO  IPNF  IZERO  ORTHO  IMODE
   2  0  1  0  6  0  2  0  0  0  0

!  FRAME  CONTROL  PARAMETERS
!  NNP  NMEM  NTYPE  M  MODE1  MODE2  GRAV  C1  C2  DT  TIME  FACTOR
   11  10  2  5  1  2  9.81  2  2  0.01  50  1.2

!  OUTPUT  INTERVALS  AND  PLOTTING  CONTROL  PARAMETERS
!  KP  KPA  KPLOT  JOUT  DSTORT  DFACT  XMAX  YMAX  NLEVEL  NUP  IRESID  KDUMP
   0  10  10  0  1  1  1  1  1  2  0  0

!  ITERATION  CONTROL  AND  WAVE  VELOCITIES
!  MAXIT  MAXCIT  FTEST  WAVEX  WAVEY  THETA  DXMAX  DYMAX  D  OMEGA  F
   10  5  0.0001  0  0  0  1.5  0  0  0  0

!  NODAL  POINT  INPUT
NODES
!  N  X(N)  Y(N)  NF1  NF2  NF3  KUP1  KUP2  KUP3  IOUT
   1  0  0  1  1  1  0  0  0  0  ! Fixed node
   2  0.01  0  0  1  0  0  0  0  0  ! Floor node
   3  0.01  1.5  0  1  0  0  0  0  0  ! Floor node
   4  0.01  3  0  1  0  0  0  0  0  ! Floor node
   5  0.01  4.5  0  1  0  0  0  0  0  ! Floor node
   6  0.01  6  0  1  0  0  0  0  0  ! Floor node
   7  0.01  7.5  0  1  0  0  0  0  0  ! Floor node
   8  0.01  9  0  1  0  0  0  0  0  ! Floor node
   9  0.01  10.5  0  1  0  0  0  0  0  ! Floor node
   10  0.01  12  0  1  0  0  0  0  0  ! Floor node
   11  0  12  1  1  1  0  0  0  0  ! Fixed node

!  INTER-STOREY  DRIFT  INPUT
DRIFT  ANGLE
!  N1  N2

!  MEMBER  TOPOLOGY  or  GEOMETRY
ELEMENTS
!  N  MT  NODE1  NODE2  NODE3  NODE4  IOUT
   1  1  1  2  0  0  0  ! Spring connection
   2  2  2  3  0  0  0  ! Floor beam
   3  2  3  4  0  0  0  ! Floor beam
   4  2  4  5  0  0  0  ! Floor beam
   5  2  5  6  0  0  0  ! Floor beam
   6  2  6  7  0  0  0  ! Floor beam
   7  2  7  8  0  0  0  ! Floor beam
   8  2  8  9  0  0  0  ! Floor beam
   9  2  9  10  0  0  0  ! Floor beam
   10  1  10  11  0  0  0  ! Spring connection

PROPS
!  SECTION  PROPERTY  INFORMATION
!  N  MTYPE  LABEL

   1  SPRING
!  ITYPE  IHYST  ILOS  IDAMG  KX  KY  GJ  WGT  RF  RT
   1  0  0  0  1160000  0  0  0  0  0

   2  FRAME  BEAM
!  ITYPE  IPIN  ICOND  IHYST  ILOS  IDAMG  ICOL  IGA  IDUCT
   1  0  0  0  0  0  0  0
!  ELASTIC  SECTION  PROPERTIES:
!  E  G  A  AS  I  WGT  END1  END2  FJ1  FJ2
   5.60E+06  2.24E+06  0.42  3.50E-01  1.26  20  0.00E+00  0.00E+00  0.00E+00  0.00E+00

!  Seismic  Weight  (kN)
WEIGHTS  0
!  N  WX  WY  WM
   1  0  0  0
   11  0  0  0

!  External  (static) nodal  loads  (Gravity Load)  (kN)
LOADS
!  N  FX  FY  FM
   1  0  0  0
   2  0  0  0

EQUAKE  C:\temp\EQs\EQ1.TXT
!  IBERG  ISTART  DELTAT  ASCALE  END  VEL  DIS  TSCALE
   3  1  0.005  1  -1  0  0  1
```

B.3 – SDOF-1 model

```
!       DESCRIPTION     OF      THE     ANALYSIS
        1 Storey        1 bay
!       Units           kN, m
!       PRINCIPAL       ANALYSIS        OPTIONS
!       IPANAL          IFMT            IPLAS           IPCONM          ICTYPE          IPVERT          INLGEO          IPNF            IZERO           ORTHO           IMODE
        2               0               1               0               6               0               2               0               0               0               0

!       FRAME           CONTROL         PARAMETERS
!       NNP             NMEM            NTYPE           M               MODE1           MODE2           GRAV            C1              C2              DT              TIME            FACTOR
        2               1               1               5               1               2               9.81            2               2               0.01            50              0.85

!       OUTPUT          INTERVALS       AND             PLOTTING        CONTROL         PARAMETERS
!       KP              KPA             KPLOT           JOUT            DSTORT          DFACT           XMAX            YMAX            NLEVEL          NUP             IRESID          KDUMP
        0               10              10              0               1               1               1               1               1               2               0               0

!       ITERATION       CONTROL         AND             WAVE            VELOCITIES
!       MAXIT           MAXCIT          FTEST           WAVEX           WAVEY           THETA           DXMAX           DYMAX           D               OMEGA           F
        10              5               0.0001          0               0               0               1.5             0               0               0               0

!       NODAL           POINT           INPUT
NODES
!       N               X(N)            Y(N)            NF1             NF2             NF3             KUP1            KUP2            KUP3            IOUT
        1               0               0               1               1               1               0               0               0               0               !       Fixed node
        2               0.01            0               0               1               1               0               0               0               0               !       Floor node

!       INTER-STOREY    DRIFT           INPUT
DRIFT   ANGLE
!       N1              N2

!       MEMBER          TOPOLOGY        or              GEOMETRY
ELEMENTS
!       N               MT              NODE1           NODE2           NODE3           NODE4           IOUT
        1               1               1               2               0               0               0                                               !       Spring connection

PROPS
!       SECTION         PROPERTY        INFORMATION
!       N               MTYPE           LABEL

        1               SPRING
!       ITYPE           IHYST           ILOS            IDAMG           KX              KY              GJ              WGT             RF              RT
        1               0               0               0               232000          0               0               0               0               0

!       Seismic         Weight          (kN)
WEIGHTS 0
!       N               WX              WY              WM
        2               240             0               0

!       External        (static) nodal  loads           (Gravity Load)  (kN)
LOADS
!       N               FX              FY              FM
        1               0               0               0
        2               0               0               0

EQUAKE  temp\EQs\EQ15.TXT
!       IBERG           ISTART          DELTAT          ASCALE          END             VEL             DIS             TSCALE
        3               1               0.005           1               -1              0               0               1
```

B.4 – SDOF-2 model

```
!    DESCRIPTION   OF      THE     ANALYSIS
     1 Storey      1 bay
!    Units         kN, m
!    PRINCIPAL     ANALYSIS OPTIONS
!    IPANAL        IFMT     IPLAS   IPCONM  ICTYPE  IPVERT  INLGEO  IPNF  IZERO  ORTHO  IMODE
     2             0        1       0       6       0       2       0     0      0      0

!    FRAME         CONTROL  PARAMETERS
!    NNP           NMEM     NTYPE   M       MODE1   MODE2   GRAV    C1    C2     DT     TIME   FACTOR
     2             1        1       5       1       2       9.81    2     2      0.01   50     0.85

!    OUTPUT        INTERVALS AND     PLOTTING CONTROL PARAMETERS
!    KP            KPA      KPLOT   JOUT     DSTORT  DFACT   XMAX  YMAX  NLEVEL NUP    IRESID KDUMP
     0             10       10      0        1       1       1     1     1      2      0      0

!    ITERATION     CONTROL  AND     WAVE     VELOCITIES
!    MAXIT         MAXCIT   FTEST   WAVEX    WAVEY   THETA   DXMAX DYMAX D      OMEGA  F
     10            5        0.0001  0        0       0       1.5   0     0      0      0

!    NODAL         POINT    INPUT
NODES
!    N             X(N)     Y(N)    NF1      NF2     NF3     KUP1  KUP2  KUP3   IOUT
     1             0        0       1        1       1       0     0     0      0      !  Fixed node
     2             0.01     0       0        1       1       0     0     0      0      !  Floor node

!    INTER-STOREY  DRIFT    INPUT
DRIFT ANGLE
!    N1            N2

!    MEMBER        TOPOLOGY or      GEOMETRY
ELEMENTS
!    N             MT       NODE1   NODE2   NODE3   NODE4   IOUT
     1             1        1       2       0       0       0                              !  Spring connection

PROPS
!    SECTION       PROPERTY INFORMATION
!    N             MTYPE    LABEL
     1             SPRING
!    ITYPE         IHYST    ILOS    IDAMG   KX      KY      GJ    WGT   RF     RT
     1             0        0       0       181000  0       0     0     0      0

!    Seismic       Weight   (kN)
WEIGHTS 0
!    N             WX       WY      WM
     2             240      0       0

!    External      (static) nodal   loads   (Gravity Load)  (kN)
LOADS
!    N             FX       FY      FM
     1             0        0       0
     2             0        0       0

EQUAKE temp\EQs\EQ15.TXT
!    IBERG         ISTART   DELTAT  ASCALE  END     VEL     DIS   TSCALE
     3             1        0.005   1       -1      0       0     1
```

Appendix C – Earthquake records

Using NZS1170.5 earthquake spectra:

- Soil type C
- Sp = 1.0
- Risk factor = 1.0 for 1/500y and 1.8 for 1/2500y.
- Wellington city zonation, z = 0.4
- Distance to fault = >20km
- Damping for design spectrum: 2%.

The earthquake spectra and target spectra are shown below for 2% damping and are scaled over a period range of 0.64s (0.4T1) to 3.0s (the corner period > 1.3 T1).

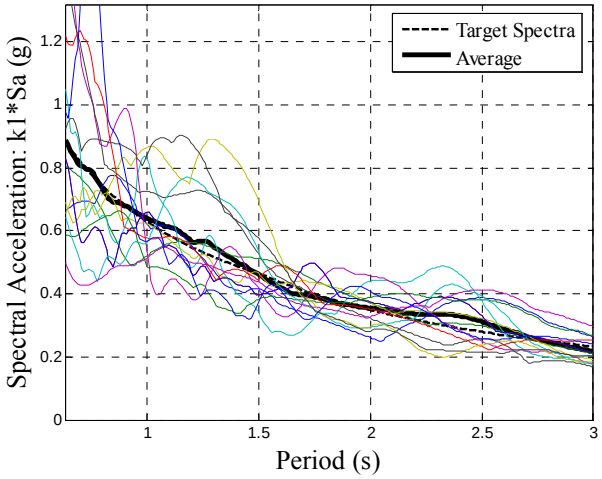

Note, the scaling limit according to NZS1170.5 (between 0.3 and 3) is exceeded for 3 EQs.

EQ	Near field or far field	Location	Dist. to source [km]	Time step	Scale Factor	
					1/500y	1/2500y
1	NF	Northridge, Los Angeles Dam	5.92	0.005	1.2	2.16
2	NF	Norhtridge, Sylmar - Olive view Med Ctr	5.3	0.005	0.6	1.08
3	FF	Tabas, Iran (BOS_L1)	26.1	0.02	4.49	8.08
4	FF	Nothridge, N Hollywood – Coldwater Can	14.6	0.005	2.18	3.92
5	FF	Northridge, Canoga Park – Topanga Clan	15.8	0.005	1.82	3.28
6	N/A	Artificial EQ (generated using SPECTRA)	-	0.01	1.22	2.20
7	FF	Superstition Hills, El Centro Imp. Co. Cent	13.9	0.005	2.16	3.89
8	FF	Superstition Hills, Plaster City	21	0.005	4.49	8.08
9	FF	Cape Mendocino, Fortuna Fortuna Blvd	23.6	0.005	2.68	4.82
10	NF	Loma Prieta, Los Gatos Pres Center	3.88	0.005	0.55	0.99
11	FF	Northridge, LA – N Faring Rd	23.9	0.005	3.22	5.80
12	NF	Chi Chi, TCU068	9.96	0.005	0.56	1.01
13	FF	Landers, Yemo Fire Station	24.9	0.005	2.65	4.77
14	FF	Loma Prieta, Hollister Diff. Army	25.8	0.005	1.29	2.32
15	NF	Tabas, Iran	2	0.005	0.85	1.53

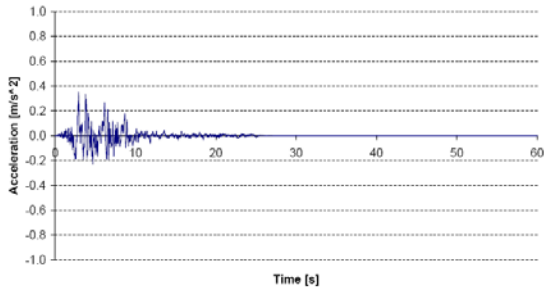

Earthquake record 1

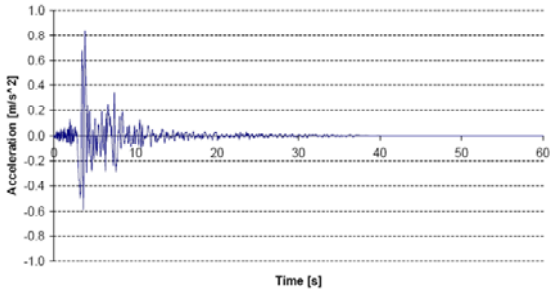

Earthquake record 2

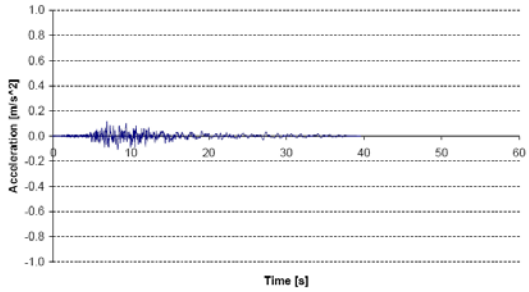

Earthquake record 3

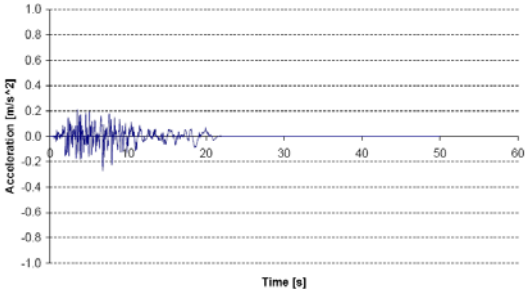

Earthquake record 4

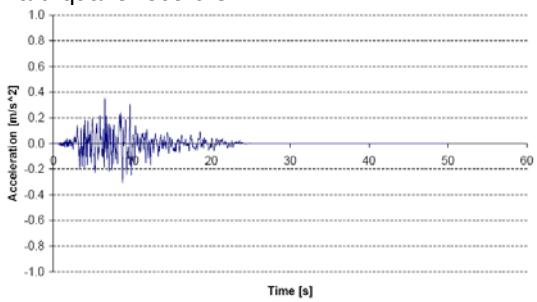

Earthquake record 5

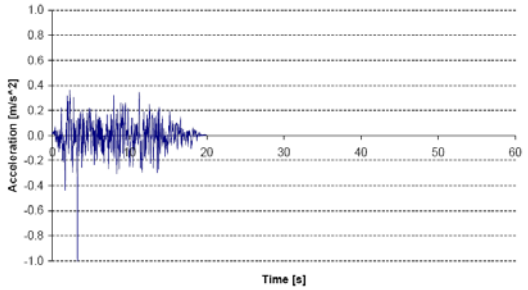

Earthquake record 6

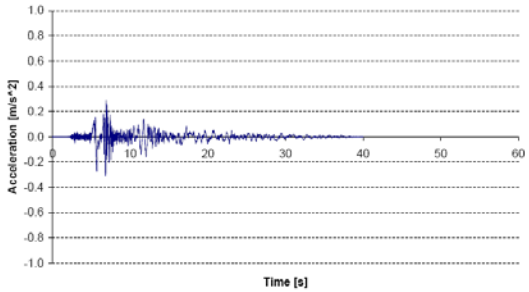

Earthquake record 7

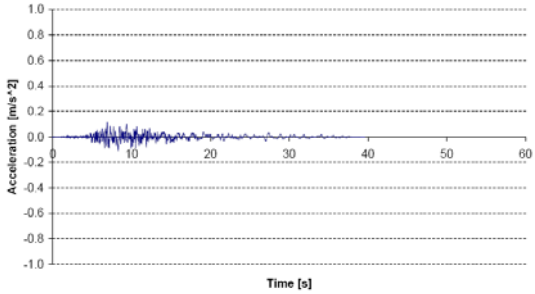

Earthquake record 8

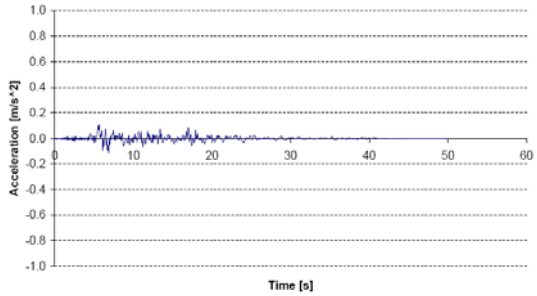

Earthquake record 9

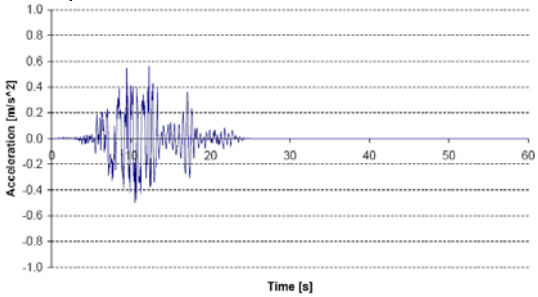

Earthquake record 10

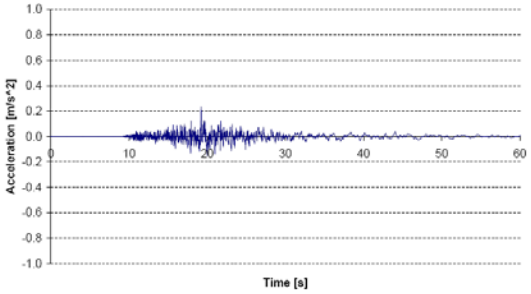

Earthquake record 11

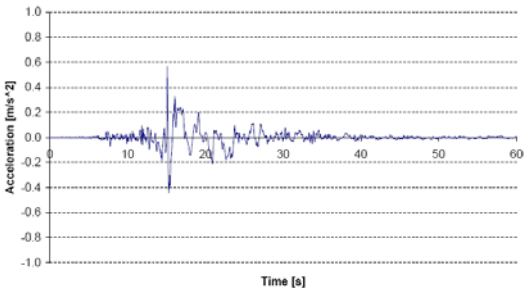

Earthquake record 12

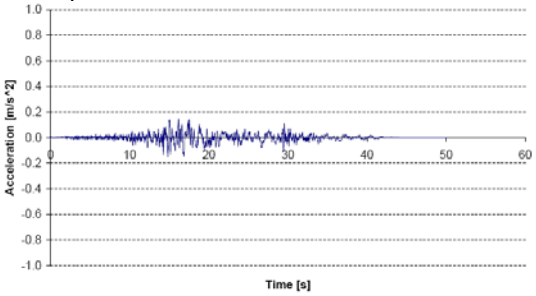

Earthquake record 13

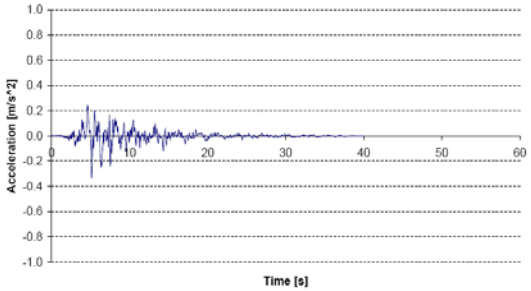

Earthquake record 14

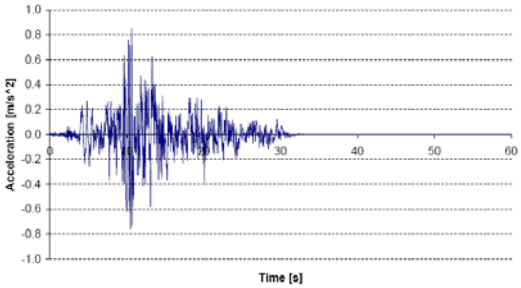

Earthquake record 15

Appendix D – Graphs numerical analysis floor unit

D.1 - Results Design A

The next figures show the results for the first design, with $\lambda = 0.33$.

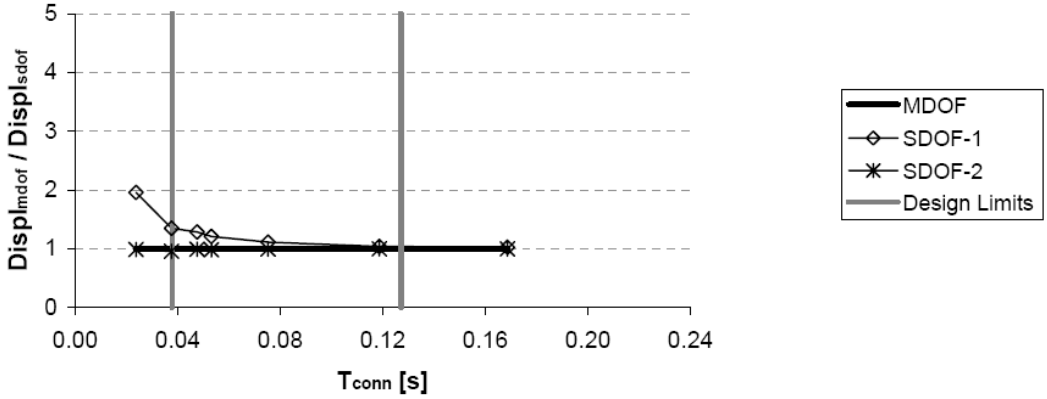

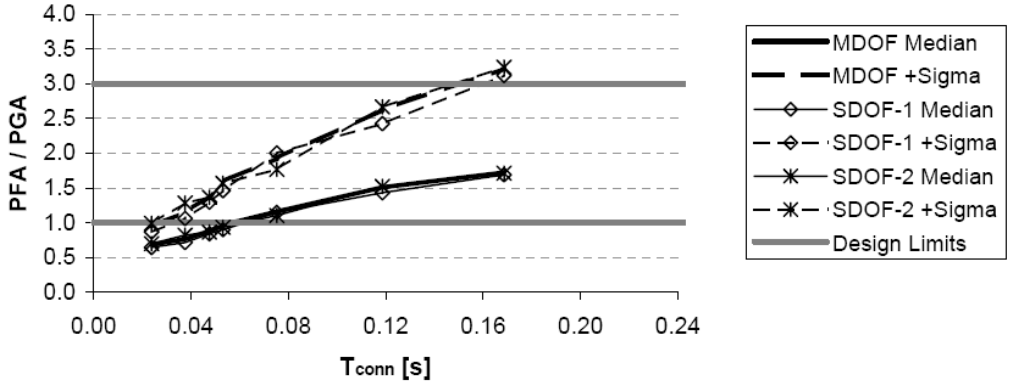

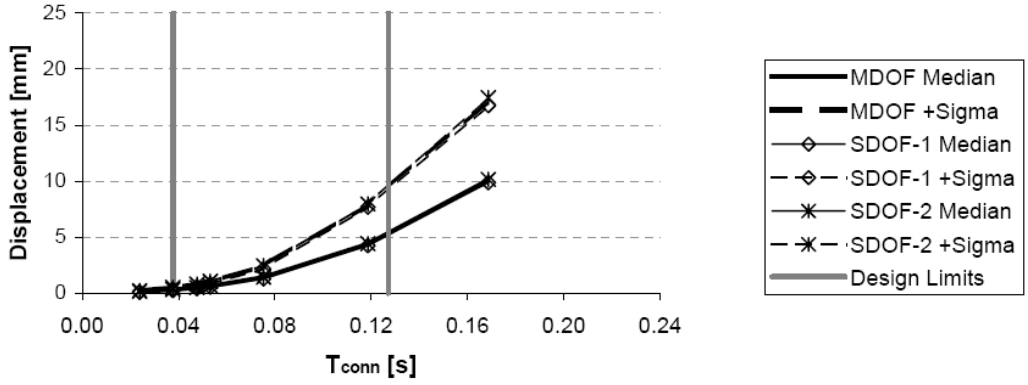

D.2 - Results Design B

The next figures show the results for the second design, with $\lambda = 0.66$.

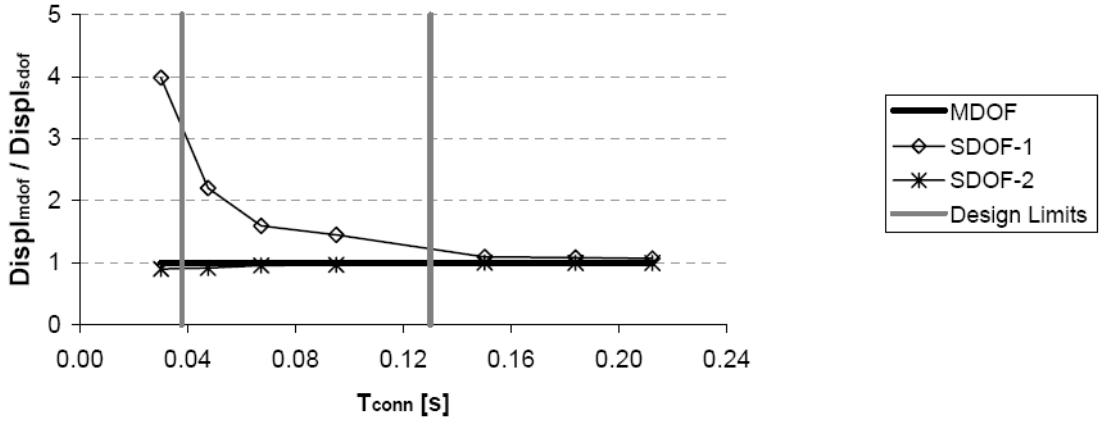

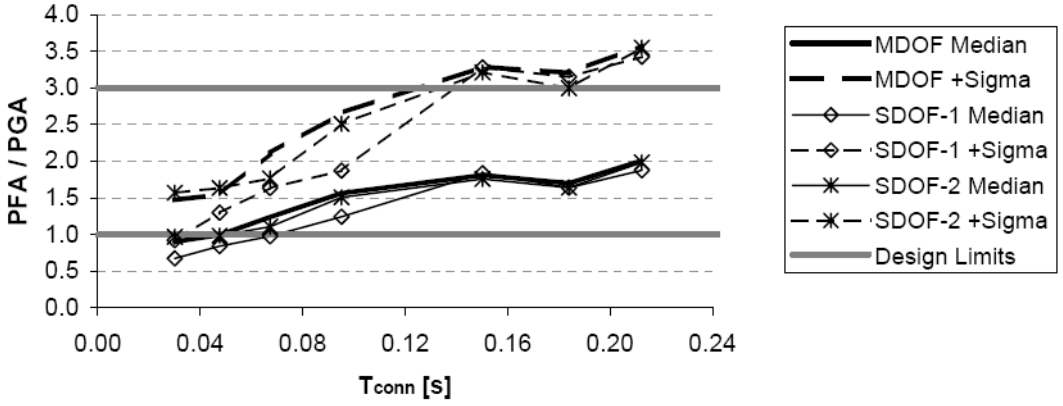

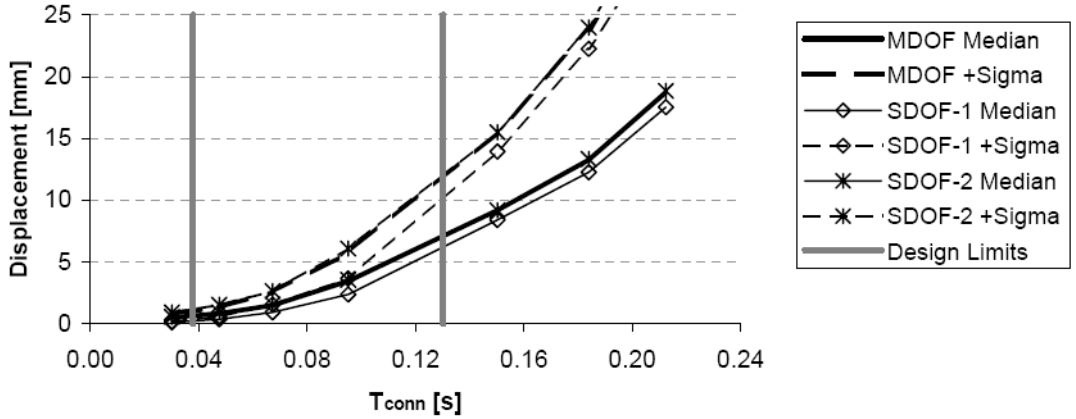

D.3 - Results Design C

The next figures show the results for the third design, with $\lambda = 1.00$.

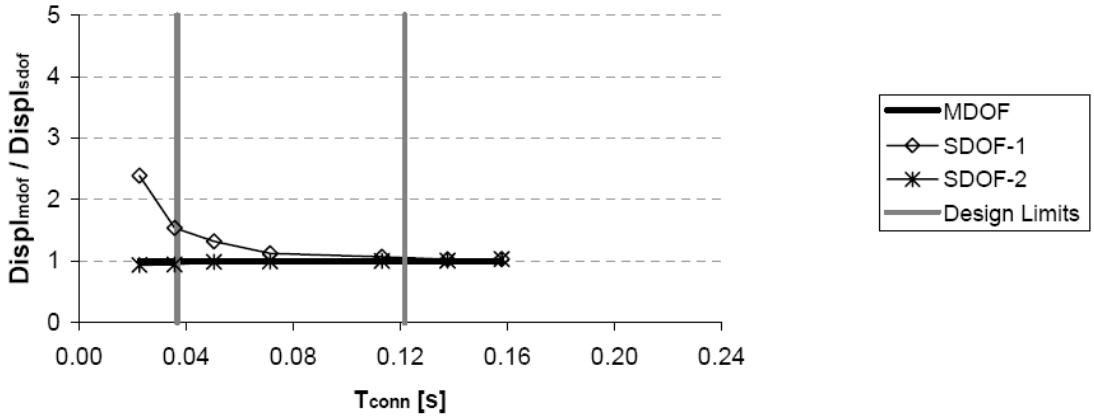

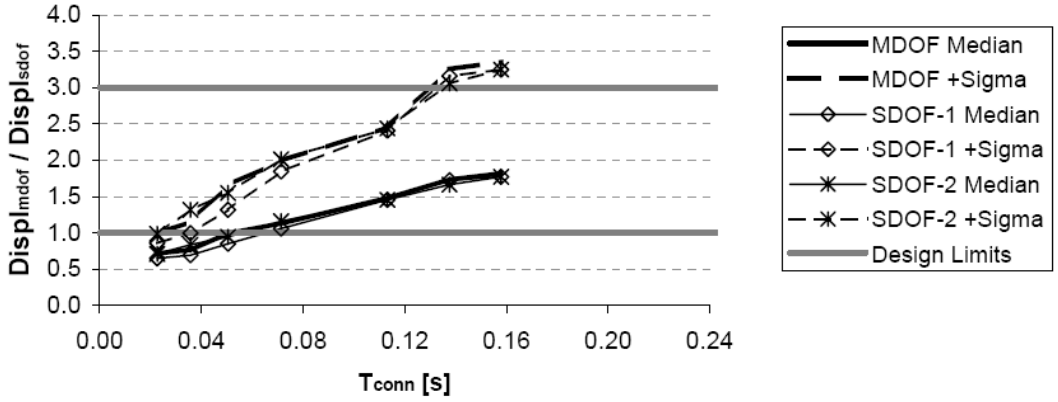

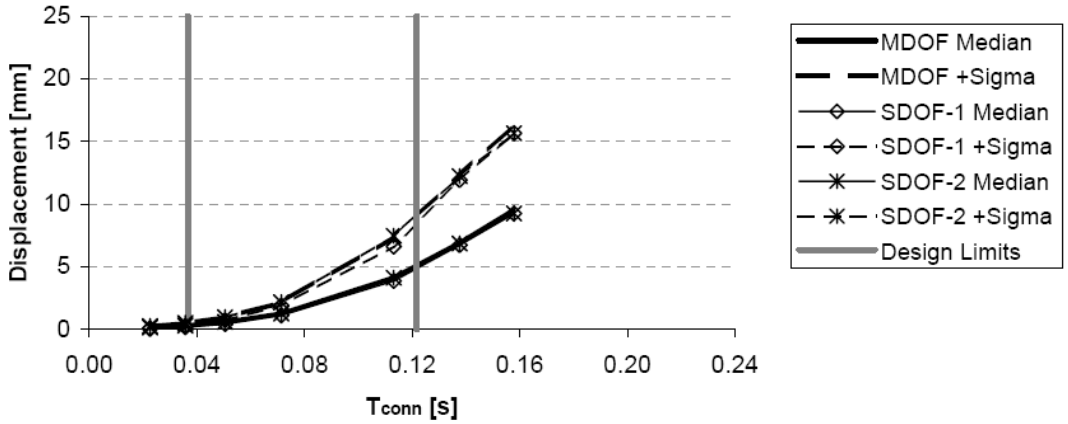

D.4 - Results Design D

The next figures show the results for the forth design, with $\lambda = 1.50$.

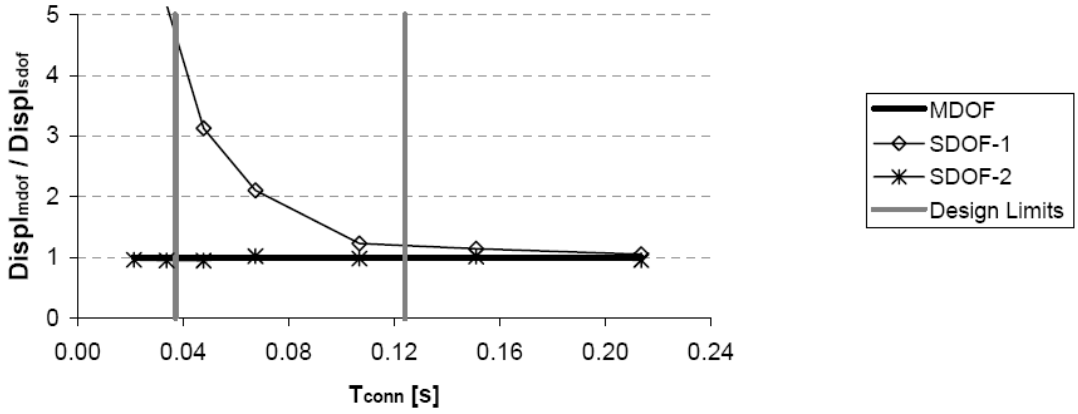

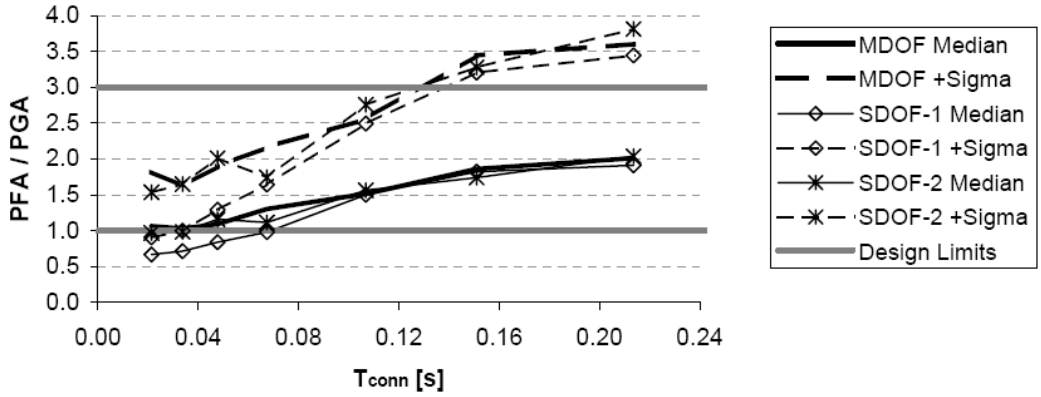

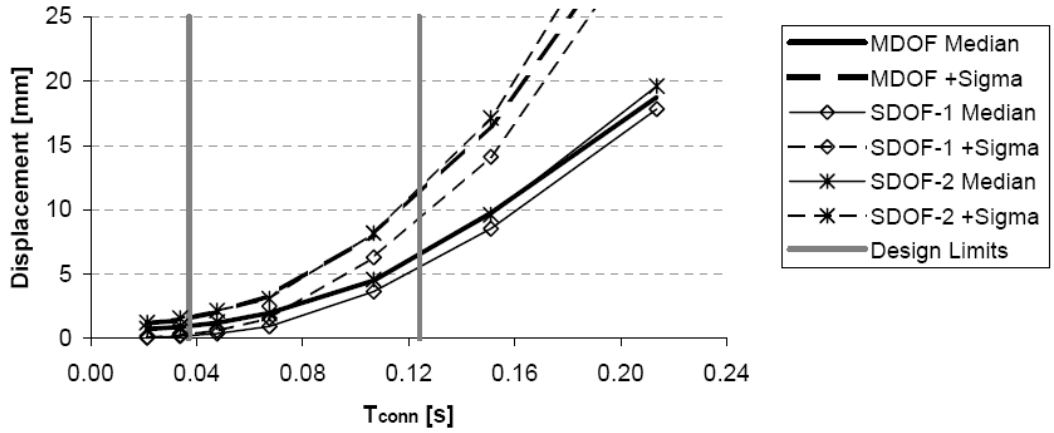

D.5 - Results Design E

The next figures show the results for the fifth design, with $\lambda = 2.00$.

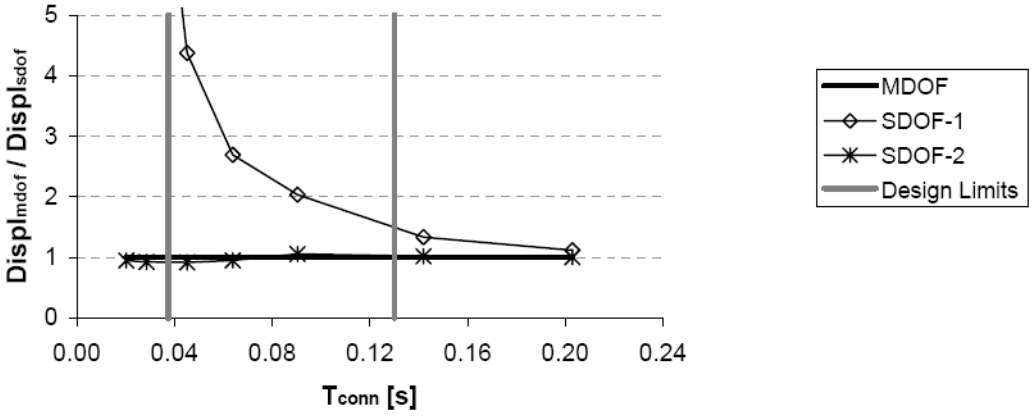

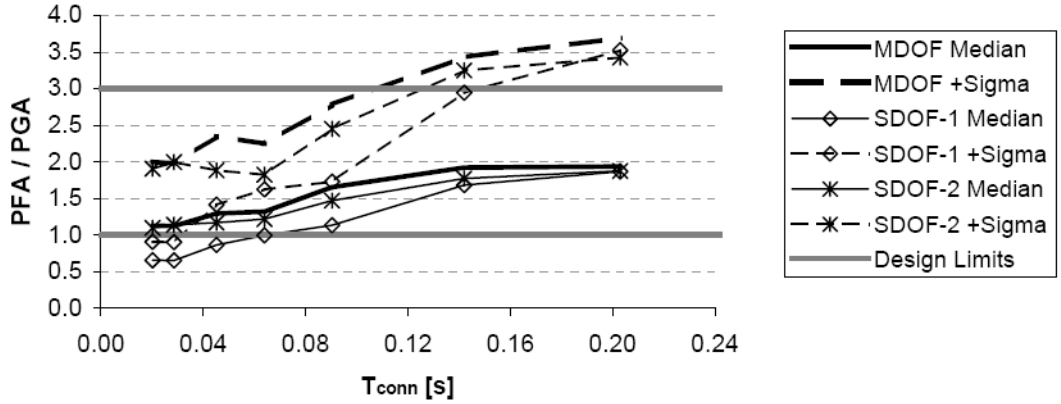

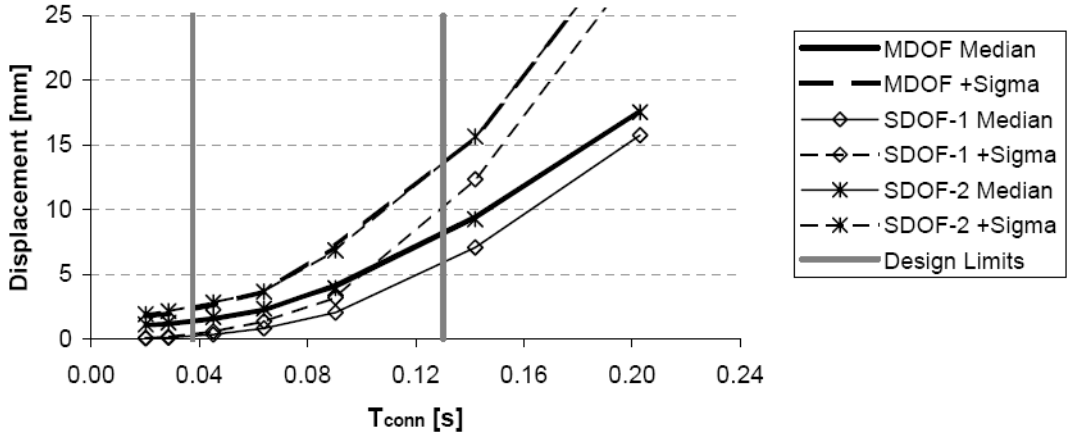

Appendix E – Graphs numerical analysis multi-storey building

E.1 – 1/50 year event

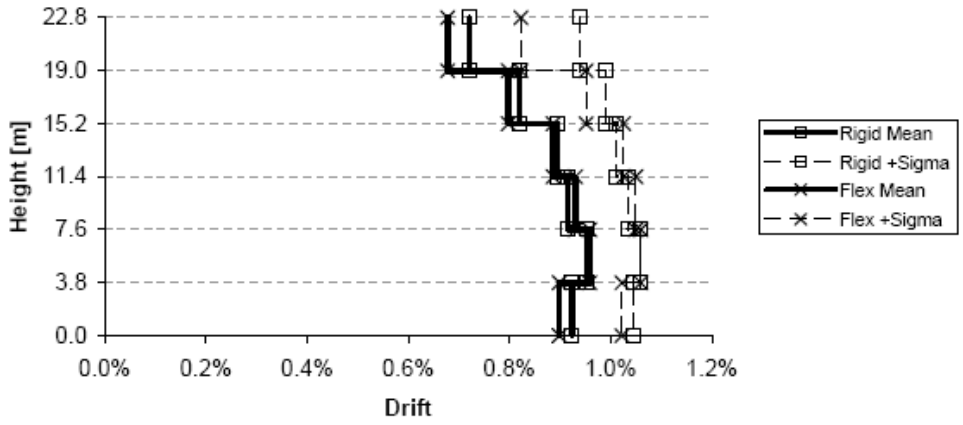

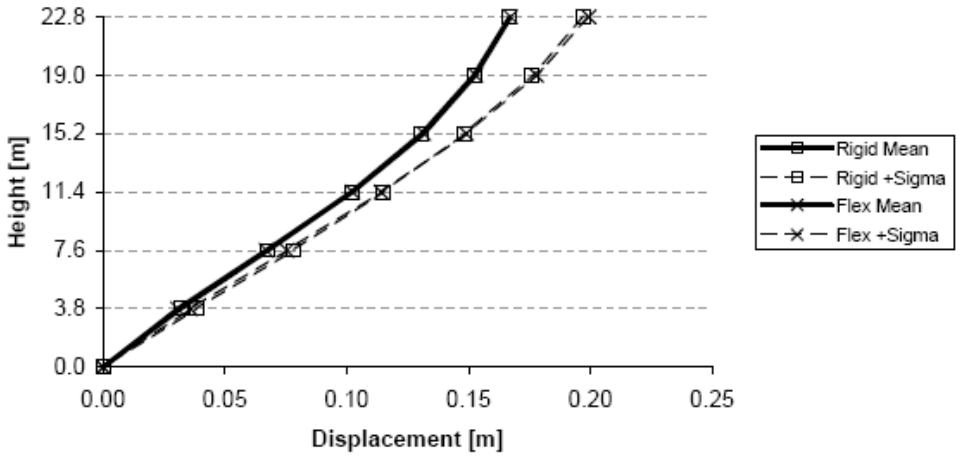

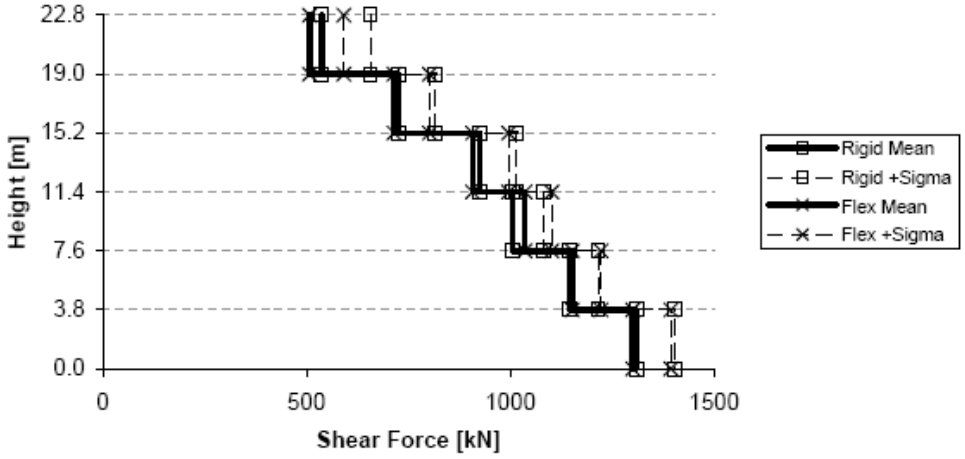

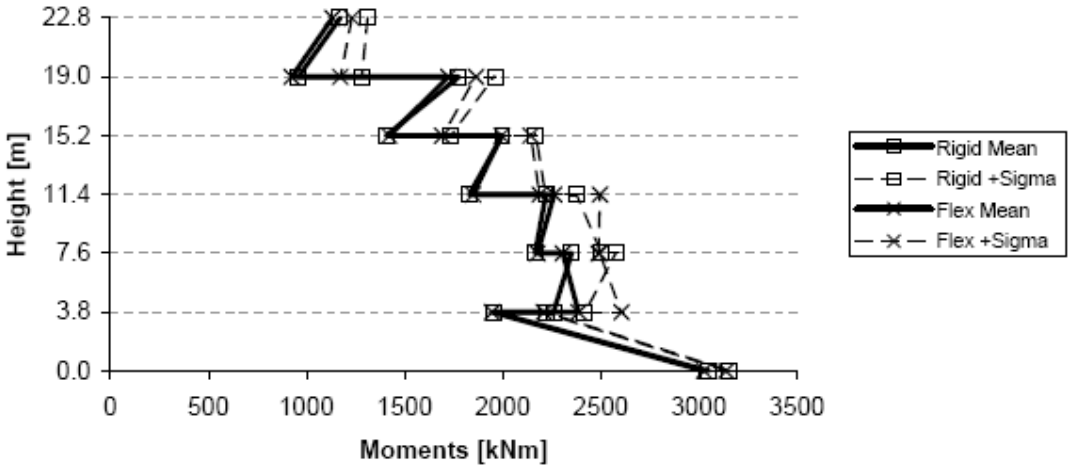
22.8
19.0
15.2
11.4
7.6
3.8
0.0
Height [m]
0
500
1000
1500
2000
2500
3000
3500
Moments [kNm]
Rigid Mean
Rigid +Sigma
Flex Mean
Flex +Sigma

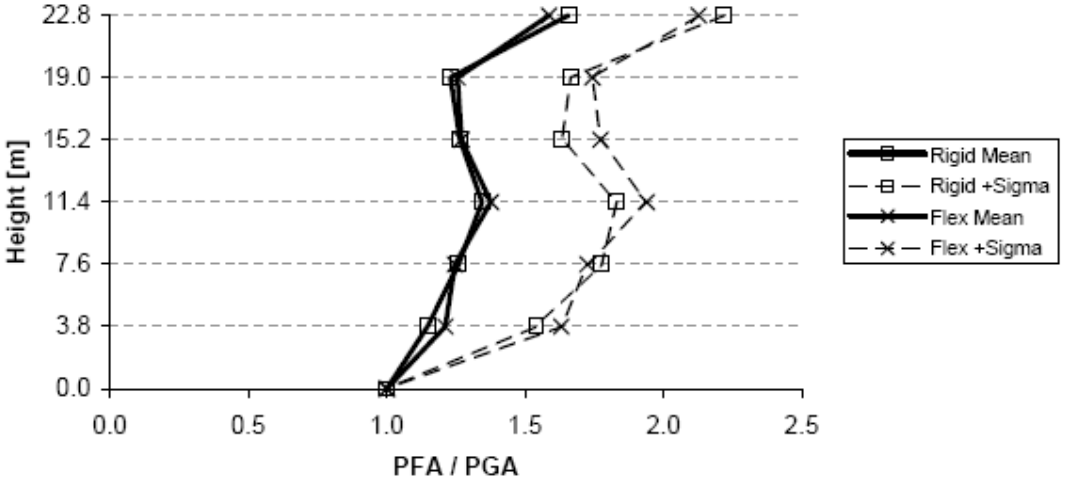
22.8
19.0
15.2
11.4
7.6
3.8
0.0
Height [m]
0.0
0.5
1.0
1.5
2.0
2.5
PFA / PGA
Rigid Mean
Rigid +Sigma
Flex Mean
Flex +Sigma

E.2 – 1/500 year event

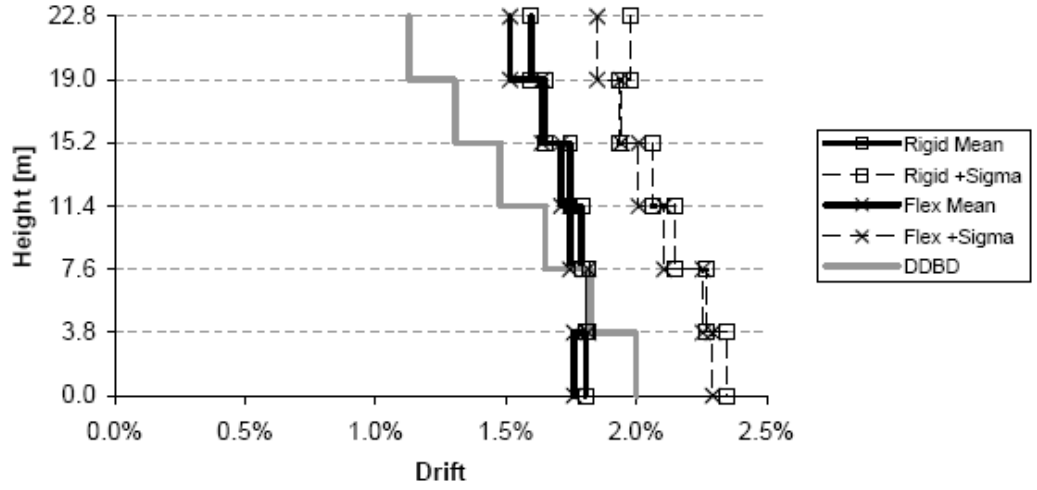

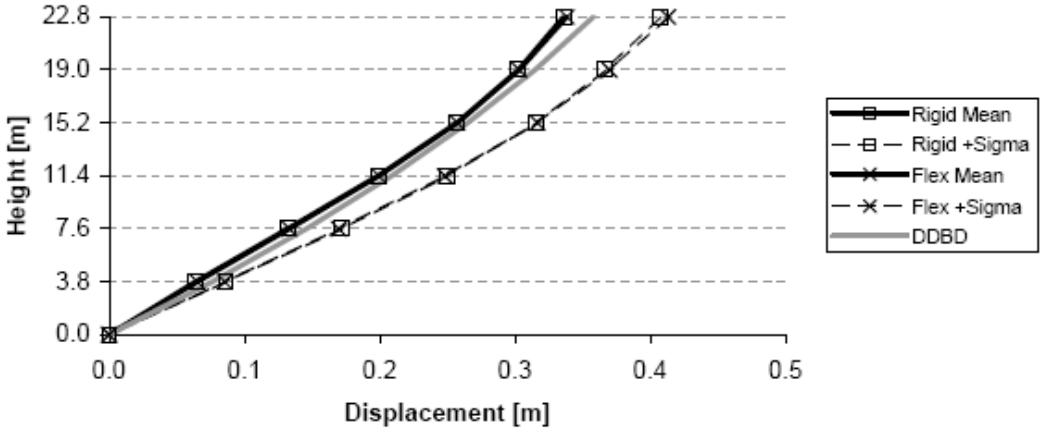

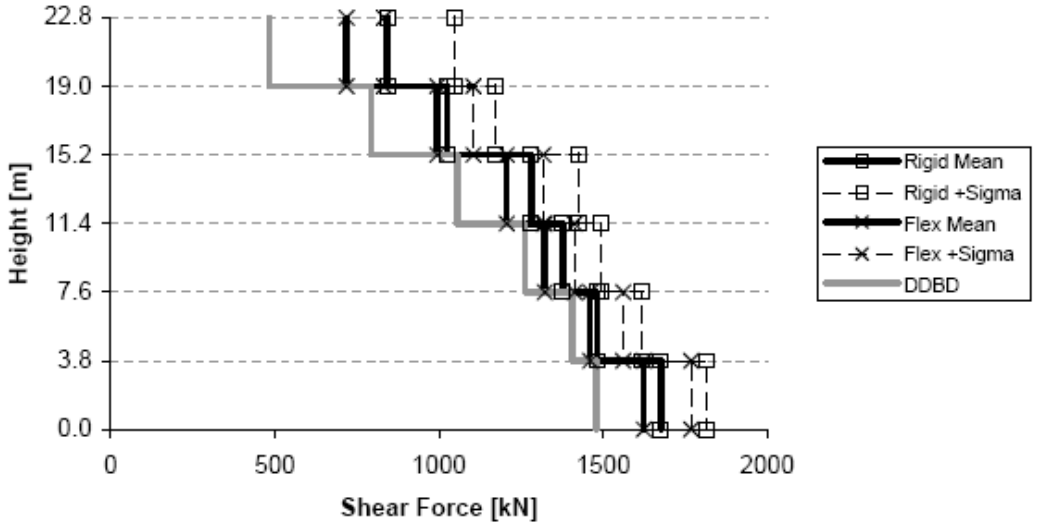

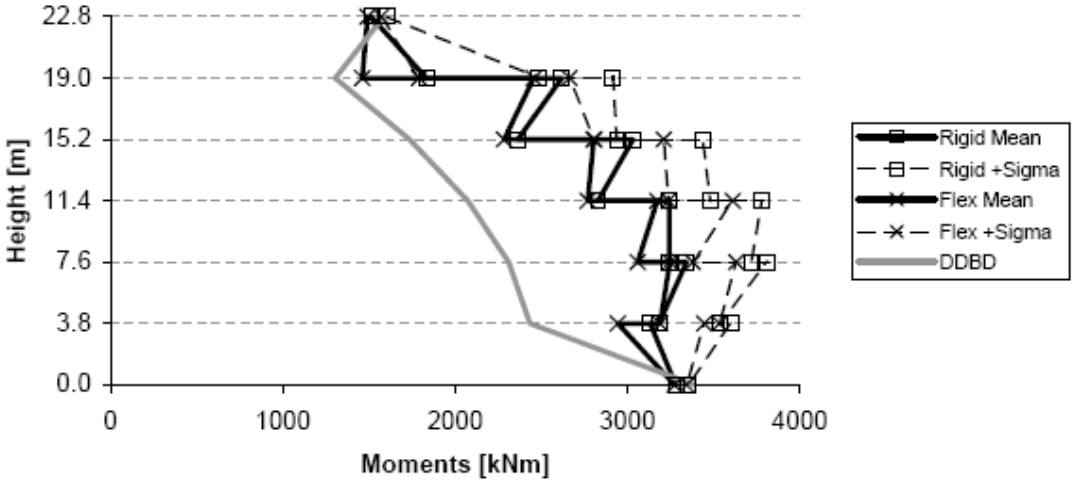
22.8
19.0
15.2
11.4
7.6
3.8
0.0
Height [m]
0
1000
2000
3000
4000
Moments [kNm]
Rigid Mean
Rigid +Sigma
Flex Mean
Flex +Sigma
DDBD

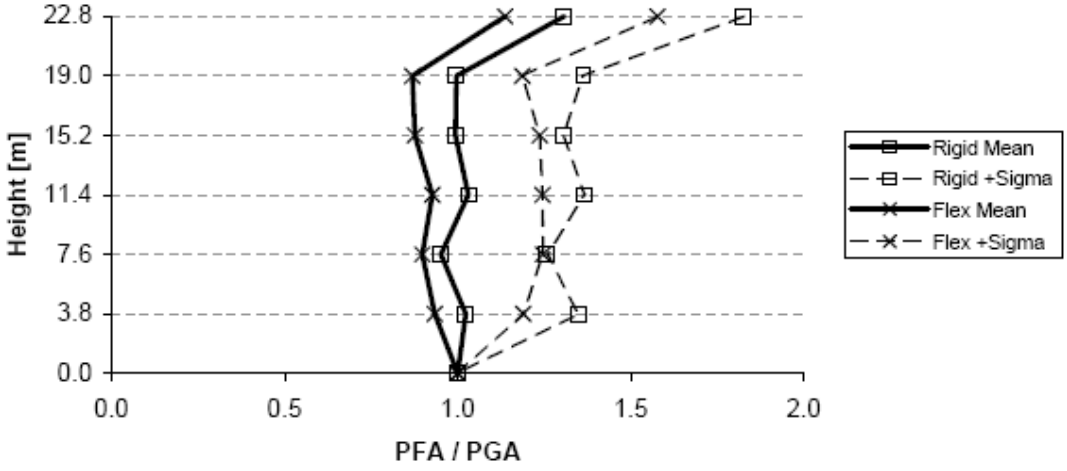
22.8
19.0
15.2
11.4
7.6
3.8
0.0
Height [m]
0.0
0.5
1.0
1.5
2.0
PFA / PGA
Rigid Mean
Rigid +Sigma
Flex Mean
Flex +Sigma

E.3 – 1/2500 year event

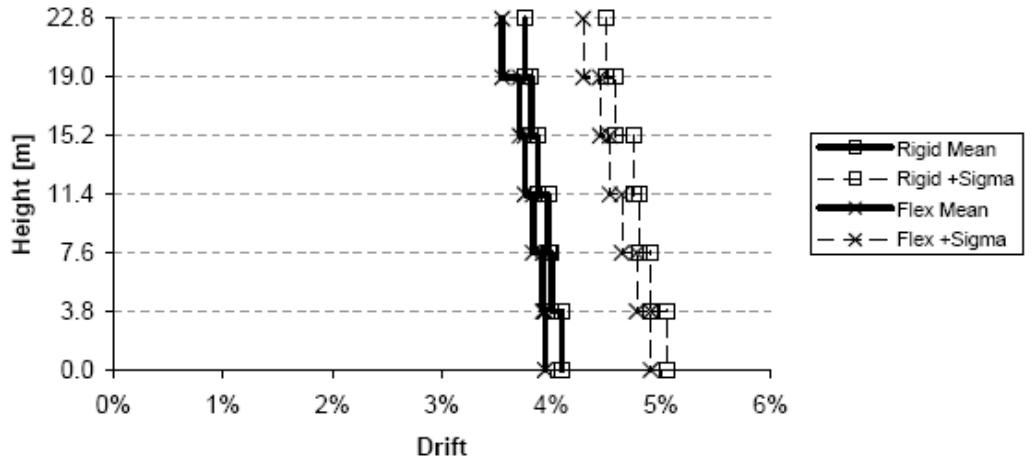

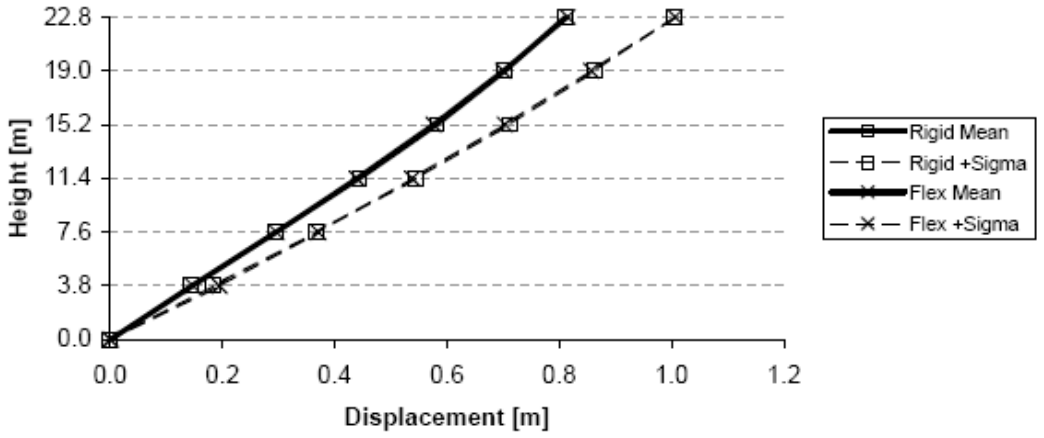

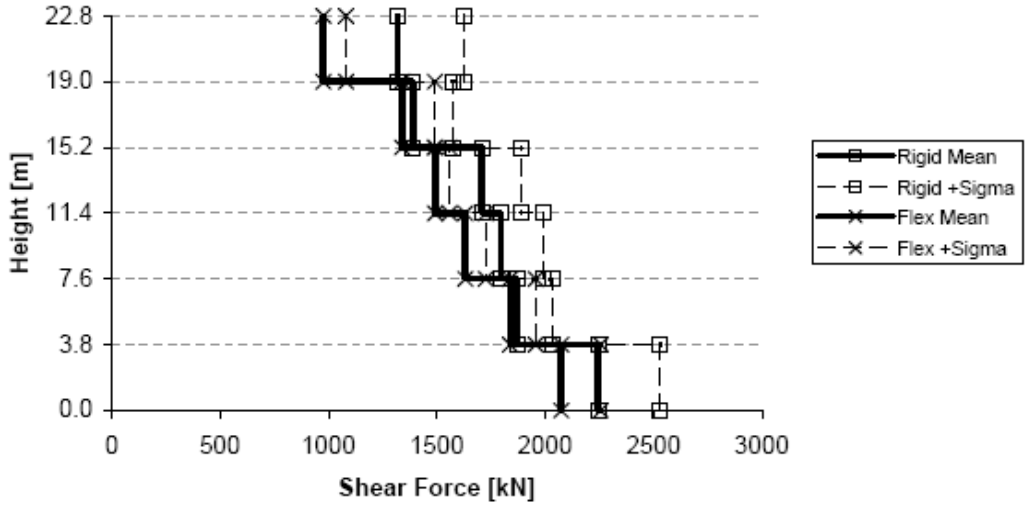

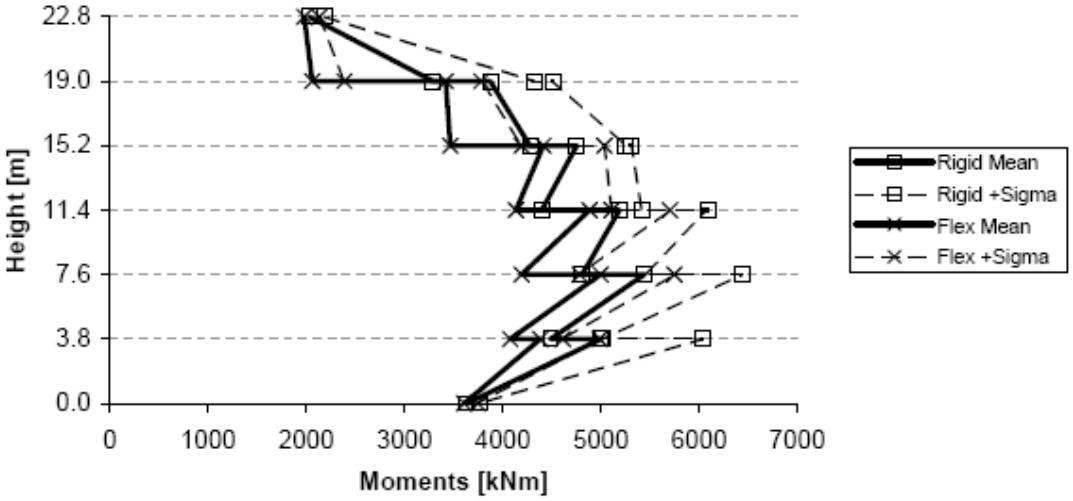
22.8
19.0
15.2
11.4
7.6
3.8
0.0
Height [m]
0
1000
2000
3000
4000
5000
6000
7000
Moments [kNm]
Rigid Mean
Rigid +Sigma
Flex Mean
Flex +Sigma

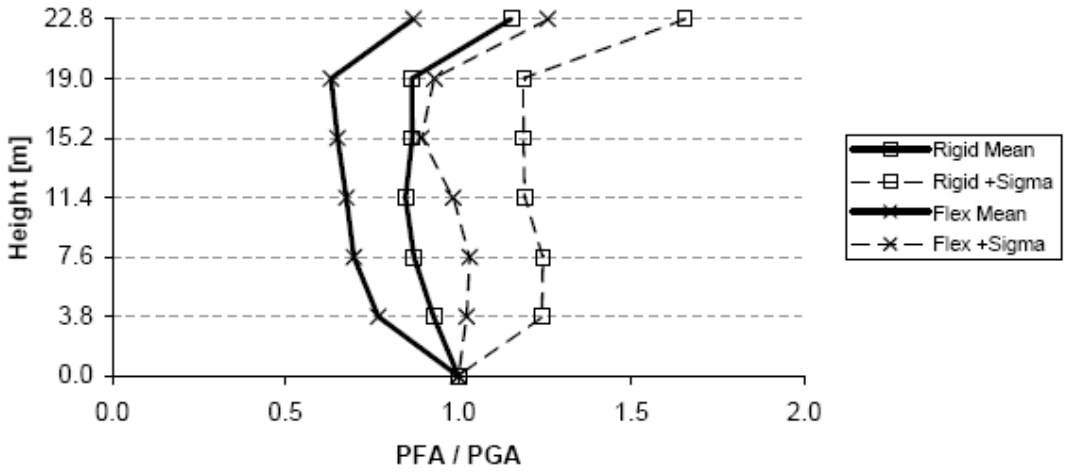
22.8
19.0
15.2
11.4
7.6
3.8
0.0
Height [m]
0.0
0.5
1.0
1.5
2.0
PFA / PGA
Rigid Mean
Rigid +Sigma
Flex Mean
Flex +Sigma